AD

USAAVLABS TECHNICAL REPORT 66-35

THEORETICAL AND EXPERIMENTAL INVESTIGATION OF THE AERODYNAMIC PROPERTIES OF AIRFOILS NEAR STALL IN A TWO-DIMENSIONAL NONUNIFORMLY SHEARED FLOW

By

W. G. Brady

G. R. Ludwig

June 1966

U. S. ARMY AVIATION MATERIEL LABORATORIES
FORT EUSTIS, VIRGINIA

CONTRACT DA 44-177-AMC-268(T)

CORNELL AERONAUTICAL LABORATORY, INC.
BUFFALO, NEW YORK

Disclaimers

The findings in this report are not to be construed as an official Department of the Army position unless so designated by other authorized documents.

When Government drawings, specifications, or other data are used for any purpose other than in connection with a definitely related Government procurement operation, the United States Government thereby incurs no responsibility nor any obligation whatsoever; and the fact that the Government may have formulated, furnished, or in any way supplied the said drawings, specifications, or other data is not to be regarded by implication or otherwise as in any manner licensing the holder or any other person or corporation, or conveying any rights or permission, to manufacture, use, or sell any patented invention that may in any way be related thereto.

Disposition Instructions

Destroy this report when no longer needed. Do not return it to the originator.

DEPARTMENT OF THE ARMY
U. S. ARMY AVIATION MATERIEL LABORATORIES
FORT EUSTIS, VIRGINIA 23604

This report has been reviewed by the U. S. Army Aviation Materiel Laboratories, and the results and conclusions are considered to be technically sound. The report is published for the exchange of information and the stimulation of new ideas.

Task 1P125901A14203
Contract DA 44-177-AMC-268(T)
USAAVLABS Technical Report 66-35
June 1966

THEORETICAL AND EXPERIMENTAL INVESTIGATION OF THE AERODYNAMIC PROPERTIES OF AIRFOILS NEAR STALL IN A TWO-DIMENSIONAL NONUNIFORMLY SHEARED FLOW

CAL Report AF-2035-S-1

by

W. G. Brady
G. R. Ludwig

Prepared by

Cornell Aeronautical Laboratory, Inc.
Buffalo, New York 14221

for

U. S. ARMY AVIATION MATERIEL LABORATORIES
FORT EUSTIS, VIRGINIA

BLANK PAGE

SUMMARY

The results of a continuing program of theory and experiment concerned with the aerodynamic characteristics of airfoils in nonuniformly sheared flows are presented. Development of a digital computer program to calculate airfoil pressure distributions in a particular type of two-dimensional, inviscid flow with nonuniform shear was completed, and airfoil pressure distributions were computed for specific configurations.

Wind-tunnel tests were performed with an airfoil in a two-dimensional, nonuniform flow with approximately the same free-stream velocity profile as that used in the computer program. Airfoil pressure distributions were obtained with the airfoil at several locations in the nonuniform flow, and throughout a range of angles of attack including angles at which complete separation occurred. It was found that the separation characteristics varied with the location of the airfoil in the sheared flow. Also, promotion or delay of separation was related qualitatively to variations in the adverse pressure gradient on the airfoil's upper surface; and it was observed that the trends are similar to those found in uniform flow. Finally, it was found that if lift coefficients referenced to stagnation streamline free-stream dynamic pressures $[(c_\ell)_s]$ are plotted against angles of attack measured from zero lift $(\bar{\alpha})$, the resulting data fall into a relatively narrow band centered on the uniform flow experimental c_ℓ versus α curve.

Computed pressure distributions were in good agreement with the corresponding experimentally measured pressure distributions. It would appear, therefore, that observed anomalous aerodynamic behavior near flow separation of airfoils in nonuniform flows is a direct result of the effects of the inviscid sheared flow on the airfoil pressure distribution.

The validated analytical technique for computing pressure distributions on an airfoil in an inviscid nonuniform flow provides a powerful tool for investigation of such anomalous behavior.

FOREWORD

The work described in this report was accomplished by the Cornell Aeronautical Laboratory, Inc. (CAL), Buffalo, New York, for the U. S. Army Aviation Materiel Laboratories (USAAVLABS), Fort Eustis, Virginia. The work was performed during the 12-month period starting in January 1965 under Contract DA 44-177-AMC-268(T), "Theory of Airfoils in Nonuniform Sheared Flows". Mr. P. Cancro administered the project for USAAVLABS. This work is a continuation of a research program carried out at CAL over a period of years from 1959 under Contracts DA 44-177-TC-439 and DA 44-177-AMC-70(T). Mr. W. G. Brady and Dr. G. R. Ludwig are authors of this report. Mr. Brady's primary responsibility was the analytical work, and Dr. Ludwig's primary responsibility was the experimental program. The invaluable contributions of Mr. J. Nemeth and Mr. C. Ryan of CAL are appreciated.

BLANK PAGE

CONTENTS

ILLUSTRATIONS

LIST OF SYMBOLS

c Airfoil chord, inches.

c_d Uniform flow section drag coefficient; $c_d = \frac{\text{DRAG PER UNIT SPAN}}{\frac{1}{2}\rho(U_o)^2 c}$.

$(c_d)_R$ Sheared flow section drag coefficient, referred to free-stream velocity at airfoil midchord position; $(c_d)_R = \frac{\text{DRAG PER UNIT SPAN}}{\frac{1}{2}\rho(U_R)^2 c}$.

c_ℓ Uniform flow section lift coefficient; $c_\ell = \frac{\text{LIFT PER UNIT SPAN}}{\frac{1}{2}\rho(U_o)^2 c}$.

$(c_\ell)_R$ Sheared flow section lift coefficient, referred to free-stream velocity at airfoil midchord position; $(c_\ell)_R = \frac{\text{LIFT PER UNIT SPAN}}{\frac{1}{2}\rho(U_R)^2 c}$.

$(c_\ell)_s$ Sheared flow section lift coefficient, referred to free-stream velocity along airfoil stagnation streamline; $(c_\ell)_s = \frac{\text{LIFT PER UNIT SPAN}}{\frac{1}{2}\rho(U_s)^2 c}$.

$\bar{c}_\ell$ Sheared flow section lift coefficient, referred to average free-stream velocity in wind-tunnel section; $\bar{c}_\ell = \frac{\text{LIFT PER UNIT SPAN}}{\frac{1}{2}\rho(\bar{U})^2 c}$.

$c_{m_{c/4}}$ Uniform flow section moment coefficient about the airfoil quarterchord, positive nose up; $c_{m_{c/4}} = \frac{\text{MOMENT PER UNIT SPAN}}{\frac{1}{2}\rho(U_o)^2 c^2}$.

$(c_{m_{c/4}})_R$ Sheared flow section moment coefficient about the airfoil quarterchord, positive nose up; $(c_{m_{c/4}})_R = \frac{\text{MOMENT PER UNIT SPAN}}{\frac{1}{2}\rho(U_R)^2 c^2}$.

C_p Uniform flow pressure coefficient; $C_p = \frac{p - p_o}{\frac{1}{2}\rho(U_o)^2}$.

$(C_p)_R$ Sheared flow pressure coefficient, referred to free-stream velocity at airfoil midchord position; $(C_p)_R = \frac{p - p_o}{\frac{1}{2}\rho(U_R)^2}$.

$(C_p)_s$ Sheared flow pressure coefficient, referred to free-stream velocity along airfoil stagnation streamline; $(C_p)_s = \frac{p - p_o}{\frac{1}{2}\rho(U_s)^2}$.

D_s Distance upstream and downstream of airfoil midchord where sheared flow dividing streamline is assumed to be at its free-stream location (see Figure 2), inches.

D_w Distance upstream and downstream of airfoil midchord where wind-tunnel wall vortex sheet singularity strengths are assumed to have reached their free-stream values (see Figure 2), inches.

$f(\psi)$ Function defined by Equation (1).

$g(x)$ Displacement of dividing streamline (see Figure 2), inches.

h Vertical height of airfoil midchord above tunnel centerline, inches.

K Shear parameter; $K = \frac{c}{U_R} \frac{dU_R}{dy}$.

$\bar{K}$ Smoothing parameter; see Equation (A-44).

L Vertical distance from tunnel centerline to wall (see Figure 2), inches.

$p(x,y)$ Static pressure at (x, y), pounds per square foot.

p_o Static pressure in free stream, pounds per square foot.

U_o Uniform flow free-stream velocity, feet per second.

$U(y)$ Sheared flow free-stream velocity, feet per second.

U_R Sheared flow free-stream velocity at $y = h$, feet per second.

U_S Sheared flow free-stream velocity of stagnation streamline, feet per second.

U_1 Free-stream velocity at lower wind-tunnel wall, feet per second.

U_2 Free-stream velocity at upper wind-tunnel wall, feet per second.

U_3 Free-stream velocity along vertical centerline in wind tunnel, feet per second.

$\bar{U}$ Average free-stream velocity in wind-tunnel test section, feet per second.

u Velocity component in x-direction, feet per second.

v Velocity component in y-direction, feet per second.

x Coordinate along axis parallel to wind-tunnel walls, positive downstream; $x = 0$ at airfoil midchord, inches.

x_L x-coordinate of airfoil leading edge, inches.

x_T x-coordinate of airfoil trailing edge, inches.

ΔY_s Vertical distance above the airfoil midchord reference height, h, where $U(y) = U_s$ in the free-stream velocity profile, inches, (see sketch, p. 33).

y Coordinate perpendicular to x-axis, positive up; $y = 0$ at wind-tunnel centerline, inches.

$\bar{\alpha}$ Airfoil angle of attack measured from zero lift angle of attack, positive leading edge up, degrees.

α Airfoil angle of attack, positive leading edge up, degrees.

γ_{A1} Singularity strength of vortex sheet representing airfoil aft lower surface.

γ_{A2} Singularity strength of vortex sheet representing airfoil aft upper surface.

γ_{AL} Singularity strength of vortex sheet representing airfoil leading edge surface.

γ_1 Singularity strength of vortex sheet representing lower wind-tunnel wall.

γ_2 Singularity strength of vortex sheet representing upper wind-tunnel wall.

ρ Air density, assumed constant, slugs per cubic foot.

ψ Stream function; see Equation (1).

INTRODUCTION

Many of the analytical problems of wing aerodynamics in flows at low subsonic speeds are treated successfully within the framework of potential flow theory. However, potential flow theory is inadequate for predicting analytically the interaction between a wing and a propeller slipstream when the slipstream intersects the wing and the flow in the propeller slipstream is not irrotational, i. e., when the slipstream flow has significant shear. An additional difficulty which gives rise to nonlinearities in the analytical treatment results from the interaction of the free boundaries of the slipstream flow and the wing.

A number of analytical treatments of the aerodynamics of sheared flows have been published; typical are References 1 through 4. Exact aerodynamic theories for uniform two-dimensional shear (constant vorticity) are available (References 1 and 4), but the available solutions for nonuniform shear (Reference 3, for example) are not particularly useful to the aerodynamicist because of limitations of the theoretical assumptions. These are primarily restrictions to small shear and shear gradient. Three-dimensional sheared flow theory (Reference 2, for example) has hardly advanced beyond attempts to arrive at a formulation which is mathematically tractable.

In view of this, the aerodynamicist is confronted with a difficult task if rational design data are to be provided for the low-speed aerodynamic characteristics of VTOL or STOL configurations in which much of the wing is immersed in a propeller wake. Reliance must be placed on experimental data, either from wind-tunnel tests or from free-flight data from prototype aircraft. In either case, without the foundation of prior experience and theoretical understanding, much guesswork and many

painful and expensive attempts at cut-and-try fixes to problems in performance, stability, and handling characteristics may be required to produce a satisfactory configuration.

The research reported here is part of a continuing program concerned with the aerodynamic characteristics of sheared flows. Initial results were obtained during a previous program of theoretical and experimental research on low-speed aerodynamics relevant to STOL and VTOL aircraft conducted for the U. S. Army Aviation Materiel Laboratories (formerly USATRECOM). References 4, 5, 6, and 7 report the results of that part of the study devoted to sheared flows. Of particular interest was the discovery that nonuniform shear in a two-dimensional flow could have a marked effect on airfoil stall characteristics (Reference 6). It is noted in Reference 6 that in the specific two-dimensional nonuniformly sheared flow treated, large variations in maximum lift were obtained near the flow centerline when the airfoil vertical position was varied by distances of the order of magnitude of the airfoil thickness.

The work reported in Reference 8 continued the preliminary experimental program of Reference 7,which was concerned with the effects of shear on a two-dimensional airfoil immersed in a three-dimensional, axially-symmetric, nonuniformly sheared flow. Also reported in Reference 8 was the initial effort on development of an analytical technique for computing the aerodynamic characteristics of an airfoil in two-dimensional, inviscid, nonuniformly sheared flow.

The research reported here continued the development of this analytical technique. A digital computer program was developed to compute pressure distributions on a two-dimensional airfoil in a particular nonuniformly sheared flow. Experimental airfoil pressure distribution data were obtained in the wind tunnel for a two-dimensional,

free-stream velocity profile nearly the same as that in the theory. These data were obtained to enable the accuracy of the analytical techniques to be verified. It was expected that the availability of an accurate theory would be of great value in investigations to determine the mechanism responsible for the unusual stall characteristics of the airfoil in nonuniformly sheared flows, as well as to obtain a more general understanding of sheared flow aerodynamic phenomena.

THEORETICAL PROGRAM

BACKGROUND - FUNDAMENTAL THEORETICAL CONSIDERATIONS

The research program, of which the work reported here is a part, is motivated by the lack of a general understanding of sheared flow aerodynamics. In particular, an understanding of the mechanisms inherent in the maximum lift behavior of airfoils in sheared flows should enable the aircraft designer to take advantage of this behavior. For example, experimental results obtained in Reference 6 indicate that large variations in maximum lift can occur with small changes in vertical position on an airfoil in two-dimensional, nonuniformly sheared flows with large shear and shear gradients.

The unusual and interesting maximum lift behavior in a particular nonuniformly sheared flow, demonstrated experimentally in Reference 6, could arise from any one or a combination of a number of possible mechanisms. Among those possibilities are the following:

1. Subtle wind-tunnel wall effects associated with the sheared flow.
2. An altering of the airfoil pressure distribution, solely on the basis of the inviscid sheared flow, so as to modify the separation of the airfoil boundary layer.
3. An interaction of the boundary layer with the inviscid sheared flow.

It might seem reasonable to test the various hypotheses selectively for their relative importance by means of carefully controlled wind-tunnel experiments; however, this approach can be time-consuming

and expensive. The large number of potentially important variables and the probable importance of nonlinearities make an all-experimental type of investigation even less attractive. If an accurate inviscid aerodynamic theory for nonuniformly sheared flow were available, however, the experimenter would have a very powerful added tool to use in conjunction with carefully chosen experiments. In particular, such an inviscid theory should enable the experimenter to identify, or at least to isolate, viscous effects. If, at the same time, the theory is capable of predicting wind-tunnel wall effects, then an additional uncertainty in the test program could be eliminated.

The theoretical study initiated during the work reported in Reference 8, and continued during the present program, has the ultimate objective of providing an analytical technique for predicting aerodynamic characteristics of airfoils in arbitrary two-dimensional, inviscid, nonuniformly sheared flows. The assumptions and conditions underlying the investigation are as follows:

1. The flow and the airfoil section are two-dimensional.
2. The flow is inviscid and incompressible.
3. The mathematical flow model must allow for large shear and shear gradients in the free stream.
4. The mathematical flow model must be consistent with large disturbances in the flow field.

The reason for specifying condition 4 above is related to the experimental findings that a sheared flow can either promote or retard flow separation at large angles of attack. Therefore, the large disturbances corresponding to these large angles of attack must be tolerated by the mathematical model. The linearizing techniques used in thin airfoil theory, therefore, would not be valid for those cases in which high angles of attack are considered.

The main characteristic of a sheared flow which distinguishes it from a nonsheared flow is the fact that it is rotational. The powerful techniques of potential theory, including conformal mapping, which can be used for two-dimensional, irrotational flow problems, are generally not applicable to rotational flows.

Rather than Laplace's equation, the stream function ψ must satisfy

$$\nabla^2\psi = f(\psi) ; \tag{1}$$

i. e., $\nabla^2\psi$ is a constant along a streamline (along which the stream function is also a constant). It can be shown that, in two-dimensional flow, this constant is the vorticity; i. e., the vorticity is a constant along a streamline in an inviscid two-dimensional, rotational flow. Except for the case of uniform shear ($f(\psi)$ = constant), or the exceptional case $f(\psi) = \bar{c}\psi$, $\bar{c}$ = constant, one is faced with solving a nonlinear, partial differential equation.

A general survey of available theory for the aerodynamics of sheared flows was presented in Reference 8. It was concluded there that the available theories were inadequate for the purposes of the present research. In particular, the requirements that a suitable theory permit large shear and shear gradients and be consistent with large disturbances in the flow field were not satisfied. In view of this, a new approach was adopted, based on a numerical technique. Although the resultant digital computer program was outlined in Reference 8, this outline is repeated here for the sake of completeness. The basic ideas behind the implementation of the computer program are presented in the body of this report. The fundamental equations and details of the actual program which was developed for use on an IBM 7044 digital computer are presented in the appendix of this report.

A digital computer program for computing an axially symmetric, free-streamline flow (finite impinging jet) was reported in Reference 9. The success of this program indicated a method of approach which should permit the calculation of the aerodynamic characteristics, including pressure distributions, of any two-dimensional airfoil at arbitrary angle of attack (in nonseparated flow) in two-dimensional, nonuniformly sheared flows with arbitrary shear. The only restriction appears to be that the free-stream velocity profile is such that it can be approximated by piecewise linear segments. Examples of such profiles are shown in Figure 1.

It should be recalled that the fundamental difficulty in treating two-dimensional, inviscid, nonuniformly sheared flows analytically is related to the fact that the fundamental governing equation (Equation (1)) is nonlinear for general nonuniformly sheared flows. This equation states that the vorticity in the flow is a constant along streamlines; inasmuch as the shape of the streamline is one of the unknowns in the problem, the functional form of the right-hand side of Equation (1) is not known beforehand. If the free-stream velocity profile can be approximated by piecewise linear segments, as in Figure 1, then the streamlines passing through those points at which the velocity gradient changes (points (a), (b), and (c) in Figure 1, for example) separate regions of constant vorticity throughout the flow. Thus, the relationship to the free-streamline flow problem (free-boundary problem) is clear; as part of the solution of the problem, the shape of those streamlines separating regions of constant vorticity must be determined. In effect, a problem with a nonlinear governing equation and known boundary conditions is replaced by a problem with a linear governing equation ($\nabla^2\psi$ = constant) within regions with free (and, hence, unknown) boundaries.

Based on the above approach, a theory was formulated for finding the pressure distribution on any airfoil at angle of attack in a nonuniformly

sheared flow with a piecewise-linear velocity profile. The computer program has been written for a two-dimensional velocity profile like that of Figure 1(b). This velocity profile has the advantage of being the simplest nonuniformly sheared flow to which the theory can be applied ; this is a worthwhile consideration for the initial calculations. Details of the theory and its implementation on the CAL IBM 7044 digital computer are presented in the following sections of this report.

It is difficult to assess with any exactness the implications of the restriction to piecewise-linear velocity distributions. In effect, a free-stream vorticity distribution like that of the solid line in the following sketch has been replaced with one like that of the dashed line.

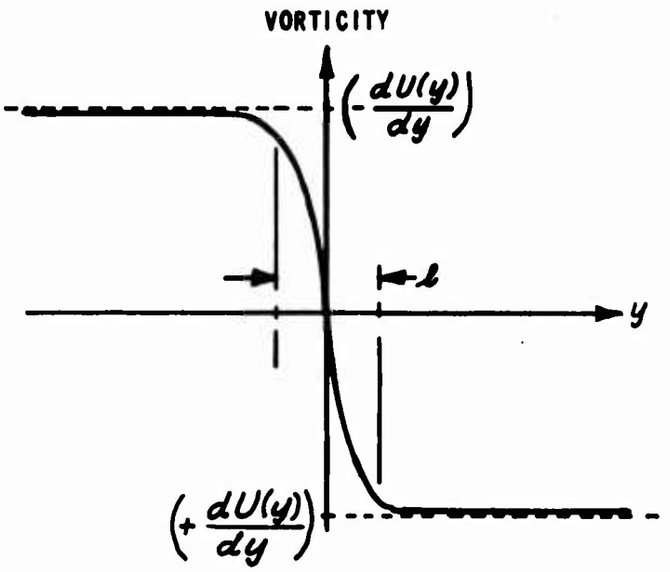

Perhaps the best way to consider this aspect is that the theory represents a limiting case of infinite shear gradient and that this is the only restriction on the model. It might be that the ratio of the distance ℓ to airfoil thickness as well as the ratio of ℓ to the displacement of the airfoil chord away from the discontinuity must be small for the approximation to be valid.

DESCRIPTION OF COMPUTER PROGRAM

Details of the formulation and implementation of the computer program are presented in the appendix. A brief outline of the basic ideas incorporated and certain numerical techniques of importance to the program are discussed in the following paragraphs.

Figure 2 is a schematic drawing of the two-dimensional flow model assumed for the computer program. A Cartesian coordinate system is used. The x-axis is parallel to the wind-tunnel walls and positive in the direction of the flow. The origin is centered vertically between the walls, and $x = 0$ is located at the airfoil midchord. The wind-tunnel walls and the airfoil surface are represented by bound vortex sheets of varying strength. The free-stream velocity variation in the y-direction is piecewise linear and symmetric about $y = 0$ (point (a) in Figure 2). On either side of the streamline which passes through point (a) (denoted henceforth as the "dividing streamline"), the distributed vorticity is constant. If the assumed free-stream velocity profile, $U(y)$, is symmetric ($U_1 = U_2$ in Figure 2), as is the case in the work presented here, the vorticity on either side of the dividing streamline is equal in magnitude but of opposite sign. If the airfoil is of nonsymmetric profile, or is nonsymmetrically disposed in the wind tunnel (for example, at zero angle of attack but not centered between the walls, or at angle of attack), the resulting disturbance flow will distort the dividing streamline in some fashion. This distorted shape is denoted by $g(x)$ in Figure 2. Equation (1) states that the vorticity in a rotational flow is constant along streamlines; therefore, the dividing streamline still separates regions of constant vorticity. If the shape of the dividing streamline $g(x)$ were known, then it would be possible to compute the variation in strength of the bound vortex sheets representing the wind-tunnel walls and airfoil surface. Given this information, plus information locating

the position of the stagnation streamline which intersects the airfoil, the pressure distribution on the airfoil surface can be computed.

An important part of the computer program is an iterative technique for determining the function $g(x)$ numerically. Mass-flow continuity is the basis for this iterative technique in the developed computer program. If an initial shape $g_0(x)$ is assumed, the strengths of the singularity distributions (vortex sheets representing the wind-tunnel walls and the airfoil surface) can be determined. Once these distributions are known, the first iterated streamline shape, $g_1(x)$, is determined by first computing, at each value of x considered, the vertical point ($g_1^*(x)$, say) in the flow where the mass flow is equal to that on either side of the dividing streamline in the undisturbed free stream, and then by taking the average of $g_0(x)$ and $g_1^*(x)$. Thus

$$g_1(x) = \frac{1}{2}\left[g_0(x) + g_1^*(x)\right].$$

Given $g_1(x)$, again the singularity strength distributions for the bound vortex sheets, representing the wind-tunnel walls and the airfoil, can be obtained, from which the second iterated streamline shape, $g_2(x)$, can be determined. If the iterative process converges, $\lim_{i\to\infty} g_i(x) = g(x)$. Hopefully, the rate of convergence is such that this limit is very nearly attained after only a few iterations.

The singularity strength distributions required to satisfy the boundary conditions at the wind-tunnel walls and the airfoil surface are those which correspond to the $g(x)$ evaluated in the final iteration. The flow field is thus completely determined. Velocities on the airfoil surface can then be converted to static pressures by means of the Bernoulli equation for rotational flow,

$$\frac{1}{2}\rho(u^2+v^2) + p = \frac{1}{2}\rho\left[U(y)\right]^2 + p_0 . \qquad (2)$$

applied along the airfoil stagnation streamline. The proper value of $U(y)$ in the free stream to be used in Equation (2) is determined by computing the mass flow between the wind-tunnel wall and the airfoil. The value of $U(y)$ which corresponds to this mass flow in the undisturbed free stream is the correct value.

DISCUSSION OF COMPUTER PROGRAM

The strengths of the singularity distributions (vortex sheets) representing the wind-tunnel walls and airfoil surface must be evaluated in order to be able to calculate airfoil pressure distributions. This is done in the computer program by breaking up the vortex sheets into small segments. For each of these segments, the singularity strength is assumed constant. The integrals over each segment of the vortex sheets for use in the equations for velocity components (Equations (A-2), (A-3), (A-6), and (A-7) of the appendix) can then be evaluated in closed form. Hence, the velocity components are expressible as finite series in terms of the vortex sheet singularity strengths. The vortex sheets representing the wind-tunnel walls are assumed to have known constant strengths upstream and downstream of the airfoil. The boundary conditions for no normal flow across the wind-tunnel walls and airfoil surface (Equations (A-8) and (A-9) of the appendix) are next applied at the center of each of the vortex sheet segments. If these boundary conditions were the only conditions to be satisfied, a determinate set of linear simultaneous algebraic equations would result. However, in addition, the Kutta-Joukowski condition at the airfoil trailing edge must be satisfied. This constraint is implemented in the computer program by requiring that the sum of the singularities representing the upper and lower airfoil surfaces vanish in the limit as the trailing edge is approached. This results in an additional equation, and the problem is now overdetermined. The problem can be made determinate by

relaxing the flow-tangency requirement at one of the vortex sheet segments. However, additional considerations arose in the solution of the set of simultaneous equations which obviated this necessity. Clearly, if the problem is properly posed in a mathematical sense, the equations which result should be determinate. The overdeterminacy of the above problem with the added Kutta-Joukowski condition most likely results from the method of numerical analysis used to obtain solutions. For example, if it had been assumed that the singularity strength of each segment of vortex sheet varied linearly, there would have been as many equations as unknowns. The choice of constant singularity strength for each segment, rather than a linear variation, was dictated primarily by the necessity to limit the number of linear equations which had to be solved.

Effectively, the process described above for determining the vortex strength distributions is the numerical solution of an integral equation. One check on the computer program was the computation of the pressure distribution on the airfoil in a uniform flow. As the airfoil involved is a Joukowski 17-percent-thick symmetric airfoil, analytic solutions for uniform inviscid, two-dimensional flow are available. Initial numerical calculations for the airfoil at an angle of attack of 10 degrees resulted in extremely irregular variation with x of computed values of C_p on the airfoil surface, as shown in Figure 3. Reference 10 discusses similar behavior exhibited by numerically computed solutions to integral equations of the first kind and presents a technique for obtaining smoothly varying solutions in an optimum sense, where it is known beforehand that the solution should be smooth. Reference 11 also considers the same problem, and extends the smoothing technique to allow the treatment of overdetermined sets of simultaneous algebraic equations. As previously noted, when the Kutta-Joukowski condition is included in the present computer program, an overdetermined set

of equations is obtained. Hence, the modified smoothing technique of Reference 11 was incorporated into the solution for the vortex strength distributions of the computer program; details are presented in the appendix. Figure 4 shows computed values of C_p on the airfoil surface at α = 10 degrees, which resulted when the smoothing technique was used in the computer program. It is evident that excellent agreement with the exact solution to the uniform, inviscid flow problem was obtained, with the exception of a 3-percent overshoot at the maximum negative computed value of C_p (suction peak). Apparently, the smoothing process works quite well in the present instance.

In contrast to the uniform flow calculation noted above, the nonuniformly sheared flow calculations required an iterative process to obtain solutions. Although there was confidence (based on the uniform impinging jet solutions obtained previously and presented in Reference 9) that a convergent iterative technique could be derived, the development of one which converged much more rapidly than that for the impinging jet constituted a major objective of the present work. In that previous case,as many as 80 iterations were required to obtain a satisfactory solution. Since the present computer program required about 12 minutes of machine time per iteration, 80 iterations would represent an unacceptable 16 hours of computer time. The technique finally employed was successful in reducing the number of iterations required; at most, five to six were sufficient to insure an acceptable solution for the configurations run thus far. This represents an hour to an hour and fifteen minutes of IBM 7044 computer time.

It should be noted that the use of mass flow continuity in the iterative process requires a known reference streamline of the flow. In the present case, a wind-tunnel wall provides this reference streamline.

EXPERIMENTAL PROGRAM

GENERAL

The experimental program was designed to provide airfoil pressure distribution data from which the accuracy of the theoretical results could be determined. At the same time, additional experimental evidence regarding airfoil maximum lift behavior in sheared flows would be obtained.

The wind-tunnel airfoil tests were of three types:

1. Uniform flow, low-turbulence tests
2. Uniform flow, high-turbulence tests
3. Sheared flow tests

The velocity profile generated for the wind-tunnel tests of the airfoil in sheared flow was similar to the particular profile considered in the theoretical treatment of the problem during this program.

The uniform-flow tests, with and without high turbulence, were designed as an experimental control. The shear screen used to generate the sheared flow also generated a high turbulence level in the flow. It was possible that this high turbulence level would in itself have had some marked effect on airfoil separation characteristics. The low and high turbulence tests in uniform flow were to resolve this possibility. In the event that the effects of turbulence in uniform flow were small, then the high-turbulence, uniform-flow airfoil pressure distribution data would provide a reference insofar as a comparison of theory and experiment is concerned. A comparison of theoretical and experimental pressure

distributions for the sheared-flow case could not be expected to be in any better agreement than the pressure distributions from uniform flow theory and experiment. The boundary layer is known to alter, somewhat, the experimental pressure distribution when compared to theory, even at angles of attack which are significantly below the stall angle.

EXPERIMENTAL APPARATUS

The experiments were made in the subsonic leg of the CAL/AF One-Foot High-Speed Wind Tunnel. This leg of the wind tunnel has a test section with a cross section of 17 inches by 24 inches and is operated as a closed-throat nonreturn tunnel. With no shear screen, the test section stagnation pressure is one atmosphere, and the practical speed range in the clear test section is from 0 to approximately 120 feet per second.

The two-dimensional airfoil used in this research has a symmetric Joukowski profile with a thickness-chord ratio of 17 percent and a chord of 6 inches. A number of static pressure orifices were distributed chordwise on the top and bottom surfaces along a section located near the center of the wing span. The wing was mounted in the wind-tunnel test section by a supporting structure which permitted independent change in geometric angle of attack and vertical location of the wing in the wind tunnel by means of manual adjustment. Figure 5 shows the wing and wing-support system mounted in the wind-tunnel test section.

Instrumentation was relatively simple. Flow calibrations in the wind-tunnel test section were performed with a conventional 3/16-inch-diameter Pitot-static probe which included static-pressure taps from which flow angularity data were obtained. Static and dynamic

pressures were measured with manometers. Thirty-two static-pressure taps distributed over the top and bottom surfaces of the wing were connected to an inclined manometer bank, and all manometer readings were recorded photographically. Free-stream static pressure was obtained from a pressure tap on the ceiling of the test section. This tap was approximately 2-1/2 chord lengths upstream of the model midchord.

The sheared flow in the wind-tunnel test section was produced by a screen placed slightly more than 3 feet (between 6 and 7 wing chords) upstream of the wing. This screen, shown in Figure 6, consisted of a number of circular rods spanning the wind-tunnel section horizontally and secured by a frame which was clamped between two sections of the wind-tunnel circuit. The spacing between rods and the rod diameters were varied so as to introduce variable losses across the flow. By proper spacing and rod size variation, the vertical distribution of losses in the flow at the screen can be such that the desired sheared-flow velocity contour can be obtained in the test section.

The theory presented in Appendix II of Reference 5 was used in the design of the screen. Application of this theory is somewhat laborious, and the results are dependent on the accuracy of the empirical relationship between local screen solidity and loss coefficient. Apparently the empirical curve presented in Reference 5 is not reliable at high values of solidity, because the use of this curve provided a velocity distribution which was considerably different from the design velocity distribution near the centerline of the test section. The final configuration used for the shear screen was tailored by a trial and error process of small modifications to the theoretical design until it was judged that further improvement could not be obtained without undue expenditure of time.

WIND-TUNNEL TESTS

Airfoil pressure distributions were measured in the wind tunnel with uniform flow and with a two-dimensional, nonuniformly sheared flow in the test section. Uniform-flow airfoil data were obtained with ambient turbulence levels (clear tunnel) and with high turbulence levels generated by screens mounted upstream of the test section. These screens were similar to the shear screen except that the horizontal rods used were uniformly spaced. Two such turbulence screens were used in separate tests, one screen with rod diameters and spacing corresponding to that portion of the shear screen with low solidity (relatively large open area ratio) and one screen corresponding to the high solidity portion of the shear screen.

During the uniform-flow tests, data were obtained with the wing model spanning the test section horizontally midway between the top and bottom walls. Pressure data were recorded within a range of angles of attack from near zero lift to beyond maximum lift. Two wind speeds were used to produce Reynolds numbers of 1.8×10^5 and 3.7×10^5, based on the airfoil chord of 6 inches.

Wind-tunnel flow calibrations were performed for both the clear-tunnel uniform-flow condition and with the turbulence screens in place. In the clear tunnel, variation of dynamic pressure in the free stream at the model location was less than 1 percent over the model chord, and variation in flow angularity in the vertical plane was less than 0.4 degree at the highest speed tested and about 0.1 degree at the lowest speed. With the low-solidity, uniform screen installed, vertical traverses of the flow at the model midchord reference station in the test section resulted in maximum variation of dynamic pressure of ± 2.8 percent and maximum flow angularity variation in the vertical plane of ± 0.25

degree. The flow with the high-solidity, uniform screen installed was considerably less uniform, with maximum variations in free-stream dynamic pressure of as much as ± 19 percent. A portion of the flow from the test section centerline to 4 inches below was more nearly uniform, and for wind-tunnel tests with this turbulence screen, the model was centered in this region.

Sheared-flow test data were obtained with the wing model situated at varying heights above and below the centerline of the sheared flow. At each position of the wing in the test section, pressure distributions were measured within a range of angles of attack from near zero lift to beyond maximum lift. The nominal Reynolds number, based on the airfoil chord and velocity at the position of the midchord, was different for each height because of the variation of velocity with height. The range of Reynolds numbers was from 1.7×10^5 at the tunnel centerline to 2.5×10^5 at 3 inches above and below the centerline. From previous experience with the wing model and wind tunnel, it was known that the boundary layers on the wind-tunnel side walls tended to interact with the wing model boundary layer, particularly near stall, so that stall occurred in a three-dimensional manner. Wind-tunnel wall suction near the intersection of the wing and the wall was used to minimize this interaction. Optimum values of the wall suction were obtained by means of lampblack and kerosene flow visualization studies, which preceded pressure tests for each configuration change.

Velocity profiles generated by the shear screen were obtained through a series of flow calibrations in the test section in a vertical plane at the model reference axis (midchord of the wing), using the 3/16-inch-diameter Pitot-static probe. Figure 7 presents velocity distributions for the final shear screen configuration used during pressure-data tests. Wing test data were obtained with the pressure-tapped

wing model segment centered 0.75 inch to one side (left looking downstream) of the wind-tunnel centerline. It can be seen that the velocity distribution approached the design distribution with reasonable accuracy but that some irregularities were present in the experimental data in the vicinity of 5 inches above and below the tunnel centerline. These irregularities are not believed to be of importance, because they were not large and because the test region extended only to 3 inches above and below the centerline. Of perhaps more concern is the rounded shape of the experimental velocity profile near the centerline. This rounded shape is not in agreement with the mathematical model and will be shown later to cause uncertainties in the data reduction technique used to define the stagnation streamline which intersects the wing. It is noted, however, that such profiles are more likely to be encountered in practice.

Figure 8 shows the flow angularity at the plane of the model midchord as determined with the static-pressure angularity taps on the 3/16-inch probe. The probe was calibrated for these measurements using standard procedures as described, for example, in Reference 12. With the probe tip fixed at some location in the flow, the probe is rotated through an arc in the vertical plane, say ±10 degrees from horizontal. The probe is then inverted and, with the probe tip at precisely the same location in the flow, the procedure is repeated. The output signals are plotted against angular position for each case. The slopes and the crossing point of the two sets of data provide the sensitivity of the probe for measuring flow angularity and a correction for the probe's dissymmetry which are independent of the characteristics of the flow itself.* The calibration was checked at several vertical locations in the sheared flow even though it was expected to be unaffected by the flow. It was found, however, that

---

* The data reduction included a small correction for the theoretical effect of shear on the measurements.

the calibration was valid only in regions far removed from the centerline of the sheared flow ($|y| > 3$ inches). In the vicinity of the center of the sheared flow, the sensitivity of the probe remained constant (as in the outer region) but the required correction for probe dissymmetry appeared to vary. (This was possibly due to the effects of curvature of the velocity profile in this central region of the flow.) Measurement of the flow angularity with sufficient precision required, therefore, that a technique similar to the probe-calibration procedure be used near the centerline of the sheared flow. At each vertical location within 3 inches from the centerline at which flow angularity was measured, the probe was rotated through an arc in the vertical plane with the probe both right-side up and inverted. The crossing point of the two sets of data provided the measure of the flow angularity independent of the apparent correction for probe dissymmetry. For locations outside of 3 inches from the centerline, the flow angularity could be determined by the substantially simpler method of using the probe calibration and the yaw-tap measurements made while the probe was traversed vertically with a fixed geometric angle for its axis. It is for this reason that Figure 8 shows a much higher density of data points in the outer region than in the central portion of the sheared flow.

A mean curve of flow angularity versus vertical location which was fitted to the data, as shown in Figure 8, has a variation of only from -0.30 degree to +0.35 degree. Accuracy of this mean curve, based on the repeatability of the measurements, is judged to be within ± 0.25 degree. The mean curve was used in calculating the effective angle of attack of the wing for each vertical location.

DISCUSSION OF EXPERIMENTAL RESULTS

Although a very large number of pressure distributions (over 200) were measured during the course of this program, only distributions which serve to illustrate the points under discussion will be presented. The section lift coefficient, c_ℓ , provides a convenient method for identifying regions where unusual phenomena may be occurring. Hence, in this report, curves of c_ℓ versus angle of attack, α , will be presented first. This coefficient, along with section drag and moment coefficients, was obtained by numerical integration of the pressure coefficient distribution on the wing section.

UNIFORM FLOW TESTS

Figure 9 shows c_ℓ versus α for the Joukowski airfoil under a variety of uniform-flow test conditions. These test conditions include tests at different free-stream velocities and tests with and without the low-solidity turbulence screen. The classical theoretical curve for a 17-percent-thick symmetrical Joukowski airfoil and a curve obtained from the strain-gauge balance measurements of Reference 5 on the same airfoil are shown for comparison. Data points obtained after the airfoil had stalled suddenly and completely are noted. It can be seen that the experimental data, including that of Reference 5, are in essential agreement, with the possible exception of the clear tunnel data point at U_0 = 118 f. p. s. and α = 7.5 degrees.

The maximum value of c_ℓ attained and the values of c_ℓ at angles larger than that for the maximum appear to be more dependent on the free-stream velocity than on whether the flow was passed through a

screen before encountering the airfoil. In general, the higher velocity free stream had a lower value of c_ℓ for a given α beyond that for maximum c_ℓ . The overall difference, however, is small. At angles below that for maximum c_ℓ , the trend appears to be reversed. All the experimental data fall below the theoretical curve in a fashion similar to that expected from experience. Data obtained with the high-solidity turbulence screen in place are not shown because of difficulties encountered in measuring the angularity of the flow. The maximum value of c_ℓ which was obtained with this screen was 1.25, which is in agreement with the data of Figure 9.

Pressure distributions for angles of 0, 7.5, and 10.0 degrees are shown in Figures 10, 11, and 12 and are compared with the inviscid potential flow theory. The agreement between theory and experiment is satisfactory at α = 0 degrees, but it begins to deteriorate near the upper surface suction peak and near the trailing edge as α is increased. The presence of the turbulence screen in the tunnel lowers the peak suction attainable on the upper surface, but it appears to delay the onset of separation from the upper surface near the trailing edge. This separation is indicated by a leveling of the value of C_p near the trailing edge and is mildly discernable in Figure 12 near $x/c \approx 0.85$ for the clear tunnel pressure distribution.

There are apparent discontinuities in the experimental data for the upper surface aft of the suction peak; for example, between x/c = 0.15 and 0.20 on Figures 11 and 12 for the clear tunnel data. The flow visualization studies showed that these irregularities correspond to the turbulent reattachment of a leading-edge separation bubble. Such bubbles occurred even at α = 0 degrees. They decreased in length as the angle of attack was increased or the flow velocity was increased. The addition of the turbulence screen to the flow did not give a measurably consistent variation to the bubble length. According to

Reference 10, which is an excellent survey of such bubbles, these laminar separation bubbles would generally be classed as short bubbles, and are evidently relatively thin.

Pressure distributions obtained on the airfoil near maximum lift and after complete stall are shown in Figures 13, 14, and 15 for 66 f. p. s. and with the low-solidity screen installed. This free-stream velocity with the turbulence screen installed corresponds most closely to the conditions obtained when the shear screen was used. Figures 13 and 14 clearly show the progressive forward movement of the separation point on the upper surface and also show the forward movement of the trailing edge of the bubble. At α = 13.0 degrees, which corresponds to maximum c_l for this case, separation occurs near x/c = 0.65. Between α = 13.0 and 16.5 degrees, the suction peak remains constant ($C_p \simeq -4.2$), but separation occurs near x/c = 0.28 for the larger angle of attack. Full separation or stall occurred at α = 16.7 degrees, as is evident in Figure 15.

Figures 16 and 17 show respectively the values of $c_{m_{c/4}}$ and c_d versus α obtained with the low-solidity screen in place. The data shown in Figures 16 and 17 must be regarded with some reserve, since they are obtained from the small difference between two large force components. The consistency of the data, however, suggests that the accuracy was at least as good as that obtained with the strain-gauge balance of Reference 5. The drag coefficient data of Figure 17 were derived from pressure distributions; hence, skin friction is not included in c_d.

In general, the uniform flow data provided the expected results, although the existence of the leading-edge bubble at low angles of attack was not expected. The addition of the turbulence screen did influence

the data very slightly, but not to the extent necessary to provide an explanation of results observed with the shear screen in place. These latter results are presented in the next section. Since there was a slight dependence on whether or not the turbulence screen was in place, the uniform flow data used for a control should be that obtained with the turbulence screen in place. The appropriate free-stream velocity is $U_0 = 66$ f. p. s., since this is approximately midway between the minimum and maximum velocities encountered with the shear screen. From the comparison of the measured and the theoretical pressure distributions for uniform flow, an increasing divergence between theory and experiment for the sheared flow can be expected as angle of attack is increased, with the theory predicting higher suction peaks on the upper surface than are evidenced in the corresponding experimental data.

SHEARED FLOW TESTS

The research reported here had as its primary objective the completion of the development of the computer program to compute airfoil characteristics in the nonuniformly sheared flow of Figure 1(b) and the validation of the theory by means of comparison with experiment. An added objective was to investigate experimentally in some detail the aerodynamic behavior and, particularly, the stalling characteristics of an airfoil in a nonuniformly sheared flow.

The significant feature of the nonuniformly sheared flow velocity profile used in the present work is that there are no free jet boundaries. It would seem that if an airfoil intersects a nonuniformly sheared flow which is wholly contained within a jet with free boundaries, as in Figure 1(c), the deformation of these free boundaries might have significant effects on the aerodynamic characteristics. Hence, the choice of a

nonuniformly sheared flow without free jet boundaries, besides simplifying the mathematical problem, allowed experimental isolation of the effect of nonuniform shear on airfoil aerodynamics from the effect of free jet boundaries.

A major problem in discussing the aerodynamics of airfoils in sheared flows is the question of a proper reference dynamic pressure. The midchord free-stream dynamic pressure is convenient for data reduction. From a practical viewpoint, the lift generated is of most interest; hence, some constant value of dynamic pressure should be used. However, in terms of boundary layer characteristics, including separation, the actual surface static pressures and associated pressure gradients are of primary importance; hence, the stagnation streamline free-stream dynamic pressure is the best reference dynamic pressure. In fact, it is this multiplicity of possible reference dynamic pressures in a sheared flow which tends to cause confusion, and it possibly leads to misleading conclusions regarding experimental aerodynamic data.

The free-stream dynamic pressure of the stagnation streamline is equal to the difference between the static pressure at the stagnation point on the airfoil and the free-stream static pressure. If taps are spaced sufficiently close together on the lower leading edge surface of the airfoil, it is possible to obtain the stagnation streamline free-stream dynamic pressure from the airfoil pressure distributions. Bernoulli's equation along the stagnation streamline is

$$p + \frac{1}{2}\rho(u^2 + v^2) = p_o + \frac{1}{2}\rho(U_s)^2$$

where p_o is the free-stream static pressure and U_s is the velocity in the sheared free stream which corresponds to the stagnation streamline. Using this relation, the pressure coefficient, $(C_p)_s$, based on the free-stream dynamic pressure of the stagnation streamline becomes

$$(C_p)_s = \frac{p - p_0}{\frac{1}{2}\rho(U_s)^2} = 1 - \frac{u^2 + v^2}{(U_s)^2} .$$

Note that since the maximum positive value of $(C_p)_s$ is 1, the appropriate free-stream dynamic pressure of the stagnation streamline is simply the maximum positive value of $(p - p_0)$ which is reached on the airfoil. In addition, the remaining two reference dynamic pressures which were mentioned above provide pressure coefficients $\bar{C}_p$ (based on an average velocity, $\bar{U}$), and $(C_p)_R$ (based on midchord velocity, U_R), which are defined by

$$\bar{C}_p = \frac{p - p_0}{\frac{1}{2}\rho(\bar{U})^2} = \left(\frac{U_s}{\bar{U}}\right)^2 - \frac{u^2 + v^2}{(\bar{U})^2}$$

$$(C_p)_R = \frac{p - p_0}{\frac{1}{2}\rho(U_R)^2} = \left(\frac{U_s}{U_R}\right)^2 - \frac{u^2 + v^2}{(U_R)^2} .$$

The section force and moment coefficients can be referred to any of the reference dynamic pressures to obtain, for example, $\bar{c}_\ell$, $(c_\ell)_R$, or $(c_\ell)_s$.

Figure 18 shows the variations of average lift coefficient, $\bar{c}_\ell$, with angle of attack which were obtained in the present investigation. In this case, $\bar{c}_\ell$ is referred to a dynamic pressure derived from the average free-stream velocity in the tunnel test section. The $\bar{c}_\ell$ defined in this way is not numerically comparable to that of Reference 6, in which experimental results were reported for the same airfoil in a nonuniformly sheared flow with free boundaries similar to that of Figure 1(c). The numerical difference arises because of the difficulty of defining an average $\bar{U}$ which is equivalent for the two sheared flows. In spite of the numerical differences, the shapes of the $\bar{c}_\ell$ versus α curves of Figure 18 are similar to those presented in Reference 6. For both sheared flows, at $\alpha = 0$, there is a positive lift for $h > 0$ and a negative lift for $h < 0$. The behavior of $\bar{c}_\ell$ ne maximum lift appears to be dependent on the magnitude of the shear. At positions well below the centerline of the velocity distribution, the stall is abrupt. At

positions near the centerline and above the centerline, the onset of stall becomes much more gradual.

The maximum usable lift as defined in Reference 6 is the value of $\bar{c}_\ell$ at which the derivative of the moment coefficient about the midchord with respect to $(c_\ell)_R$, i.e., $\frac{d(c_{m_{1/2}})_R}{d(c_\ell)_R}$, becomes zero. An apparent correlation of this maximum usable lift with the product of shear parameter and gradient of shear parameter, $(K\frac{dK}{dy})$, was noted in Reference 6. The present data (Figure 18) showed no evidence of such a correlation.

Figure 19 shows $(c_\ell)_R$ versus α for all positions of the model that were tested in the sheared flow. These data are directly comparable to the data of Figure 6 of Reference 6 (which has been reproduced here as Figure 20), if the value of r in Figure 20 is taken to be 12 inches. The test configuration in the present case differs from that of Reference 6 in the lower values of shear and the constrained edges of the nonuniformly sheared regions of the flow. The trends evident in Figures 19 and 20 are similar. Note that even in the low-shear tests (Figure 19), lift coefficients, $(c_\ell)_R$, as high as 2.0 are obtained. However, the pronounced effect of different airfoil position near the centerline of the nonuniformly sheared free jet on the shape of the lift coefficient curve (Figure 20, h/r = + 1/8 and -1/8) does not occur with the bounded nonuniform flow (Figure 19). Moreover, the maximum usable lift for the bounded nonuniform flow does not show any marked variation with airfoil position near the centerline of the flow (Figure 18 does show large variations in maximum usable lift, but these variations correspond to relatively large changes in airfoil position.) This, again, is in contrast to Reference 6, where the maximum usable lift varied from $\bar{c}_\ell \approx 0.5$ at $\frac{y}{r}$ = + 1/8 to $\bar{c}_\ell \approx 1.1$ at - -1/8. These large variations in aerodynamic behavior with the airfoil at different

positions near the centerline of the free nonuniform jet may be a consequence of the higher shear or of the fact that free boundaries are present, or a combination of both.

Figure 21 shows the drag coefficient $(c_d)_R$ plotted versus $(c_\ell)_R$. As mentioned previously, $(c_d)_R$ includes the pressure drag only and is probably not very accurate. Of interest is the fact that $(c_d)_R$ is positive in all cases. Sheared flow aerodynamic data obtained previously with the strain-gauge balance (Reference 8) had resulted in negative drag coefficients for some cases with small values of $(c_\ell)_R$.

The moment coefficient about the quarterchord, $(c_{m_{c/4}})_R$, is shown plotted versus $(c_\ell)_R$ in Figure 22. These data show a relatively large variation with differing wing positions and appear to fall roughly into two groups, one for data obtained with the wing below the centerline of the sheared flow and one for the data obtained with the wing above the centerline. The data obtained with h = -1/2 inch, which was closest to the centerline of the experimental velocity distribution, fall approximately midway between these groups. The differences in the groups of curves indicate variations in pressure distribution at constant values of $(c_\ell)_R$. Notable in Figure 22 is the evidence that the center of pressure moves continuously rearward with increasing $(c_\ell)_R$ for negative values of h, while for positive h, it remains approximately constant or even moves forward as $(c_\ell)_R$ increases up to values near the maximum. Just below the maximum values of $(c_\ell)_R$, the center of pressure of the $(+h)$ group begins to move rearward abruptly in a fashion similar to the $(-h)$ group.

It is interesting to compare pressure distributions in the regions where the above two groups show dissimilar behavior in the movement of center of pressure. This has been done in Figure 23 for h = +3 and -3 inches in the sheared flow and also for uniform flow. The

data shown were chosen to be at values of $(c_\ell)_R$ as close to each other as possible and in a range of $(c_\ell)_R$ where separation of the boundary layer should not be too influential in determining the pressure distribution. Figure 23 shows that the adverse pressure gradient aft of the suction peak on the upper surface is increased by negative shear (h = -3 inches) and decreased by positive shear (h = +3 inches) in comparison with that which is obtained in uniform flow. This behavior is consistent with the differences in the shapes of the $(c_\ell)_R$ versus α curve at high angles of attack for positive and negative shear. The steeper pressure gradient will tend to promote separation; the lower pressure gradient, to delay separation.

The upper surface pressure distributions of Figure 23, which are typical of all values of $(c_\ell)_R$ up to the maximum, do not explain, however, the seemingly haphazard variation in the maximum values of $(c_\ell)_R$ illustrated in Figure 19. From these upper surface pressure distributions it could be concluded that, since separation is promoted by negative shear and delayed by positive shear, the maximum values of $(c_\ell)_R$ should be observed when the shear is positive and a progressive deterioration in maximum $(c_\ell)_R$ should occur as the shear becomes negative. This is certainly not the case in Figure 19 where the data for h = +3 and -3 inches gave approximately the same maximum value of $(c_\ell)_R$, although it must be admitted (as mentioned in the previous paragraph) that the abrupt stall for negative shear and the gradual stall for positive shear are consistent with the upper surface pressure distributions. A partial explanation for this apparent inconsistency is that the lift also depends on the lower surface pressures, and as can be seen in Figure 23, the lift due to the lower surface for h = -3 is appreciably greater than that for h = +3.

Some degree of correlation can be brought to the c_ℓ data by using

the apparent free-stream dynamic pressure of the stagnation streamline which intersects the airfoil as a reference dynamic pressure. The method for obtaining this dynamic pressure was discussed previously. It amounts to choosing the value of dynamic pressure which will make the positive peak of $(C_p)_R$ equal to unity. For example, in Figure 23, for $h = -3$ inches, all values of $(C_p)_R$ are converted to $(C_p)_S$ simply by dividing $(C_p)_R$ by 1.25. The same factor is then used to obtain $(c_\ell)_S$ from $(c_\ell)_R$. If in addition to using $(c_\ell)_S$, the angle of attack for zero lift is subtracted from the usual angle of attack, the resulting curves for the various values of h become directly comparable. The results are plotted in Figure 24(a) as $(c_\ell)_S$ versus $\bar{\alpha} \equiv \alpha - \alpha_{c_\ell=0}$. A similar presentation of $(c_\ell)_R$ is shown in Figure 24(b) for comparison. Note that individual sets of $(c_\ell)_S$ data for a given airfoil midchord position show a greater degree of irregularity (they do not form as smooth a curve) than the corresponding $(c_\ell)_R$ data. This can be attributed to errors in determining the free-stream dynamic pressure of the stagnation streamline from the experimental pressure distributions. Unfortunately, there was a greater concentration of static-pressure taps on the upper leading-edge surface of the airfoil than on the lower leading edge. Consequently, in many cases, there was difficulty in determining accurately the maximum positive value of $(C_p)_R$, and such inaccuracies are reflected directly in $(c_\ell)_S$.

Inspection of the $(c_\ell)_R$ data (Figure 24(b)) provides several features which are worthy of note. First, all of the experimental data obtained in the sheared flow for values of $\bar{\alpha}$ greater than zero lie above the control data for the same airfoil in uniform flow at approximately the same Reynolds number. Second, the slopes $\left(\frac{\partial (c_\ell)_R}{\partial \bar{\alpha}}\right)$ of a number of the sets of sheared-flow data increase as angle of attack increases, becoming greater than that predicted by inviscid uniform flow theory. This latter observation cannot be accounted for on the basis of viscous

effects alone, since such effects on an airfoil always tend to result in reduced lift compared to that predicted by inviscid theory.

Inspection of Figure 24(a) provides a somewhat different, and more enlightening, picture. In this case, all of the experimental data at positive values of $\bar{\alpha}$ lie on or below the inviscid uniform flow theoretical curve and appear to fall into two approximate groupings, one for positions below the sheared flow centerline and one for positions near and above the sheared flow centerline. These groupings are similar to those noted previously in the $(c_{m_{c/4}})_R$ versus $(c_\ell)_R$ data (Figure 22). Such correspondence is not particularly surprising, since plotting c_m versus c_ℓ effectively cancels any error which arises through the use of incorrect or inconsistent values of reference dynamic pressure and completely eliminates the angle of attack from the presentation. The differences between the two groups of data in Figure 24(a) will be shown to be consistent with differences in the observed pressure distributions.

Figure 25 shows the pressure distribution $(C_p)_s$ on the airfoil for different wing positions. The distributions shown are for nearly equal values of $\bar{\alpha}$, with $\bar{\alpha}$ small enough that boundary-layer separation should not affect the results to any marked degree. Note that the pressure gradient after the suction peak is less steep for positive shear (h = +3 inches) than for negative shear (h = -3 inches) and also that the gradient shown by the uniform flow control data is approximately the same as that for the negative shear data. The magnitude of $(C_p)_s$ at the suction peak is influenced by the existence of a leading-edge bubble. This bubble occurred both with uniform flow and with h = -3 inches, even at low angles of attack. At h = +3 inches, however, the bubble did not appear until the angle of attack approached 10 degrees. Hence, comparison of the magnitude of the

suction peaks is not of any particular value. Comparison of the pressure gradients after the suction peak is useful because the uniform flow control experiments indicated that these gradients are not particularly sensitive to the existence of the bubble. (See, for example, Figures 10, 11, and 12.)

Similar pressure distributions are shown in Figure 26 for a higher value of $\bar{\alpha}$. The same trends are evident here as were displayed in Figure 25. Hence, it appears that the shapes of the $(c_\ell)_s$ curves near stall are consistent with the pressure distributions. These distributions indicate that separation should be delayed by positive shear and promoted by negative shear. For the airfoil used in these tests, the sharp suction peaks and large adverse pressure gradients generated in the uniform flow and the negatively sheared flow cause the formation of a leading-edge bubble which reduces the lift to values less than those predicted by uniform flow theory even at relatively low angles of attack. The favorable effect of positive shear delays the formation of the leading-edge bubble and also delays the onset of trailing-edge separation, resulting in a closer correlation with uniform-flow, inviscid theory in Figure 24(a).

From the above discussion, it would appear that a large portion of the confusion regarding the effects of nonuniform shear on the lift of an airfoil can be eliminated if a proper reference velocity is used to reduce the data to nondimensional form. This velocity is the free-stream velocity which corresponds to the stagnation streamline of the airfoil.

Incidental to the determination of the free-stream dynamic pressure of the stagnation streamline, displacement of the stagnation streamlines at the various angles of attack for each value of h tested was also determined. (See sketch on following page.)

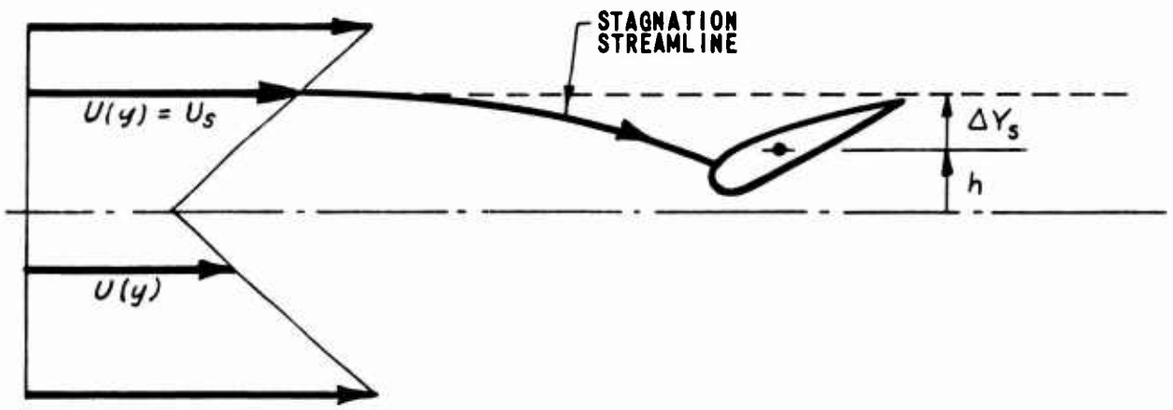

Stagnation streamline displacement, ΔY_s , is the vertical distance above the airfoil midchord reference height, h , to the location in the free-stream velocity profile where $U(y) \equiv U_s$. The ability to trace the approximate location from which the stagnation streamline originated through simple pressure measurements on a body (ignoring viscous losses due to mixing) is a unique and useful feature of two-dimensional sheared flows.

The resultant data for h = -3, -2, -1, +1, and +3 inches are plotted in Figures 27 through 31. Again, these data should be viewed with some caution, as they were derived from the stagnation point static pressure and the errors may be large. Bars are drawn through some of the particularly questionable points to indicate the possible degree of error arising from estimating the maximum positive value of $(C_p)_R$. In addition to errors due directly to the difficulty in obtaining the correct value of $(C_p)_R$ at the stagnation point, there was further magnification of these errors when the airfoil was near the centerline

of the sheared flow. The rounded velocity profile in this region made small errors in $(C_p)_R$ at the stagnation point correspond to large errors in ΔY_s . The values of ΔY_s derived experimentally for $h = +1/2$, 0, $-1/2$ were particularly suspect because of this and, hence, are not presented. The data for the wing well below the centerline of the sheared flow behave in a manner which appears to be consistent with an increase in circulation around the airfoil as angle of attack is increased. The data obtained with the airfoil above the centerline vary in a manner different from the data obtained below the centerline. No explanation for the differences in behavior of the apparent deflection of the stagnation flow streamline is advanced at present. Further computations using the non-uniform sheared flow theory may help to explain these differences in stagnation streamline deflection.

From the experimental data presented thus far, several important conclusions can be stated with respect to two-dimensional aerodynamic characteristics in the specific nonuniformly sheared flow considered during the present research:

1. The addition of turbulence to the flow through the use of a screen to generate the sheared flow is not the source of the observed differences between stalling characteristics of airfoils in sheared and in unsheared flows.

2. Much of the apparent difference in aerodynamic behavior below stall resulting from differing vertical positions in the sheared flow can be reconciled if the free-stream velocity of the stagnation streamline which intersects the airfoil is used as a reference velocity in calculating lift coefficients; see Figure 24(a). It is worth noting that, even in the relatively low shear of the present

work, the dynamic pressure of the stagnation streamline differed from the dynamic pressure referenced to the airfoil midchord by more than 50 percent in some instances.

3. There are differences in the approach to complete stall of the airfoil depending upon the vertical location of the airfoil in the sheared flow. These differences appear to be associated with the change in pressure distribution on the upper surface of the airfoil. Positive shear at the airfoil position reduces the pressure gradient on the upper surface and hence delays the occurrence of separation, while the converse is true of negative shear.

These observations suggest that it is probably not necessary to consider the direct interaction between shear in the free stream and the behavior of the boundary layer when seeking the stalling characteristics of a wing in a sheared flow. If the pressure distribution on a wing in an inviscid sheared flow is predictable, then the prediction of stalling characteristics in a real sheared flow should be equivalent to the prediction of stalling characteristics of a wing in a viscous, uniform flow, given the inviscid, uniform-flow pressure distribution. This hypothesis will be further substantiated by comparison of theoretical and experimental pressure distributions in the sheared flow in subsequent paragraphs.

COMPUTED RESULTS AND COMPARISON WITH EXPERIMENTAL RESULTS

Calculations using the developed computer program for a non-uniformly sheared flow were performed corresponding to two vertical locations of the wing with respect to the flow centerline, $h/c = -0.33$ and $h/c = +0.50$. The free-stream velocity profile used in the numerical calculations was such that the shear parameter, K, varied from ± 1 near the tunnel centerline to ± 0.33 adjacent to the wind-tunnel walls. At $h/c = -0.33$, pressure distributions were computed for $\alpha = 7.1$ degrees and $\alpha = 9.5$ degrees. At $h/c = +0.5$, the pressure distribution at $\alpha = 8.2$ degrees was computed.

Figure 32 is a comparison of computed and experimental values of $(C_p)_R$ versus x/c for $h = -2$ inches (corresponding to $\frac{h}{c} = -0.33$), $\alpha = 7.1$ degrees; Figure 33, for $h = -2$ inches, $\alpha = 9.5$ degrees (experimental data for $\alpha = 9.6$ degrees); and Figure 34, for $h = +3$ inches ($h/c = 0.5$), $\alpha = 8.2$ degrees. It can be seen that in all three cases the comparison is as good as in the corresponding uniform-flow case between the results of inviscid theory and the experimental data in a low Reynolds number turbulent flow (see Figures 10 through 12). In particular, the upper-surface pressure gradient is quite accurately predicted, although, as for the uniform-flow cases, the leading edge suction peak is overpredicted, more so as the peak $(C_p)_R$ becomes more negative.

In Figure 34, for $h = +3$ inches, the uniform-flow pressure distribution calculated from the computer program for the airfoil at $h/c = +0.5$ is also plotted for comparison. It is clear that, in agreement with experiment, the predicted pressure gradient just aft of the

leading-edge suction peak is less adverse for the h = +3 inches, nonuniformly sheared-flow configuration than for the uniform-flow configuration.

Computed $(c_\ell)_R$ and $(c_{m_{c/4}})_R$ for these three cases are plotted on Figures 35 and 36, respectively, where comparisons are made with the appropriate experimental results. Agreement is satisfactory except, perhaps, for h = -2 inches, α = 9.5 degrees ($(c_\ell)_R$ = 1.72), where experimentally the center of pressure is further aft than predicted. Computed values of $(c_{\ell_\alpha})_R$, including the uniform flow configuration, vary from -0.010 to -0.016. This reflects the slight overprediction of leading-edge peak suction for uniform flow, which undoubtedly carries over into the nonuniformly sheared-flow calculations.

Computed displacements of the airfoil stagnation streamlines are plotted in Figures 28 and 31. Relatively good agreement with the experimentally derived displacements is obtained for h = -2 inches (Figure 28). Predicted displacements in this case are 25 percent to 35 percent too high. Poorer agreement is shown for the h = +3 inches, α = 8.2 degrees case (Figure 31). If there were perfect symmetry in the experimental nonuniform velocity profile, negative stagnation streamline deflections for the airfoil at h = -3 inches at positive angles of attack would correspond to positive streamline deflections with the airfoil at h = +3 inches at negative angles of attack. The experimental stagnation streamline displacement data for h = -3 inches, with signs of α and ΔY_s reversed, is also plotted in Figure 31. The comparison of computed and experimental stagnation streamline deflection data is somewhat improved in this case. (Note that the corresponding pressure distribution for h = -3 inches, α = -8.2 degrees is plotted in Figure 34 for comparison with h = +3 inches, α = 8.2 degrees data.) In view of the uncertainties involved in the determination of experimental stagnation streamline deflections, the comparison of computed and

experimental results in this case is quite good.

DISCUSSION OF COMPUTED RESULTS

It was concluded on the basis of the experimental data that the variation in stall behavior with vertical location of the airfoil in the nonuniformly sheared flow was associated with the corresponding variation in the adverse pressure gradient aft of the suction peak on the airfoil upper surface. For the airfoil above the centerline of the nonuniformly sheared flow, the onset of trailing-edge stall was delayed somewhat, and the occurrence of complete separation was delayed to somewhat higher angles of attack than in the case of a directly comparable uniform flow (at the same Reynolds number and with similar turbulence level). Related to this behavior was a less adverse pressure gradient on the upper surface of the airfoil in the nonuniformly sheared flow than in the uniform flow. Likewise, for the airfoil below the centerline of the nonuniformly sheared flow, stall was correspondingly promoted, and in this case, the upper surface pressure gradient was more adverse than for the comparable uniform flow.

The question remains: are the experimentally demonstrated variations of adverse pressure gradient with change in vertical height associated with an interaction of the sheared flow and the boundary layer, or are they attributable solely to the modification of the pressure gradient by the sheared flow? (Note that the laminar separation bubble is an example of an interaction of the boundary layer and the outer flow.) The good agreement of the computed and experimental pressure distributions indicates that, in fact, the altered pressure distributions are primarily a result of inviscid action of the sheared flow.

The flow model upon which the digital computer program is

based involves several idealizations which could affect the computed results to some degree. The two most important are probably:

1. The flow is assumed to be inviscid.

2. The shear screen is assumed to be located a great distance upstream relative to the model chord length.

3. Flow disturbances are assumed localized in the immediate vicinity of the airfoil.

The assumption of an inviscid fluid means that both viscous mixing and the displacement effect of the boundary layer are neglected. If the disturbance arising from the airfoil is localized in the flow within two or three chord lengths of the airfoil, the effects of neglecting viscous mixing in the theoretical model are probably small. Indications from the limited calculations done thus far are that the airfoil disturbance is felt farther upstream and downstream for nonuniformly sheared flow than for uniform flow, particularly for the h = +3 inches, α = 8.2 degrees configuration.

The effect of assuming that the shear screen is very far upstream of the model is difficult to ascertain. In actuality, the shear screen was located about seven airfoil chord lengths upstream of the airfoil midchord. If the airfoil flow disturbance did extend this far upstream, then there could be an interaction of some sort. Theoretically, it would have been possible to include the shear screen in the flow model; however, limitations of computer capacity precluded this for the present.

The assumption that flow disturbances associated with the airfoil do not propagate indefinitely far upstream or downstream of the airfoil in the wind tunnel is incorporated in the computer program by fixing $g(x)$ — the displacement of the free streamline at the apex of the velocity distribution — at its free-stream value (zero in the present nonuniformly

sheared flow) for $x < -D_s$ and $x > D_s$, and by fixing the vortex strength distribution representing the wind-tunnel wall at the free-stream value for $x < -D_w$ and $x > D_w$. For the calculations at h = -2 inches, the values $(D_s)/c = (D_w)/c = 4$ were chosen. For the h = +3 inches configuration, calculations were performed for $(D_s)/c = (D_w)/c = 6$ and for $(D_s)/c = (D_w)/c = 8$. In principle, the extent of the flow disturbance upstream and downstream of the airfoil could be computed by arbitrarily choosing values of D_w and D_s, obtaining a solution, and determining whether, in fact, the vortex strengths for the wind-tunnel wall at $x = \pm D_w$ and $g(x)$ at $x = \pm D_s$ have attained their free-stream values. If not, D_s and D_w could be made larger and the calculations repeated until values of D_s and D_w were found for which $g(\pm D_s)$, $\gamma_1(\pm D_w)$, and $\gamma_2(\pm D_w)$ had attained their free-stream values. This was not practicable because of the limitations of computer storage capacity and also the practical limitation on the maximum size of matrix that can be inverted numerically with acceptable accuracy. It was found for the h = +3 inches calculations that as D_s and D_w were increased from six to eight chord lengths, the values of $g(\pm D_s)$, $\gamma_1(\pm D_w)$, and $\gamma_2(\pm D_w)$ showed even less agreement with free-stream values. This behavior, at least insofar as $\gamma_1(\pm D_w)$ and $\gamma_2(\pm D_w)$ are concerned, was also noted in several uniform flow cases that were computed with the program. For this reason, it is believed that this result may partly be associated with the numerical techniques used in the computer program. In particular, the small numerical inaccuracies associated with the smoothing procedure might have been a major contributing factor. In any case, these noted discrepancies were small in the present calculations.

The comparisons of theoretical and experimental data, particularly the pressure distributions, indicate that the theory successfully predicts the important features of the (unseparated flow) airfoil aerodynamic characteristics in the nonuniformly sheared flow

treated during the present research. It appears that the stall behavior can be accounted for on the basis of the inviscid flow pressure distribution, and that there are no unusually large viscous interaction effects between the sheared outer flow and the boundary layer. The analytical technique, therefore, should prove to be an extremely useful research tool for further investigation of the stall behavior of airfoils in nonuniformly sheared flows.

It would be most desirable to extend the computed results for the present velocity profile over a greater range of angles of attack and for additional h/c values. This would permit a theoretical check of the relatively good correlation of the experimental data for $-0.5 \leq \frac{h}{c} \leq 0.5$ in terms of $(c_\ell)_s$ versus $\bar{\alpha}$. In particular, it would be of great interest to determine how accurately the theory predicts $(\Delta c_\ell)_R$ at $\alpha = 0$. The calculations should also be extended to higher values of the shear parameter K than those considered in the current work.

The experimental airfoil data of Reference 6 were obtained in a two-dimensional, nonuniformly sheared flow with nearly four times the shear near the flow centerline as for the flow of the present tests. The sheared flow computer program should be modified and extended to the nonuniform velocity profile of the Reference 6 data, and pressure distributions should be computed for a number of the configurations of the tests of Reference 6. The shear in the Reference 6 velocity profile is probably as large or larger than the maximum obtainable in a propeller slipstream. If, as expected, the theory retains its accuracy for this level of shear, its range of validity should be adequate to cover all foreseeable practical cases.

PROSPECTS FOR ACCOUNTING FOR THREE-DIMENSIONAL EFFECTS

An important application of the results obtained from this continuing research program is, of course, to the aerodynamics of wings immersed in propeller slipstreams. The engineering prediction of the lift generated by a wing interacting with a propeller slipstream at low forward speeds has been a difficult problem. This problem is of particular importance for VTOL and STOL aircraft in which either the propeller thrust or the lift generated by deflection of propeller slipstreams is a substantial portion of the take-off lift of the aircraft.

There are at least two possible approaches to the analytical prediction of lift on a finite wing in a propeller slipstream:

1. A direct approach based on a vortex sheet flow model similar to that of the analytical technique used in the present study.
2. A lifting-line approach based on the theory for three-dimensional, nonuniformly sheared flows proposed by von Karman and Tsien (Reference 13).

Clearly, the first approach would result in a computer program of formidable complexity even in comparison with the two-dimensional flow computer program developed during the present research. The more attractive approach from a practical computational point of view is the lifting-line approximation. However, even the von Kármán-Tsien theory cannot be applied readily to the calculation of finite-wing aerodynamic characteristics because the theoretical expression for the induced angle of attack at each wing section must be rederived for each nonuniformly sheared flow velocity distribution. The derivation involves the solution of two differential equations and an integral

equation; finding these solutions undoubtedly will not be a simple process. In addition, the von Kármán-Tsien theory is a small disturbance theory, and its extension to high wing loadings near maximum lift can be justified only on the basis of a comparison of the results of analysis and experiment.

In any case, two-dimensional sectional lift data derived from two-dimensional, nonuniformly sheared flows with the same velocity profiles as those in sections vertical to the plane of the finite wing are needed in order to apply the lifting-line approximation. If experimental data were to be obtained for this purpose, a difficult and expensive test program would be required. An accurate two-dimensional airfoil theory for nonuniformly sheared flow would provide the same sort of data, and at considerably less expense.

It is believed that effort should be devoted to exploitation of the von Kármán-Tsien nonuniform flow lifting-line theory. If this effort were successful, then the two- and three-dimensional experimental flow data developed and presented in References 6 and 8 would permit an evaluation of the usefulness of such a modified lifting-line theory as an engineering tool. Additional two-dimensional sectional data for the nonuniform flow corresponding to the vertical velocity profiles of the three-dimensional nonuniform flow treated in Reference 8 will undoubtedly be required. These data could be generated from the two-dimensional theory of this report.

CONCLUSIONS AND RECOMMENDATIONS

On the basis of the work done and the results obtained, the following conclusions can be drawn relative to the aerodynamic properties of a Joukowski 17-percent-thick symmetric airfoil in the two-dimensional nonuniformly sheared flow considered in this program (uniform positive shear above the flow centerline; uniform negative shear below the flow centerline).

1. The addition of turbulence to the flow through the use of a screen to generate the sheared flow is not the source of the observed differences between stalling characteristics of airfoils in sheared and in unsheared flows.

2. The airfoil's stall behavior varies with vertical position of the airfoil in the flow. For airfoil positions above the flow centerline, (positive shear) stall is delayed; for the airfoil below the flow centerline (negative shear), stall is promoted.

3. The stall behavior is consistent with the experimentally observed variations in the adverse pressure gradients on the upper surface of the airfoil. Smaller adverse pressure gradients were observed for the airfoil positioned above the flow centerline than for the airfoil below the flow centerline.

4. Calculated pressure distributions based on an inviscid theory for an airfoil in a nonuniformly sheared flow were in good agreement with experimental pressure distributions, particularly with respect to the upper surface pressure gradients. It appears, therefore, that the experimentally observed behavior of airfoils near maximum lift in a

nonuniformly sheared flow can be attributed primarily to the effects of the inviscid pressure distribution on the upper surface boundary layer, as is the case for airfoils in uniform flows.

5. A marked degree of correlation of the data is obtained for differing vertical positions in the flow if section lift coefficients are referenced to the airfoil's stagnation streamline dynamic pressure, and angle of attack is measured from the zero-lift angle of attack. The two primary factors in determining the observed two-dimensional aerodynamic behavior of airfoils in nonuniformly sheared flows, then, appear to be the variation of stagnation streamline dynamic pressure with angle of attack for a given wing position in the sheared flow and the inviscid influence of the nonuniformly sheared flow in determining the pressure distribution on the airfoil upper surface. The former factor determines the apparent lift-curve slope well below stall,and the latter determines the stalling behavior. Both factors appear to depend on the overall distribution of shear in the flow,

6. For the particular nonuniformly sheared flow considered in this report, there was no evidence of unusual variations in maximum lift obtained as airfoil vertical position was varied in the vicinity of the flow centerline. (This is in contrast to the results reported in Reference 6 for a nonuniformly sheared flow with larger shear and unconstrained flow boundaries.)

On the basis of the results obtained, the following recommendations are made.

1. Supplemental airfoil pressure distribution data should be obtained experimentally for the particular two-dimensional, nonuniformly sheared flow in which the force and moment data of Reference 6 were obtained. Of special interest is whether correlation of $(c_L)_s$ versus $\bar{\alpha}$ with h similar to that for the data presented in this report is obtained.

2. The computer program as it is now constituted (constrained nonuniformly sheared flow of Figure 1(b)) should be used for calculations of airfoil pressure distributions for additional values of angle of attack and vertical position of the airfoil in the flow. The calculations should also be extended to higher values of the shear parameter K than those considered thus far.

3. The theory and computer program should be extended to the particular two-dimensional, nonuniformly sheared flow for which the data of Reference 6 were obtained. Calculations of airfoil pressure distributions should then be made for a range of airfoil vertical positions in the flow, and for a range of angles of attack.

It should be possible, from the results of these calculations, and from those of (2) above, to determine the mechanism responsible for the maximum lift behavior reported in Reference 6.

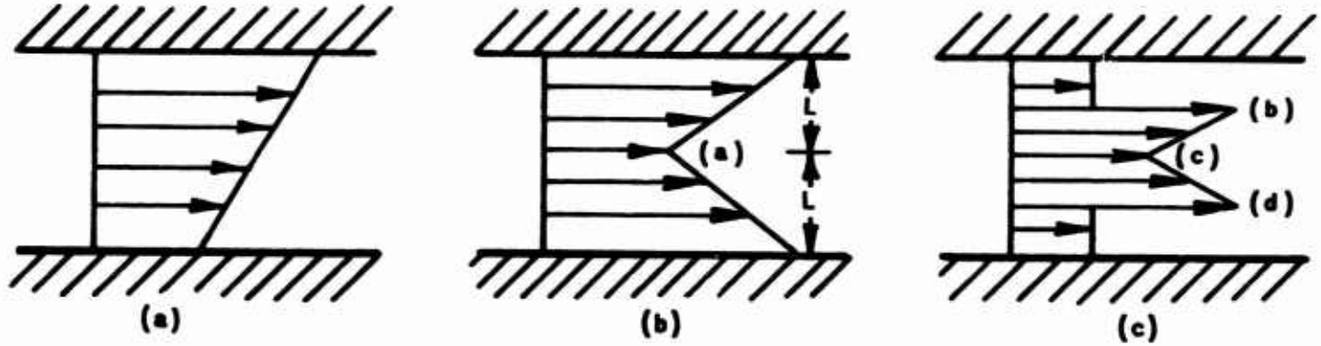

Figure 1. EXAMPLES OF FREE-STREAM VELOCITY PROFILES REPRESENTED BY PIECEWISE LINEAR SEGMENTS.

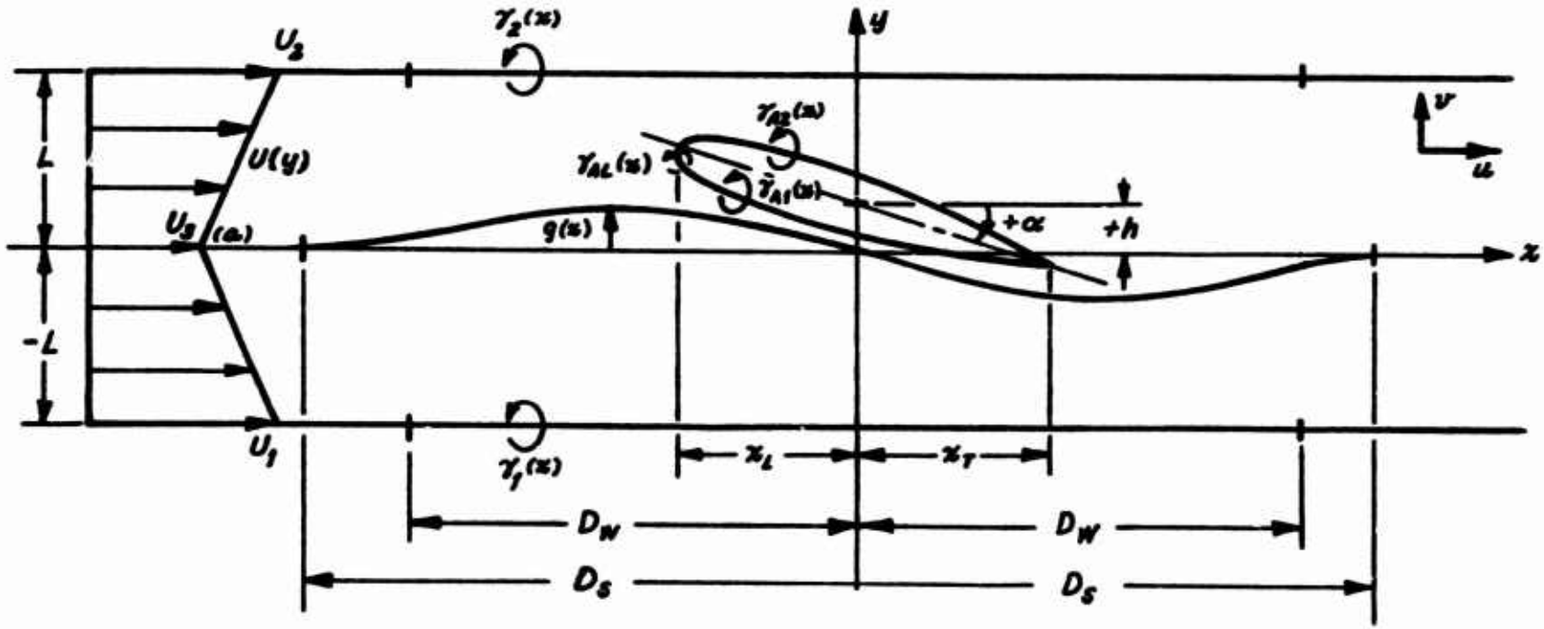

Figure 2. SCHEMATIC OF FLOW MODEL FOR IBM COMPUTER PROGRAM.

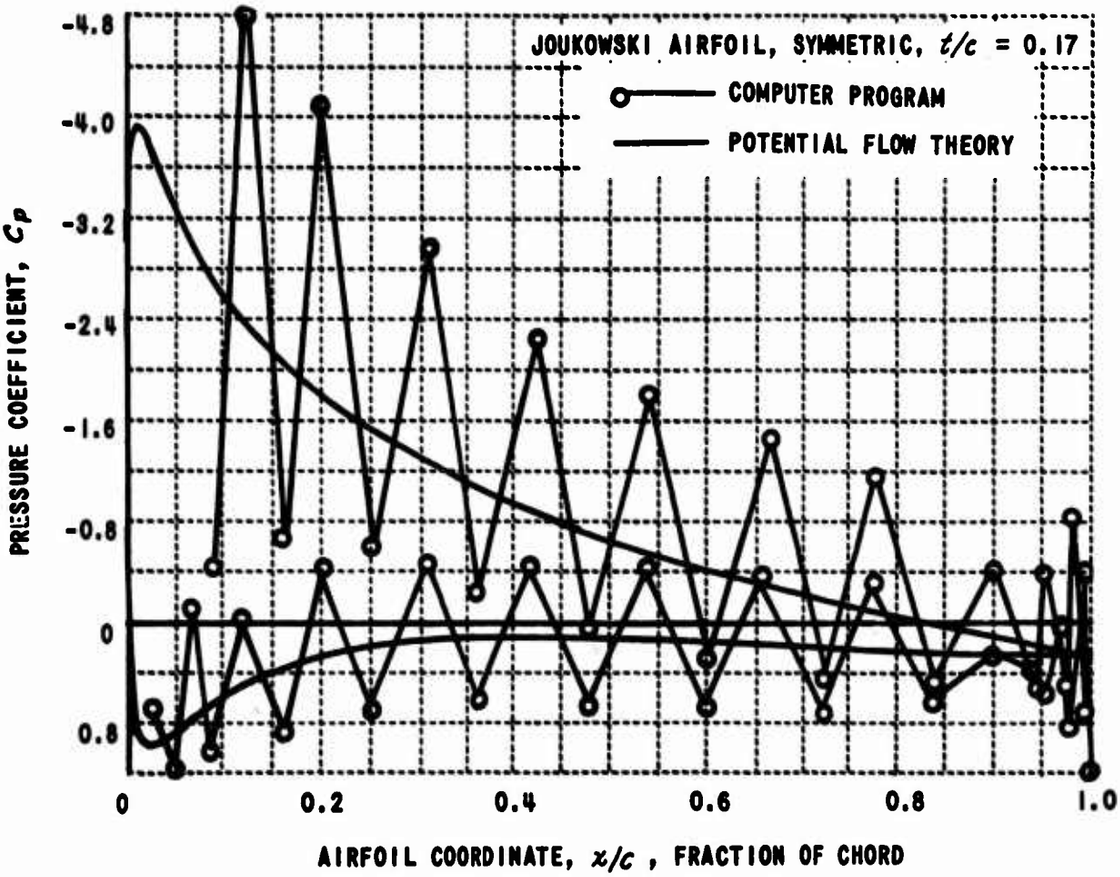

Figure 3. PRESSURE COEFFICIENT, C_p, VERSUS FRACTION OF CHORD, x/c, FOR UNIFORM FLOW FROM POTENTIAL FLOW THEORY, AND FROM COMPUTER PROGRAM WITHOUT SMOOTHING; α = 10.0 DEGREES.

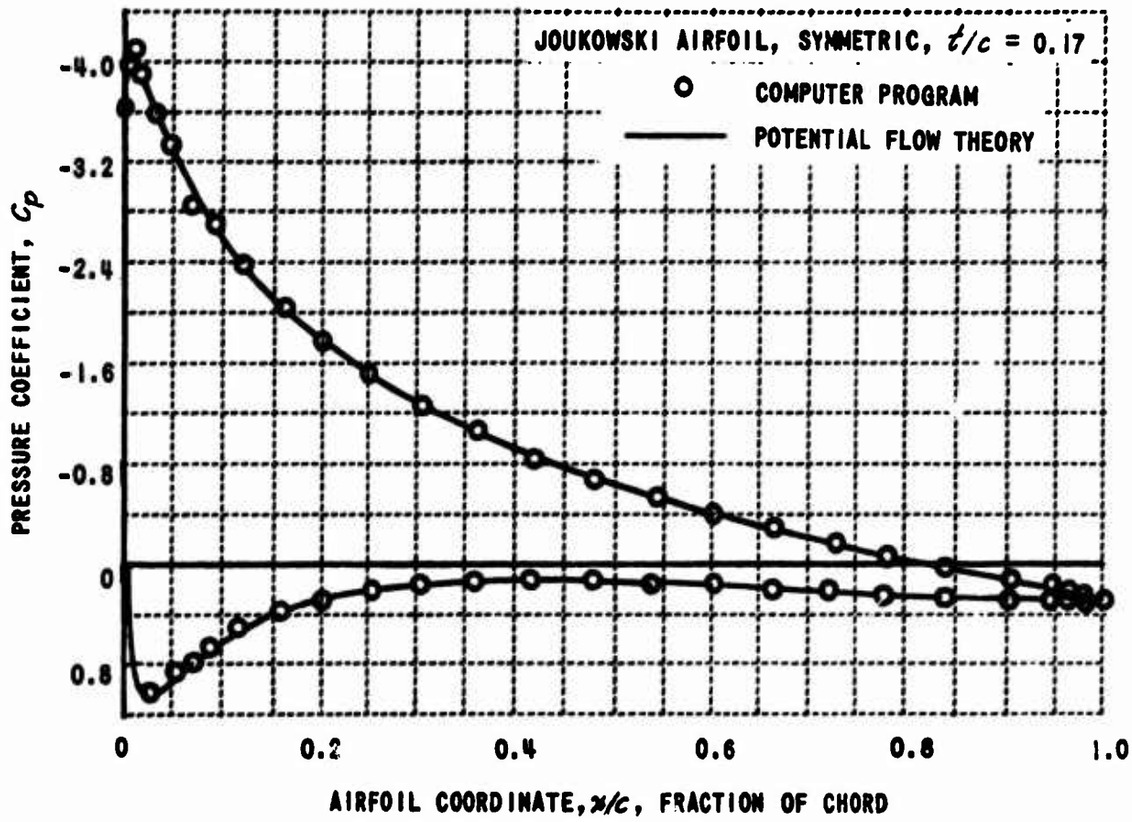

Figure 4. PRESSURE COEFFICIENT, C_p, VERSUS FRACTION OF CHORD, x/c, FOR UNIFORM FLOW FROM POTENTIAL FLOW THEORY, AND FROM COMPUTER PROGRAM WITH SMOOTHING ($\bar{R}$ = 0.10); α = 10.0 DEGREES.

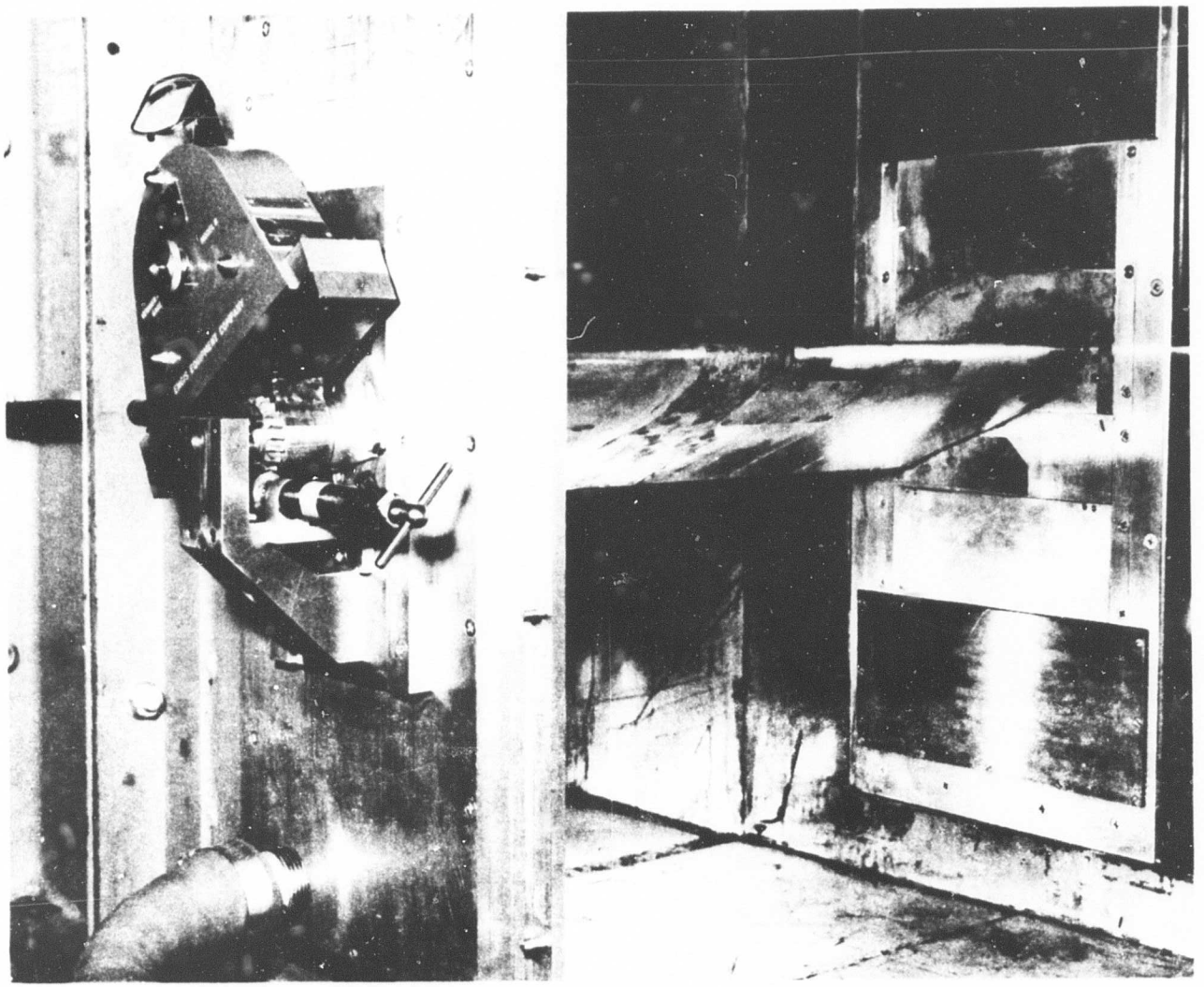

Figure 5. VIEW OF AIRFOIL MODEL INSTALLED IN WIND-TUNNEL TEST SECTION.

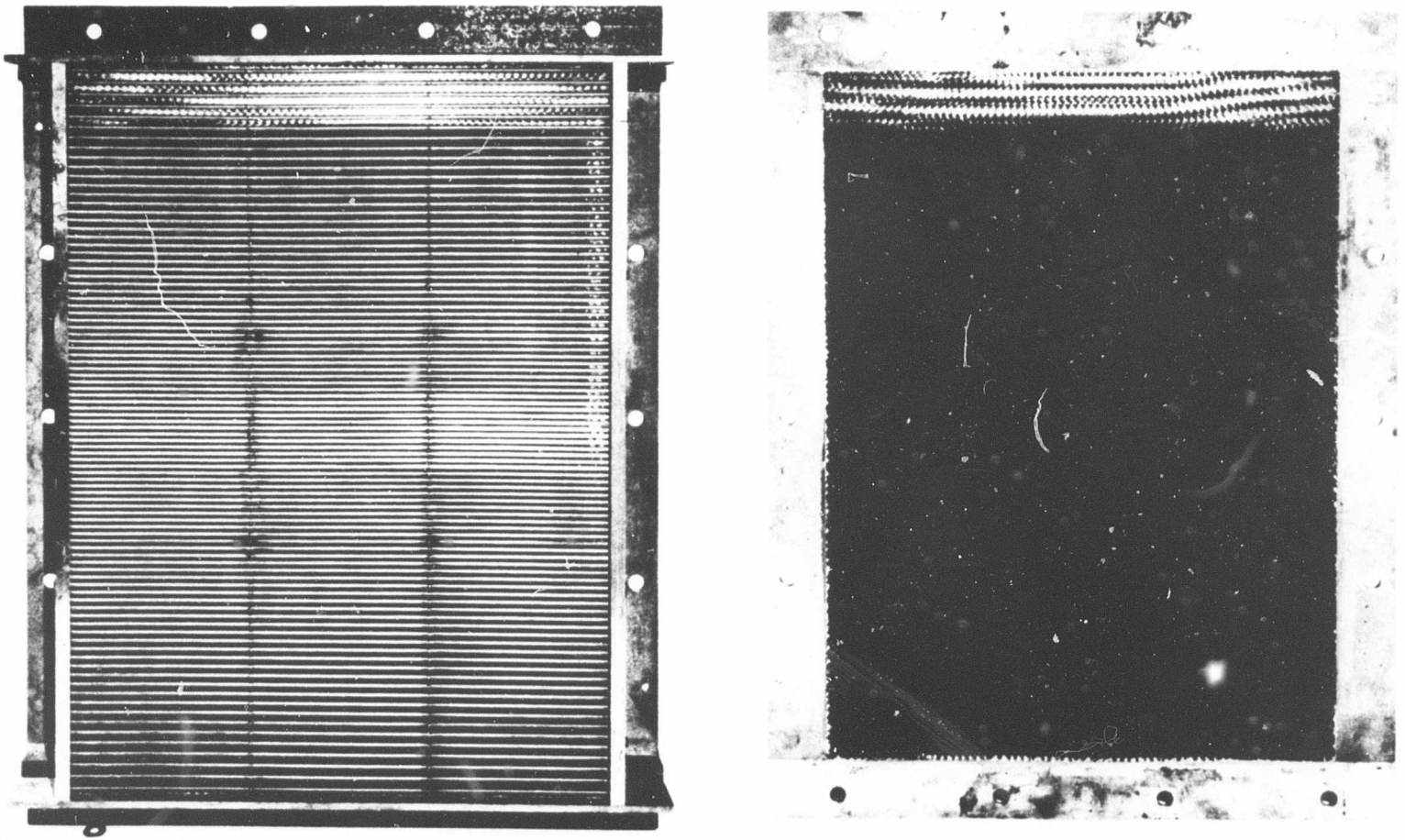

(a) LOOKING DOWNSTREAM

(b) LOOKING UPSTREAM

Figure 6. SHEAR SCREEN ASSEMBLY.

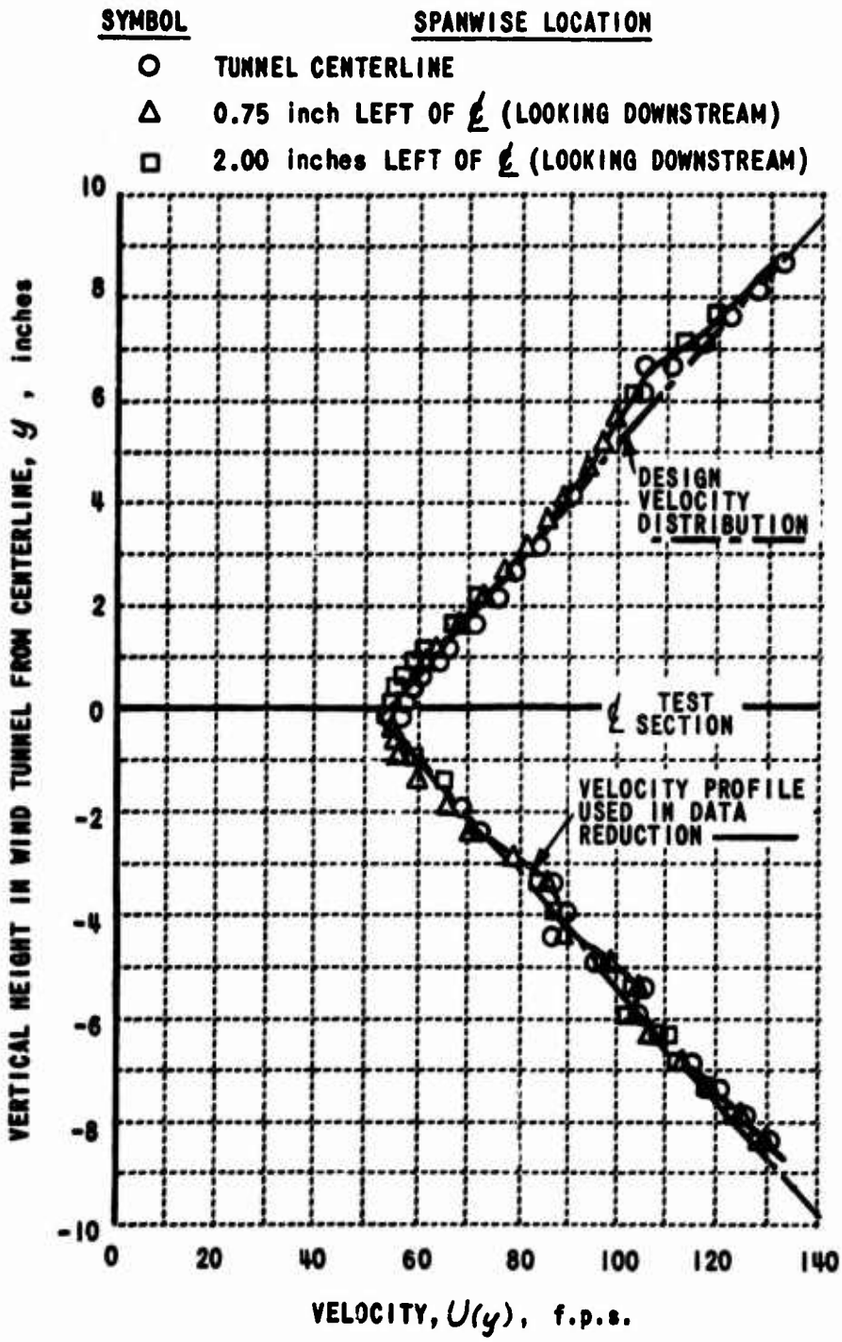

Figure 7. MEASURED FREE-STREAM VELOCITY DISTRIBUTION IN NONUNIFORMLY SHEARED FLOW AT MODEL MIDCHORD STATION.

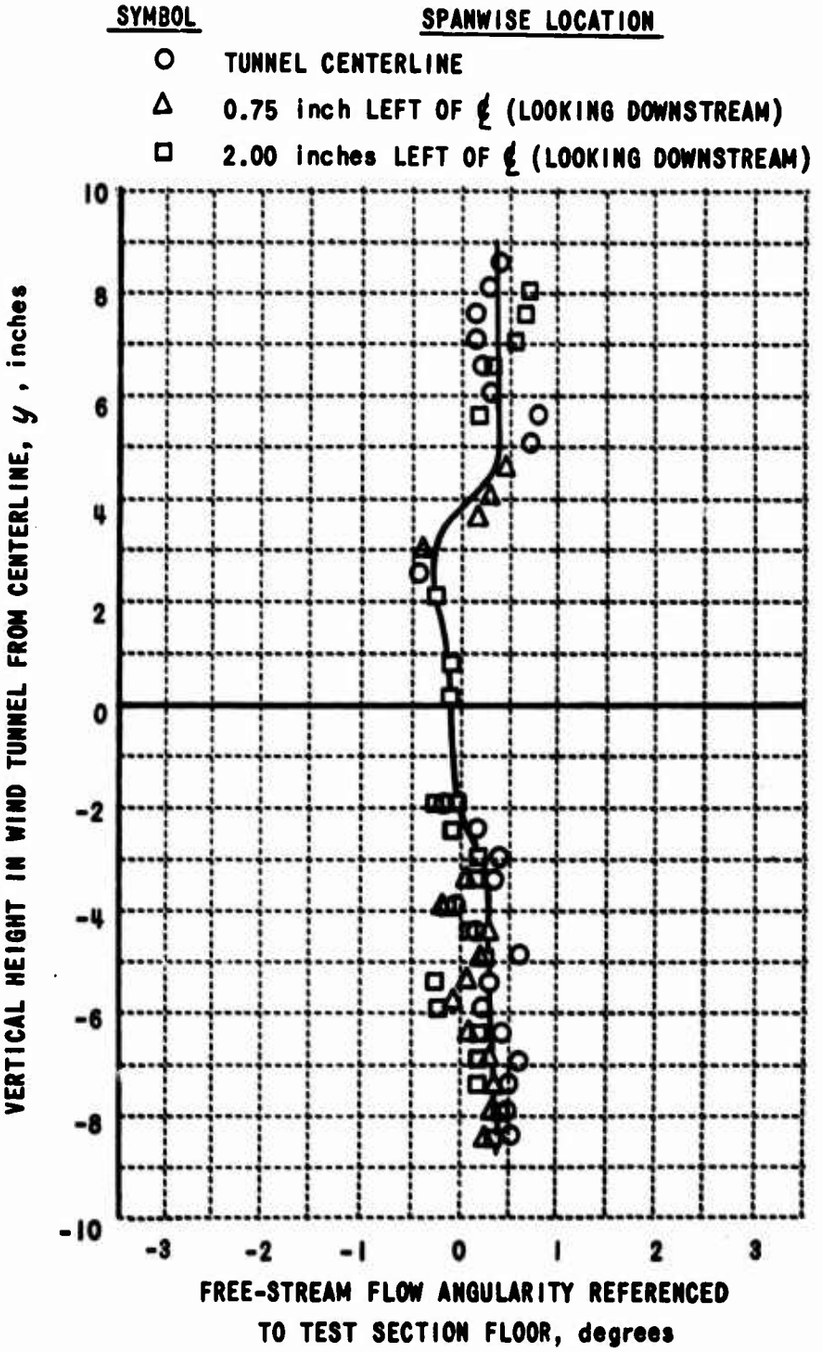

Figure 8. MEASURED FREE-STREAM FLOW ANGULARITY IN NONUNIFORMLY SHEARED FLOW AT MODEL MIDCHORD STATION.

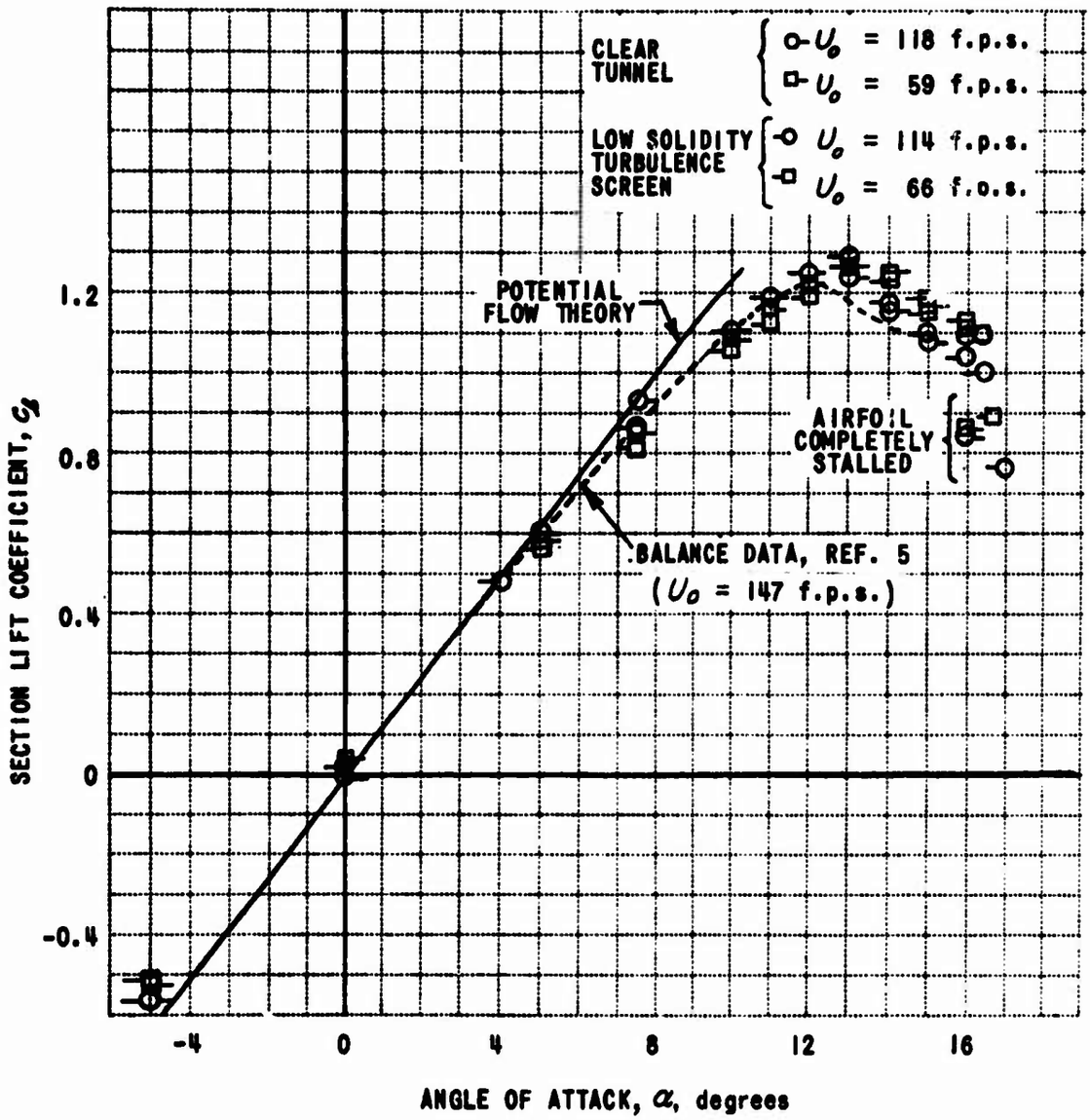

Figure 9. SECTION LIFT COEFFICIENT, c_l , VERSUS ANGLE OF ATTACK, α, FOR UNIFORM FLOW.

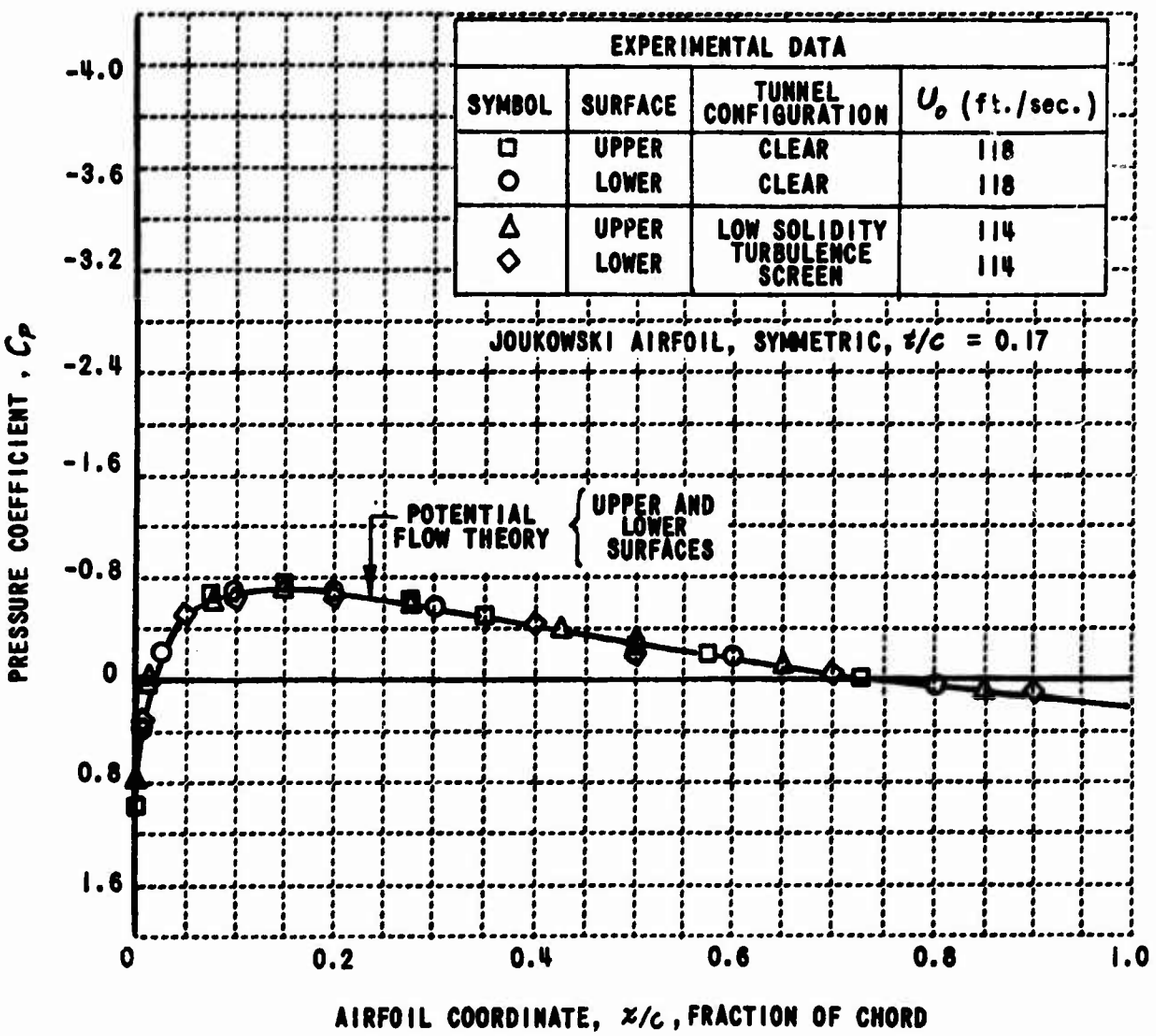

Figure 10. PRESSURE COEFFICIENT, C_p, VERSUS FRACTION OF CHORD, x/c, UNIFORM FLOW, α = 0 DEGREES.

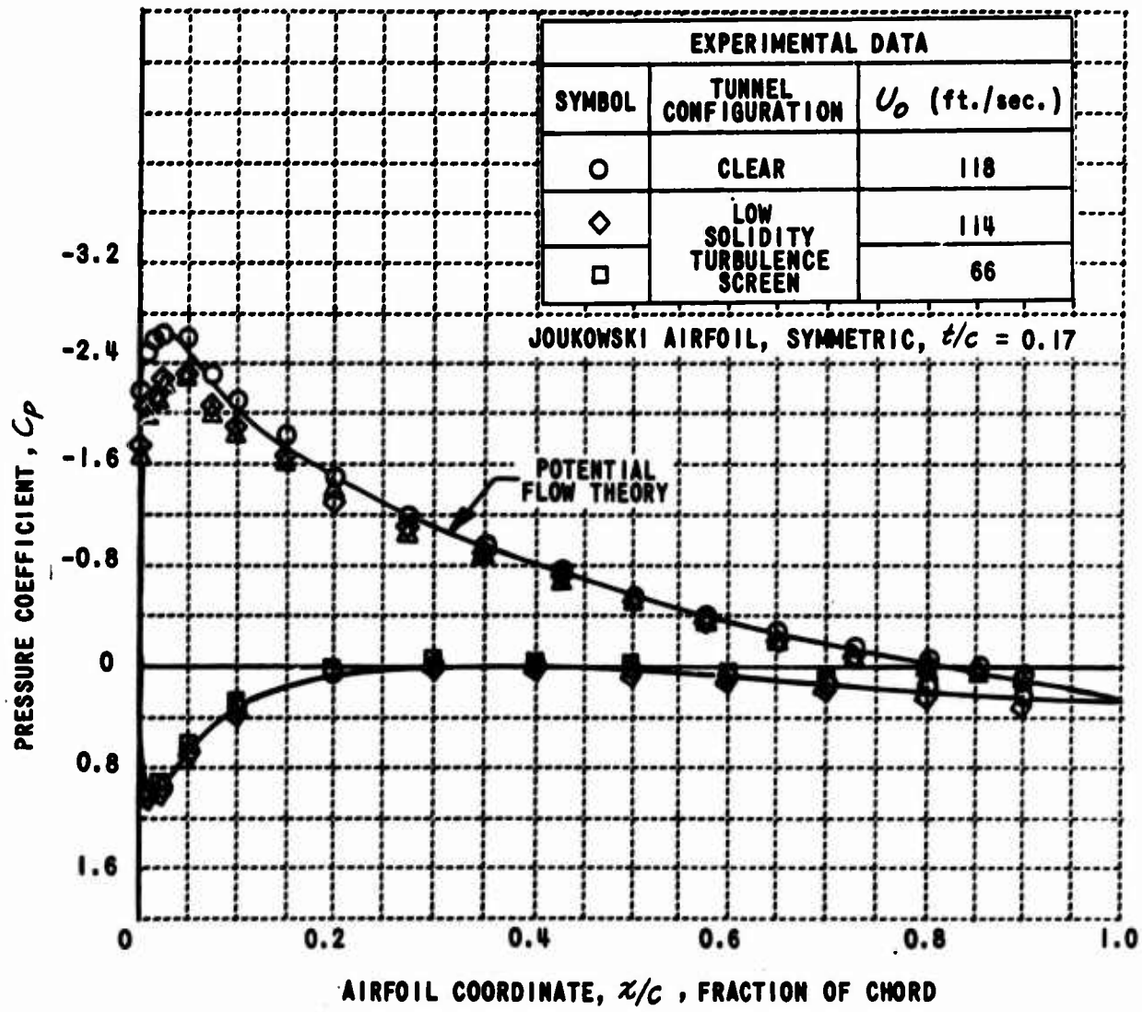

Figure 11. PRESSURE COEFFICIENT, C_p , VERSUS FRACTION OF CHORD, x/c, UNIFORM FLOW, α = 7.5 DEGREES.

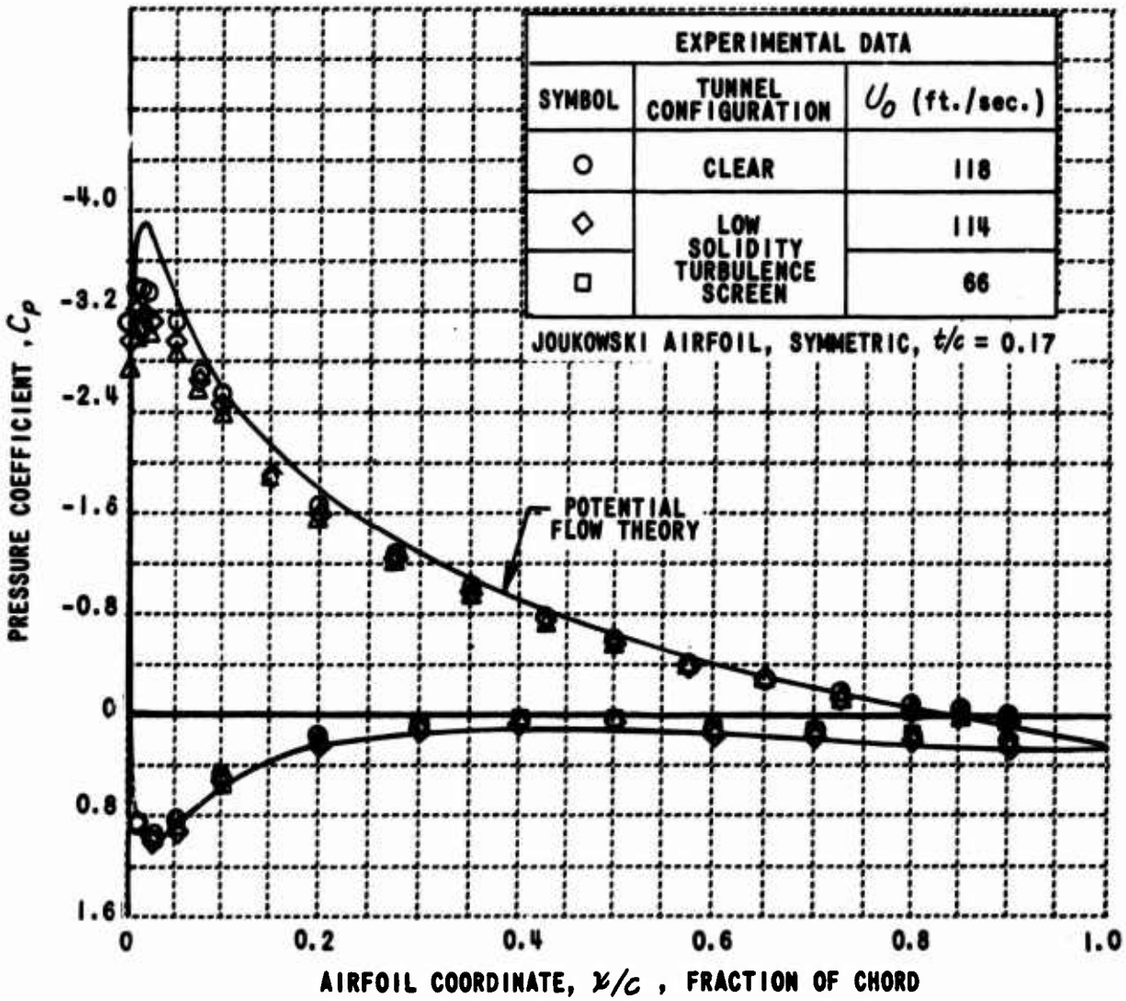

Figure 12. PRESSURE COEFFICIENT, C_p, VERSUS FRACTION OF CHORD, x/c, UNIFORM FLOW, α = 10.0 DEGREES.

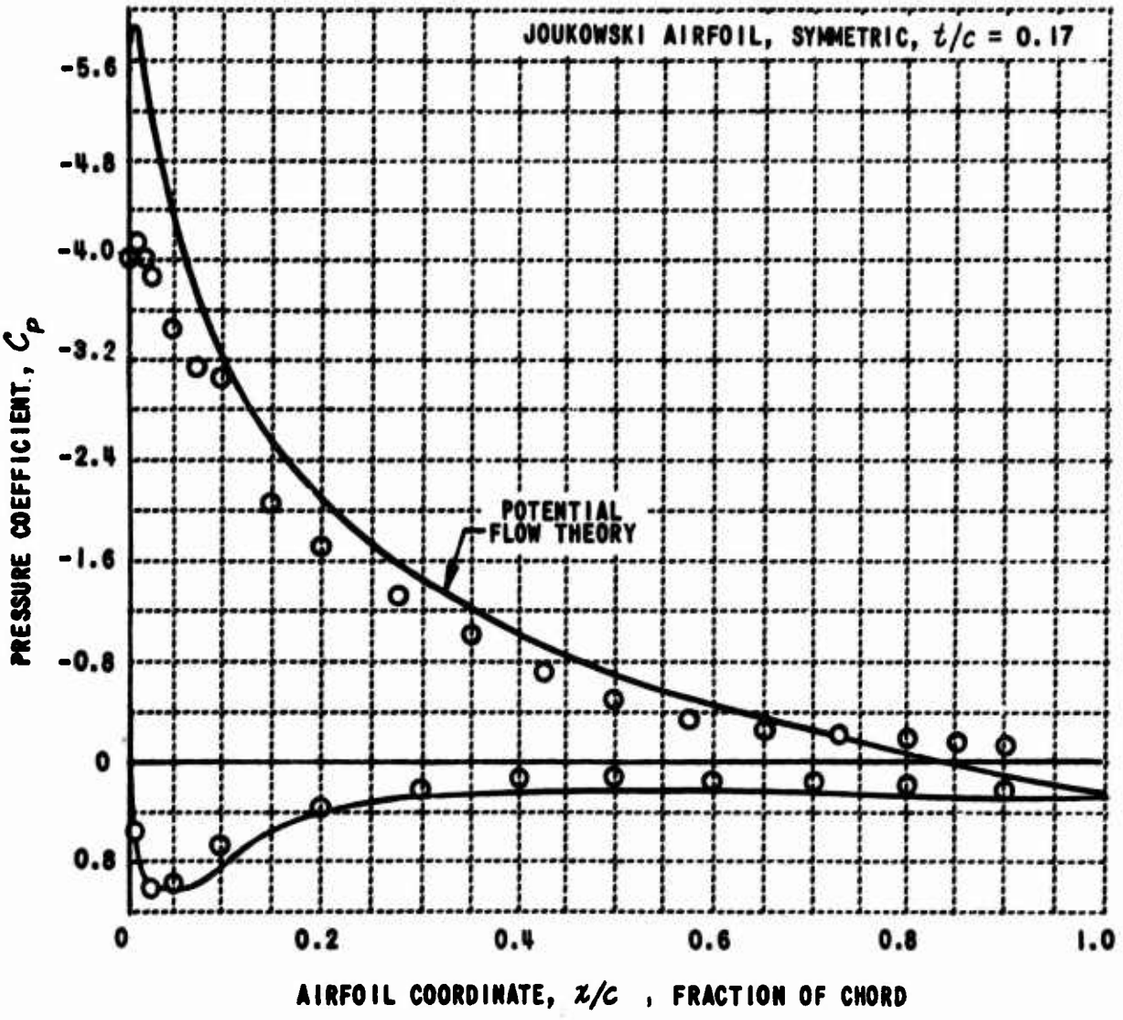

Figure 13. PRESSURE COEFFICIENT, C_p, VERSUS FRACTION OF CHORD, x/c, UNIFORM FLOW, LOW SOLIDITY TURBULENCE SCREEN, α = 13.0 DEGREES, U_o = 66 FT./SEC.

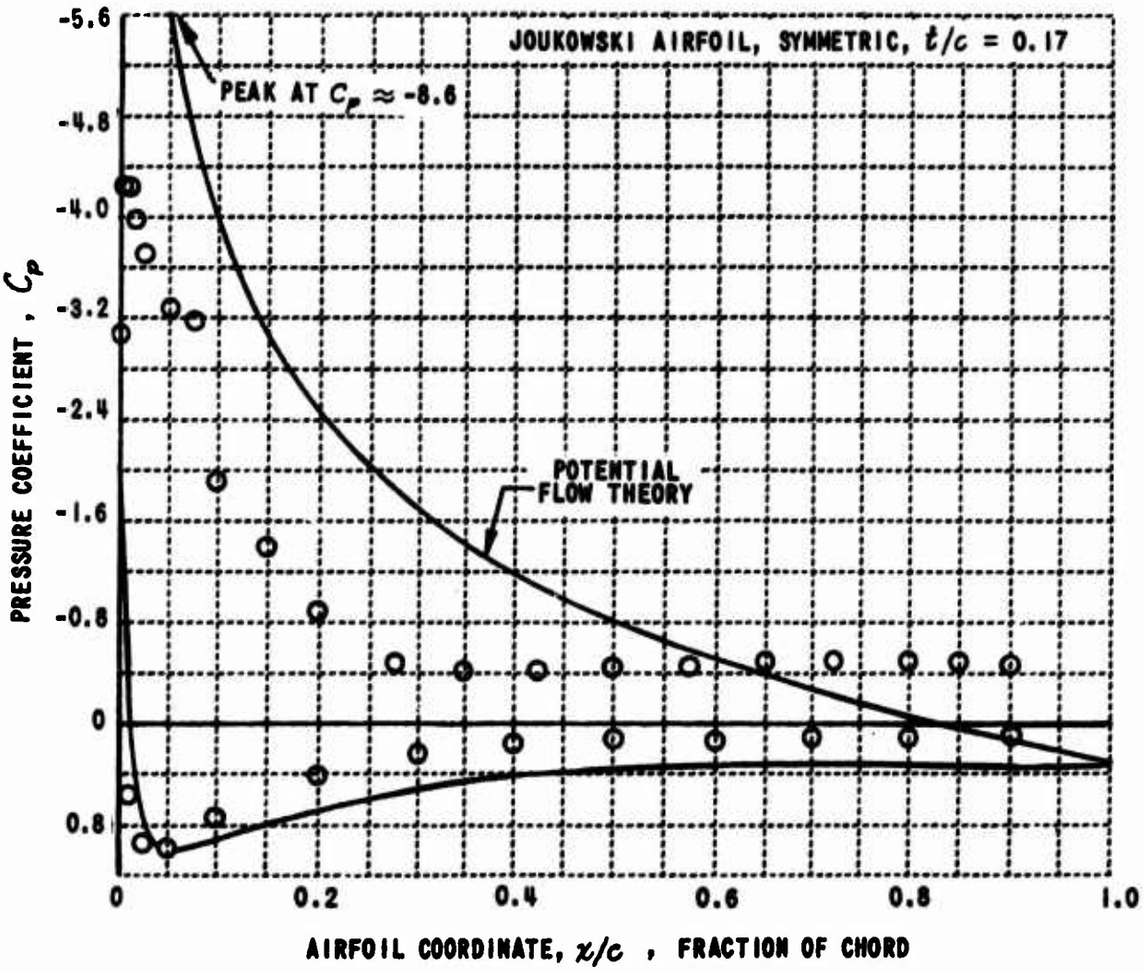

Figure 14. PRESSURE COEFFICIENT, C_p, VERSUS FRACTION OF CHORD, x/c, UNIFORM FLOW, LOW SOLIDITY TURBULENCE SCREEN, α = 16.5 DEGREES, U_o = 66 FT./SEC.

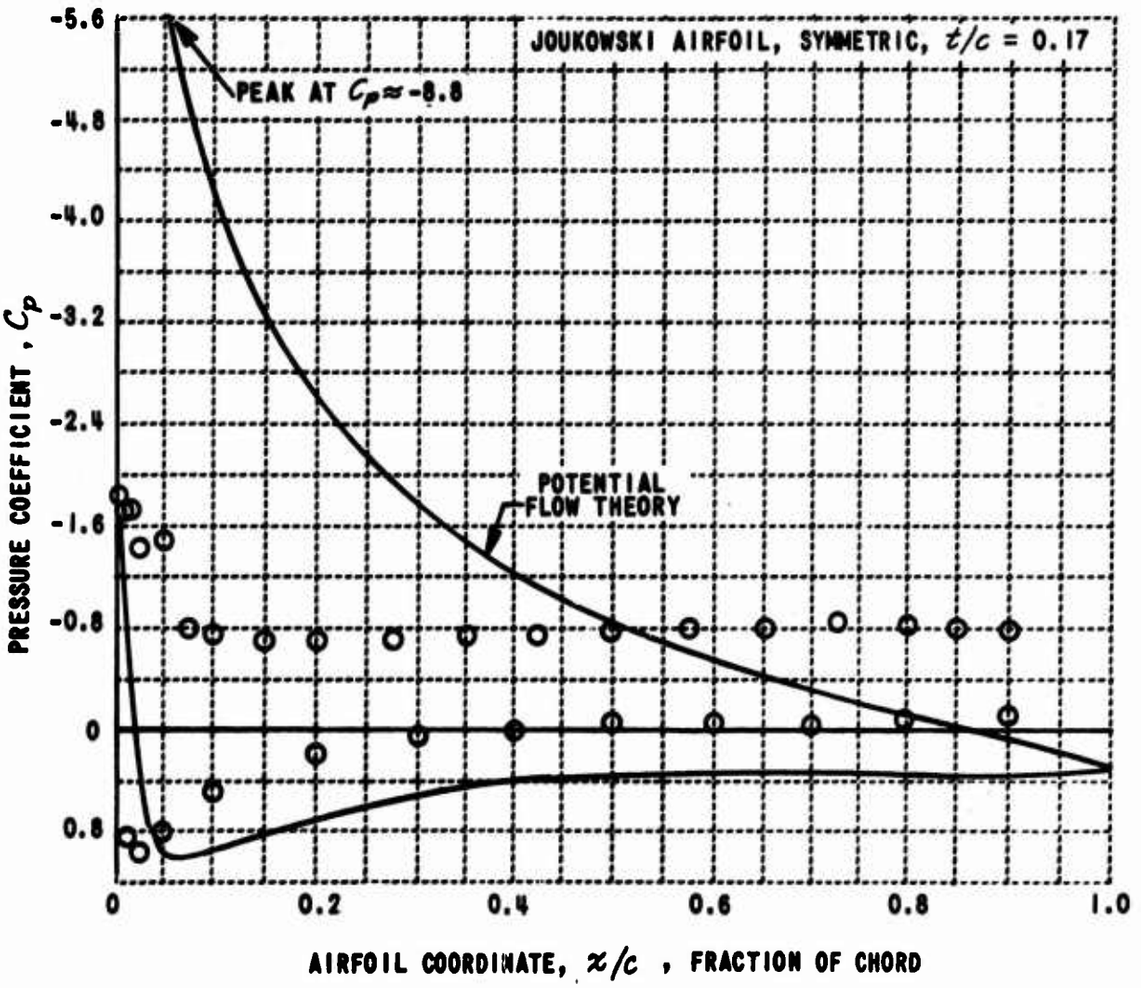

Figure 15. PRESSURE COEFFICIENT, C_p, VERSUS FRACTION OF CHORD, x/c, UNIFORM FLOW, LOW SOLIDITY TURBULENCE SCREEN, α = 16.7 DEGREES, U_o = 66 FT./SEC.

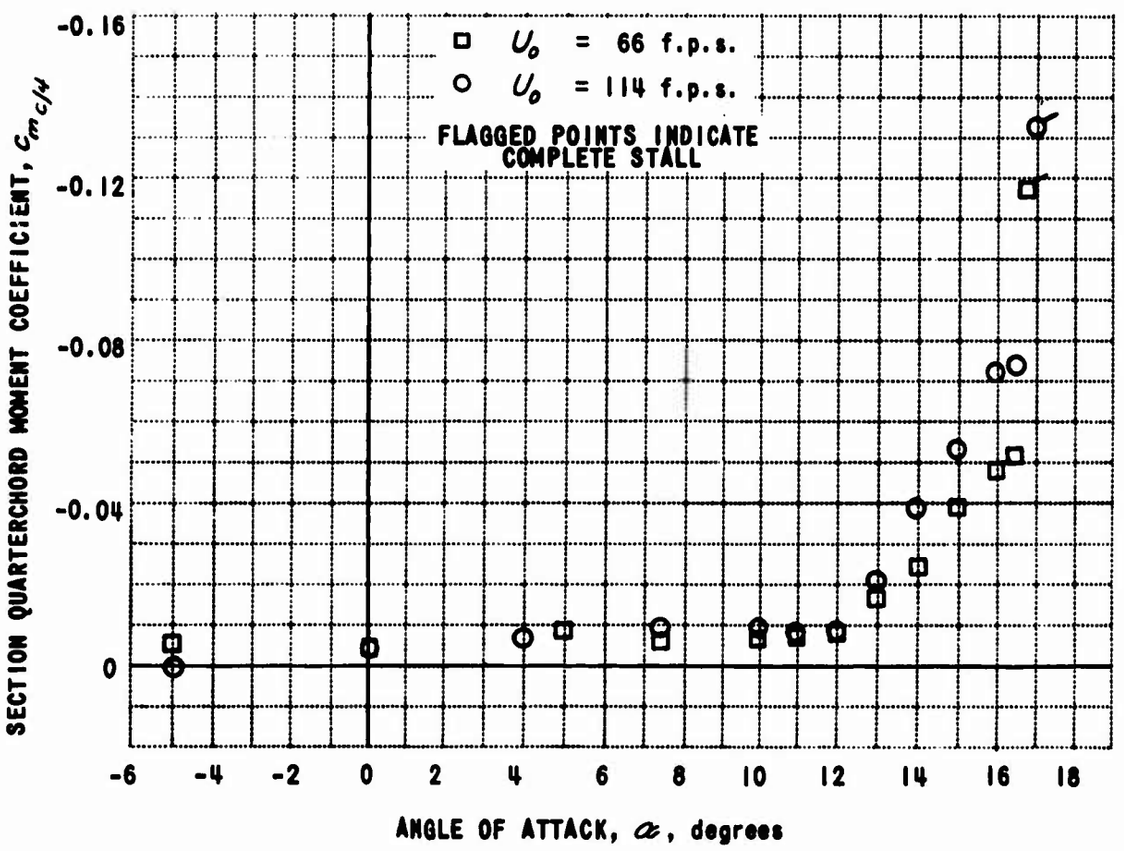

Figure 16. SECTION QUARTERCHORD MOMENT COEFFICIENT, $c_{m_{c/4}}$, VERSUS ANGLE OF ATTACK, α, IN UNIFORM FLOW WITH LOW SOLIDITY TURBULENCE SCREEN.

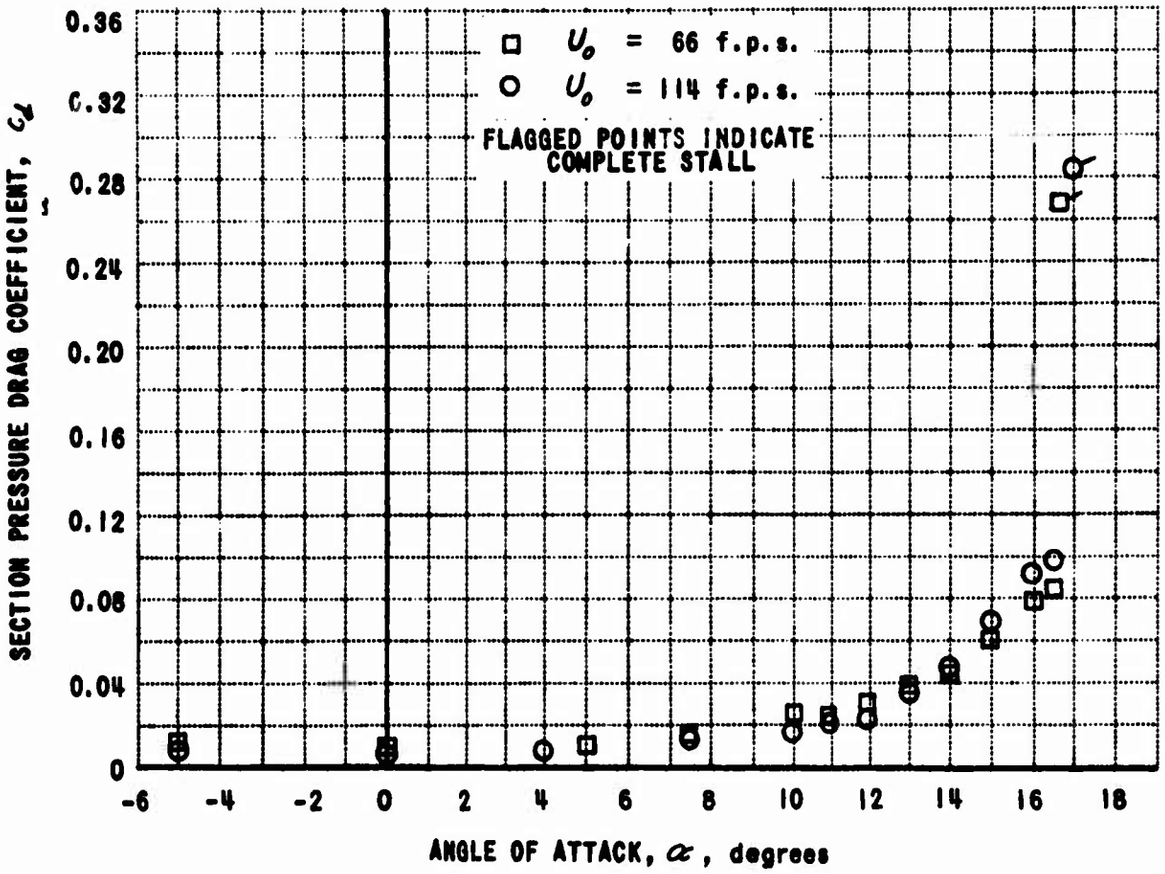

Figure 17. SECTION PRESSURE DRAG COEFFICIENT, c_d, VERSUS ANGLE OF ATTACK, α, IN UNIFORM FLOW WITH LOW SOLIDITY TURBULENCE SCREEN.

EXPERIMENTAL DATA
SYMBOL
h(inches)
+3
1.0
0.9
0.8
0.7
0.6
0.5
0.4
0.3
0.2
0.1
0
-0.1
COEFFICIENT REFERENCED TO DYNAMIC PRESSURE CORRESPONDING TO AVERAGE VELOCITY, $\bar{c}_p$

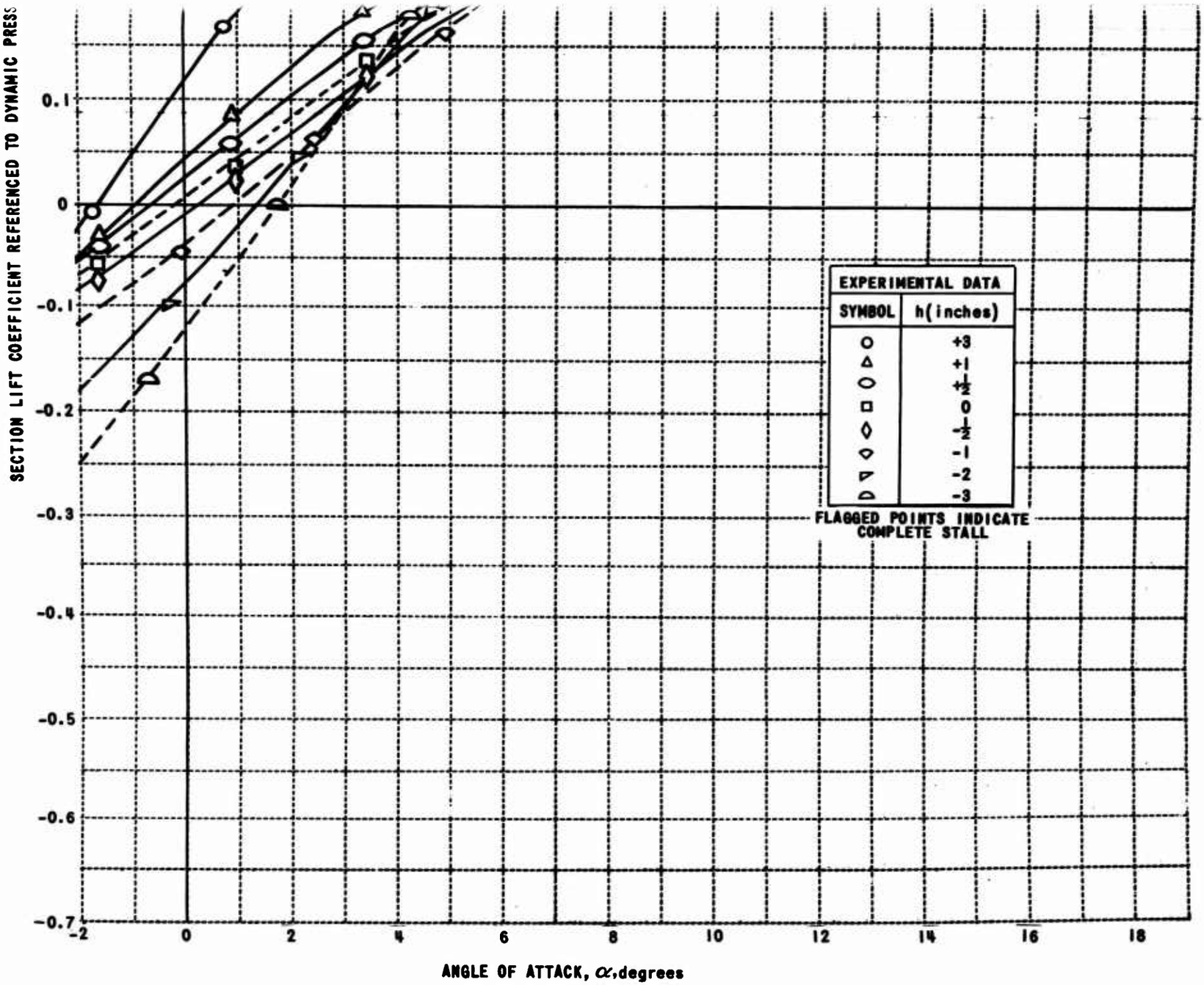

Figure 18. NONDIMENSIONAL SECTION LIFT, $\bar{c}_\ell$, VERSUS ANGLE OF ATTACK, α, NONUNIFORMLY SHEARED FLOW.

2.2
2.0
1.8
1.6
1.4
1.2
1.0
0.8
0.6
0.4
NCED TO MIDCHORD FREE-STREAM DYNAMIC PRESSURE, $(c_d)_R$

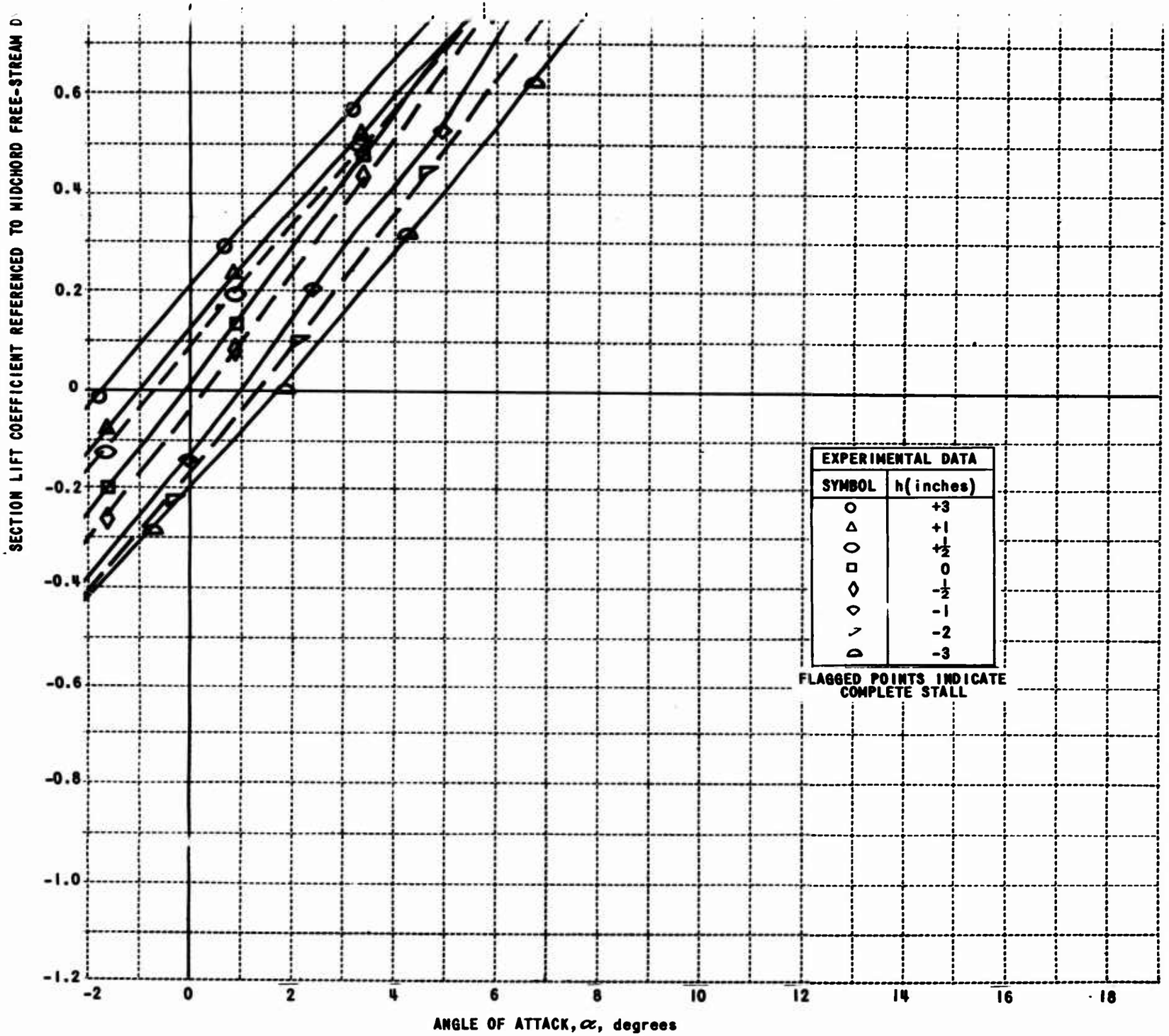

Figure 19. SECTION LIFT COEFFICIENT REFERENCED TO MIDCHORD FREE-STREAM DYNAMIC PRESSURE, $(c_\ell)_R$, VERSUS ANGLE OF ATTACK, α, NONUNIFORMLY SHEARED FLOW.

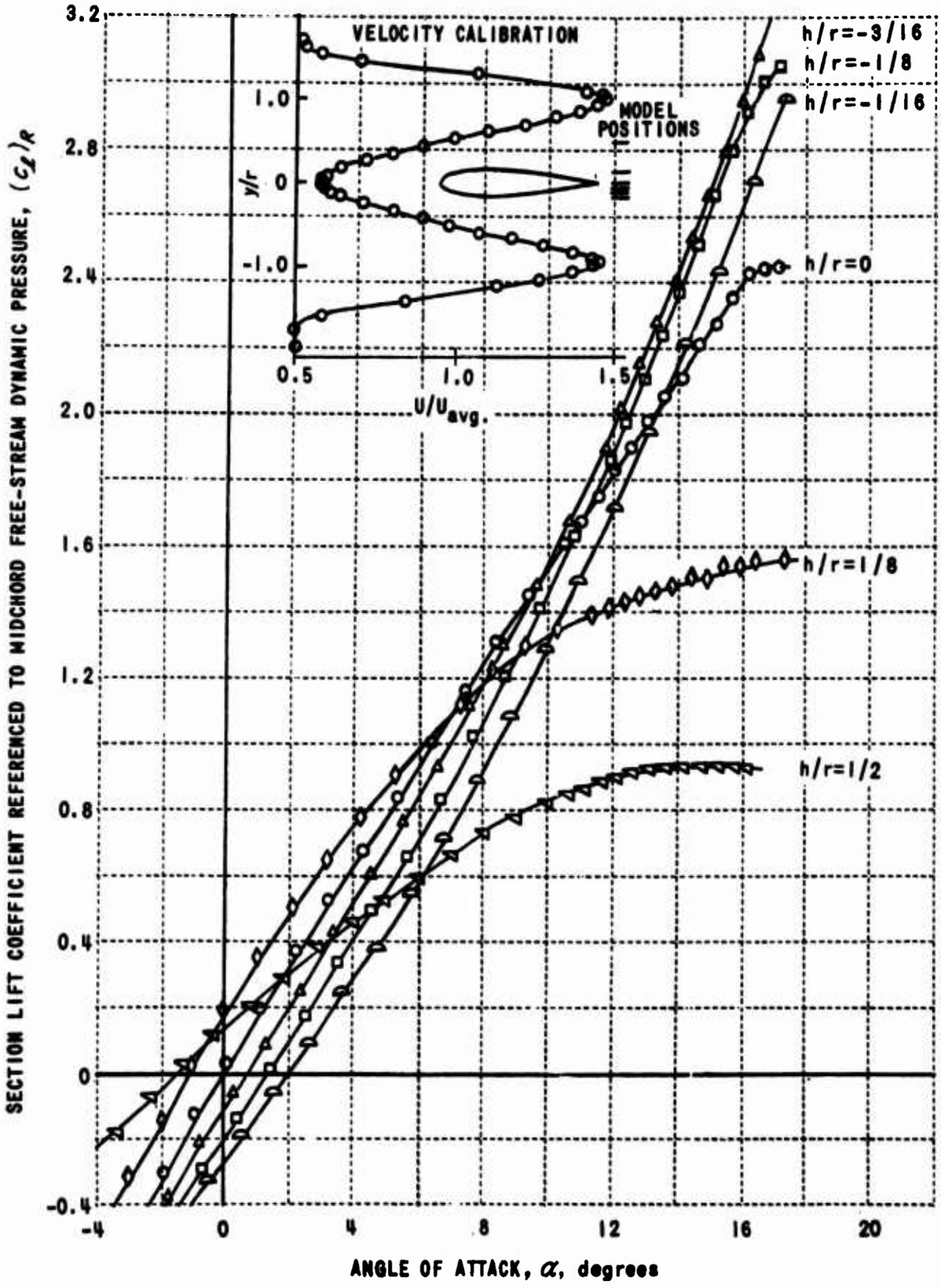

Figure 20. SECTION LIFT COEFFICIENT REFERENCED TO MIDCHORD FREE-STREAM DYNAMIC PRESSURE, $(c_\ell)_R$, VERSUS ANGLE OF ATTACK, α, NONUNIFORMLY SHEARED FLOW (REFERENCE 6).

ICIENT REFERENCED TO MIDCHORD FREE-STREAM DYNAMIC PRESSURE, $(c_\ell)_R$

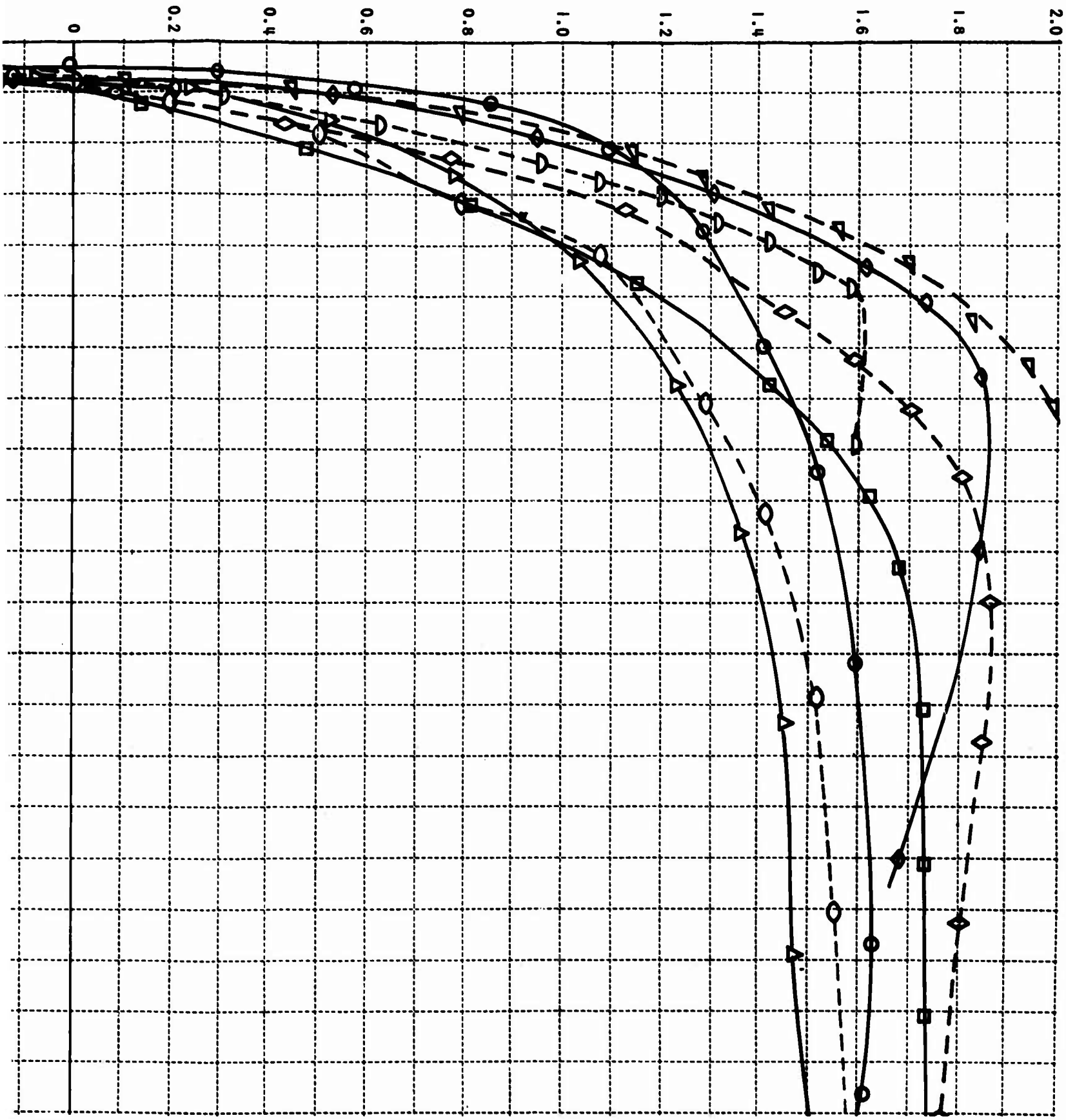

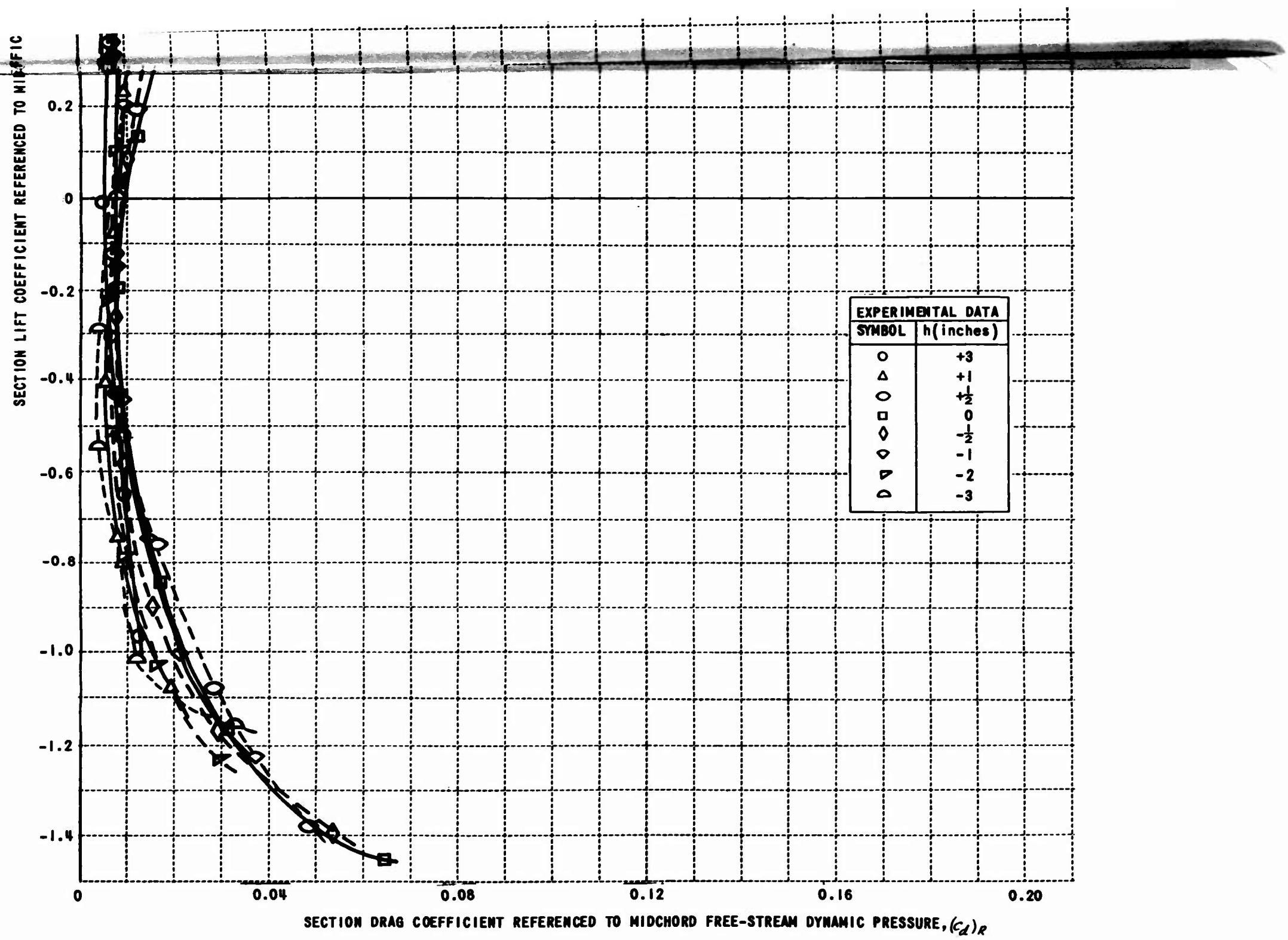

Figure 21. SECTION LIFT COEFFICIENT, $(c_\ell)_R$, VERSUS SECTION PRESSURE DRAG COEFFICIENT, $(c_d)_R$, NONUNIFORMLY SHEARED FLOW.

EXPERIMENTAL DATA
SYMBOL
h(inches)
+3
+1
+½
0
-½
-1
-2
-3
-0.16
-0.15
-0.14
-0.13
-0.12
-0.11
-0.10
-0.09
-0.08
-0.07
-0.06
EFFICIENT REFERENCED TO MIDCHORD FREE-STREAM DYNAMIC PRESSURE, $(C_{m_{c/4}})_R$

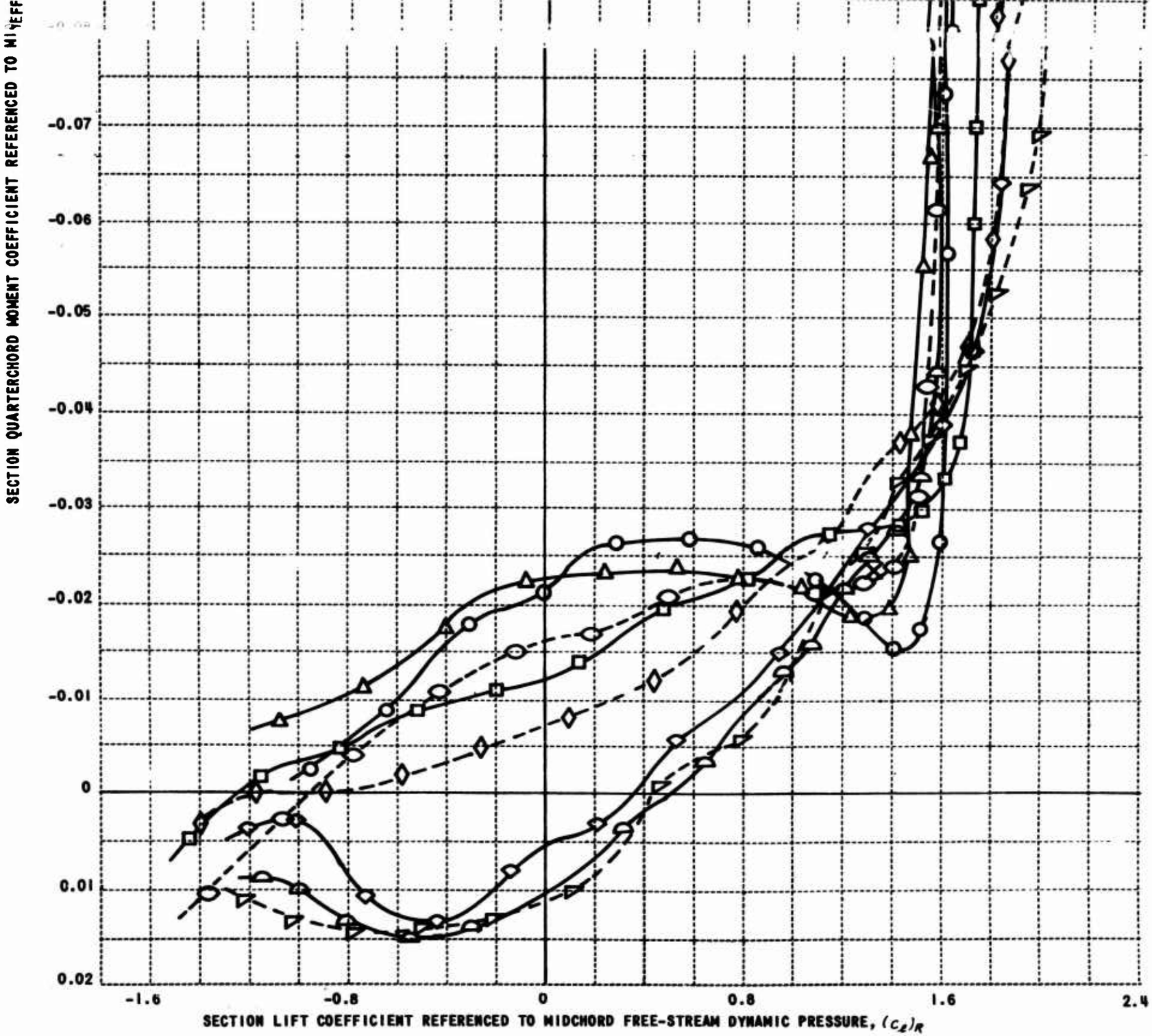

Figure 22. SECTION QUARTERCHORD MOMENT COEFFICIENT, $(c_{m_{c/4}})_R$, VERSUS SECTION LIFT COEFFICIENT, $(c_\ell)_R$, NONUNIFORMLY SHEARED FLOW.

BLANK PAGE

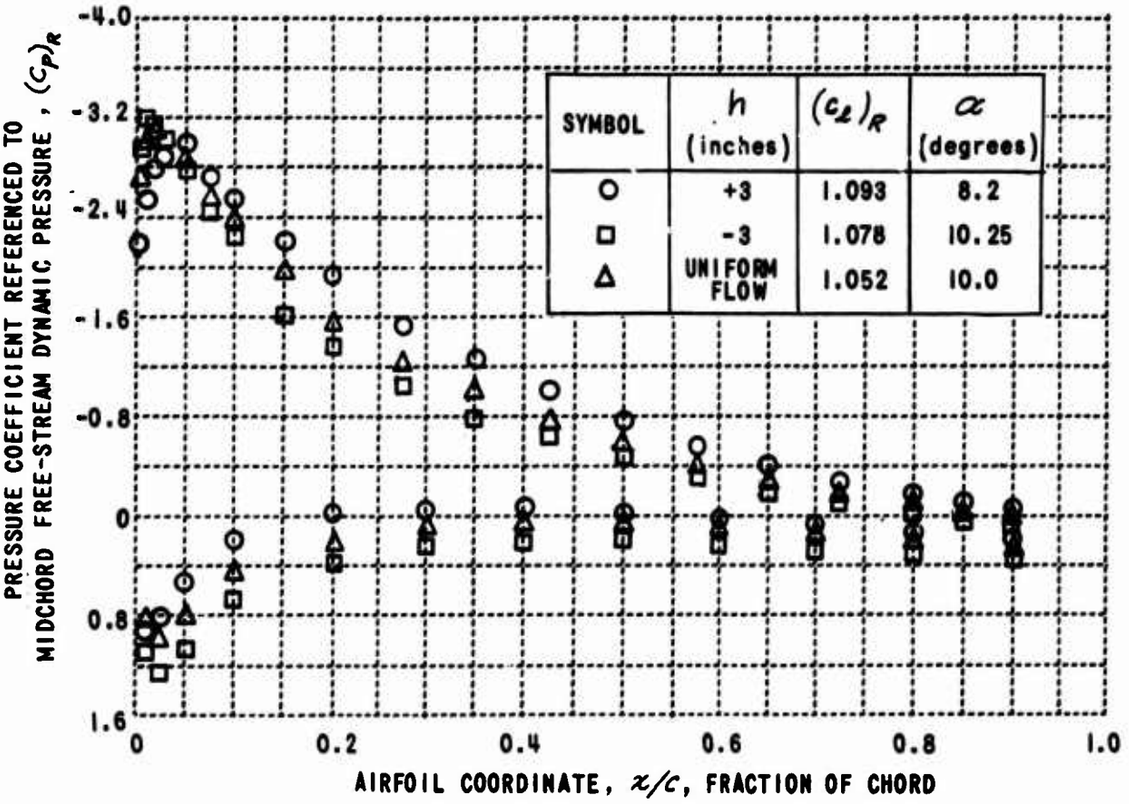

Figure 23. PRESSURE COEFFICIENT REFERENCED TO MIDCHORD FREE-STREAM DYNAMIC PRESSURE, $(C_p)_R$, VERSUS FRACTION OF CHORD, x/c, FOR UNIFORM FLOW AND NONUNIFORMLY SHEARED FLOW.

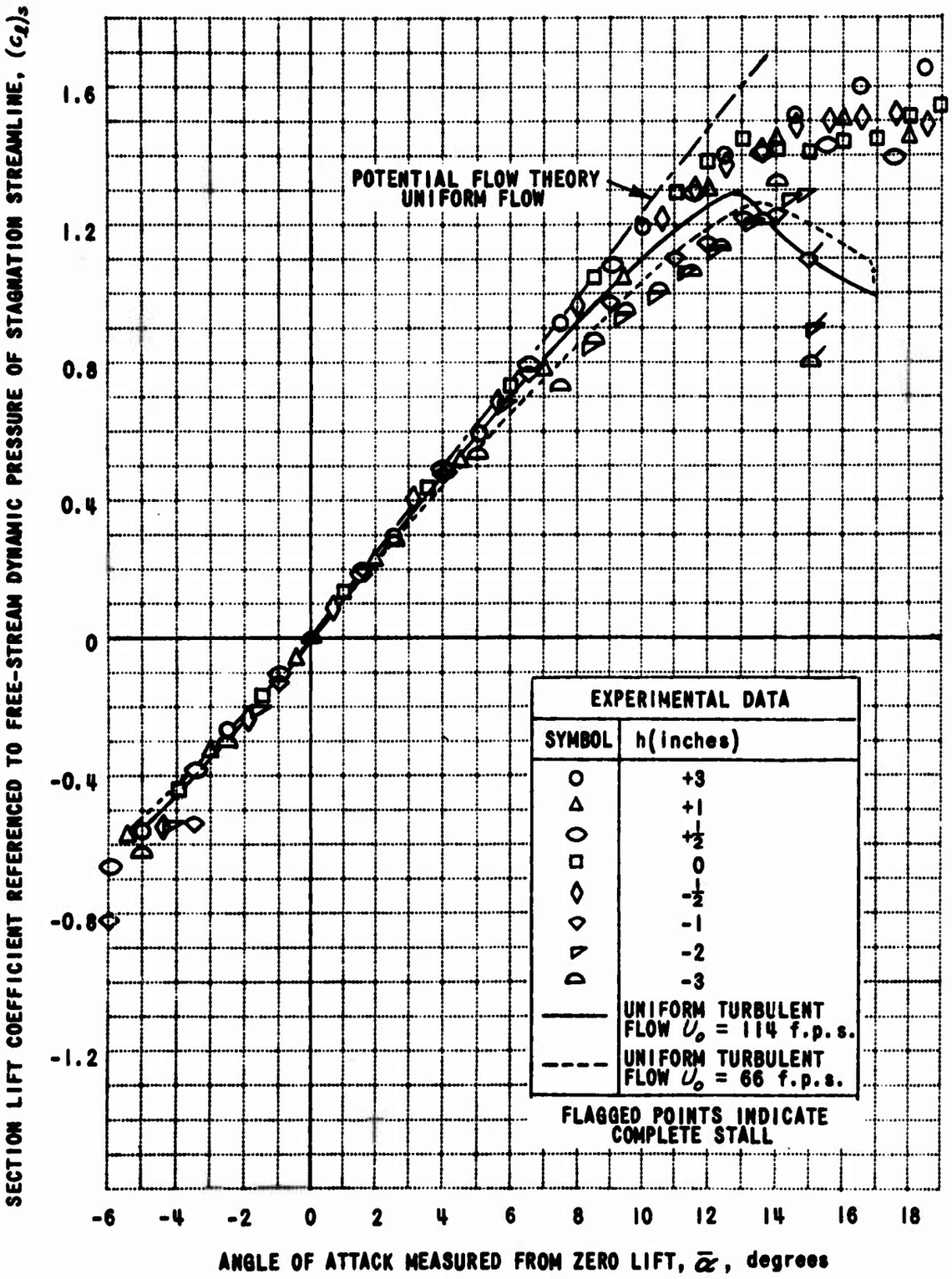

Figure 24(a). SECTION LIFT COEFFICIENT REFERENCED TO FREE-STREAM DYNAMIC PRESSURE OF STAGNATION STREAMLINE, $(c_\ell)_s$, VERSUS ANGLE OF ATTACK MEASURED FROM ZERO LIFT, $\bar{\alpha}$, NONUNIFORMLY SHEARED FLOW.

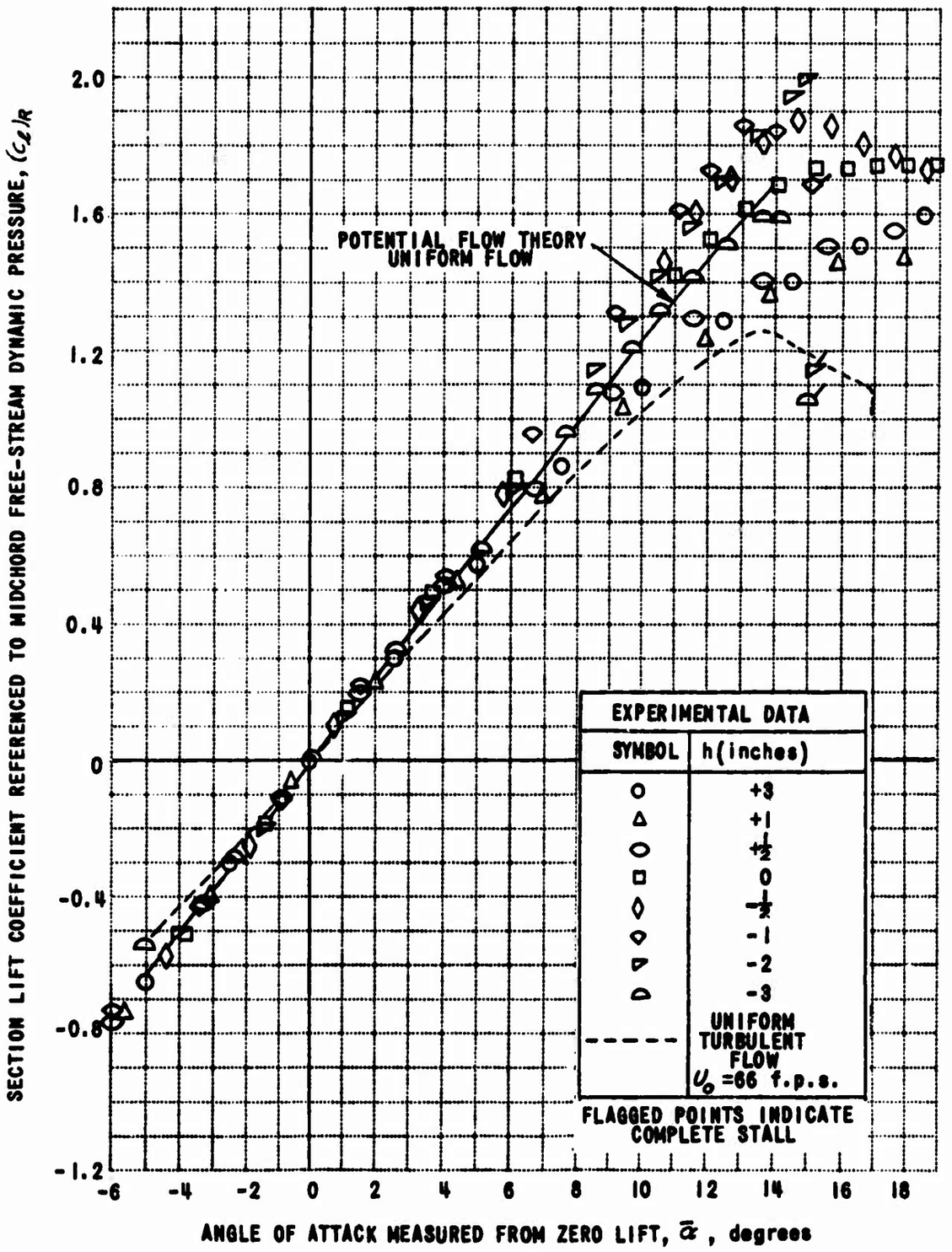

Figure 24(b). SECTION LIFT COEFFICIENT REFERENCED TO MIDCHORD FREE-STREAM DYNAMIC PRESSURE, $(c_\ell)_R$, VERSUS ANGLE OF ATTACK MEASURED FROM ZERO LIFT, $\bar{\alpha}$, NONUNIFORMLY SHEARED FLOW.

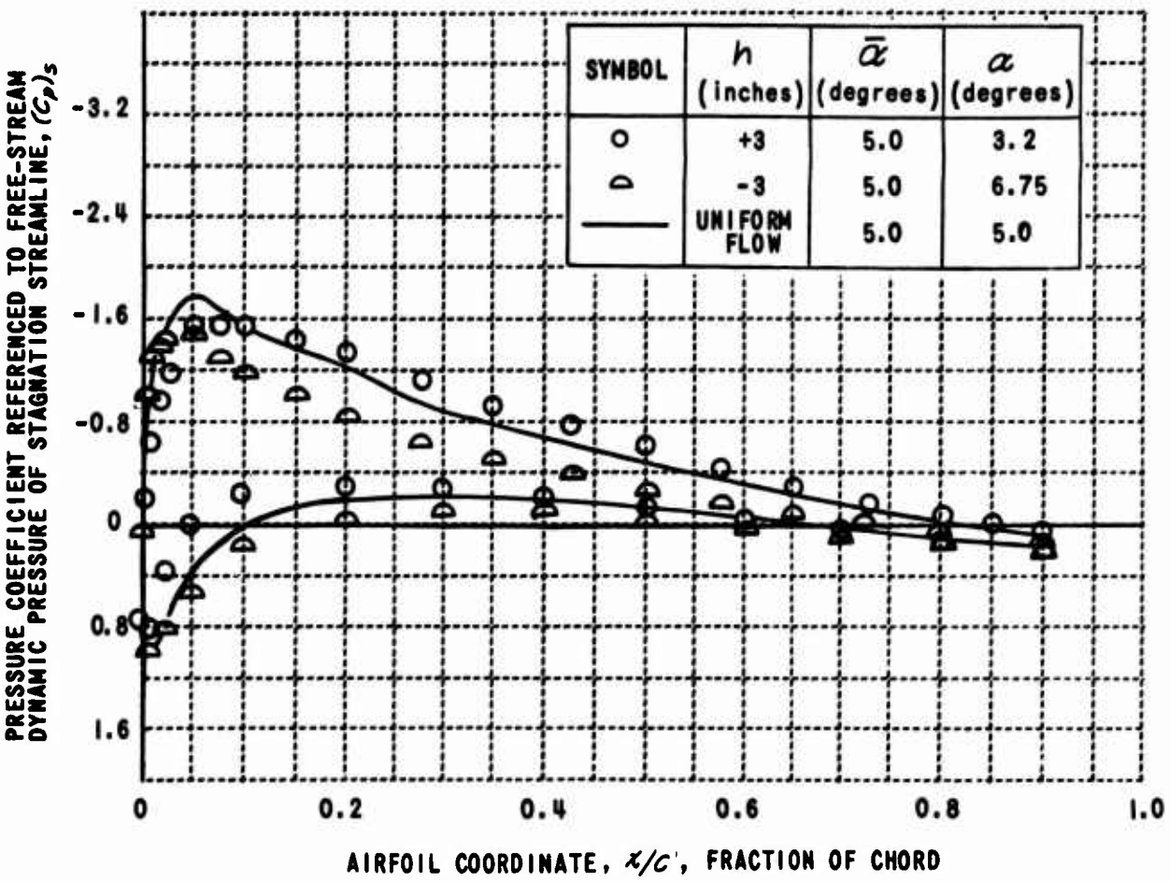

Figure 25. PRESSURE COEFFICIENT REFERENCED TO FREE-STREAM DYNAMIC PRESSURE OF STAGNATION STREAMLINE, $(C_p)_s$, VERSUS FRACTION OF CHORD, x/c, FOR $\bar{\alpha}$ = 5 DEGREES, UNIFORM FLOW AND NONUNIFORMLY SHEARED FLOW.

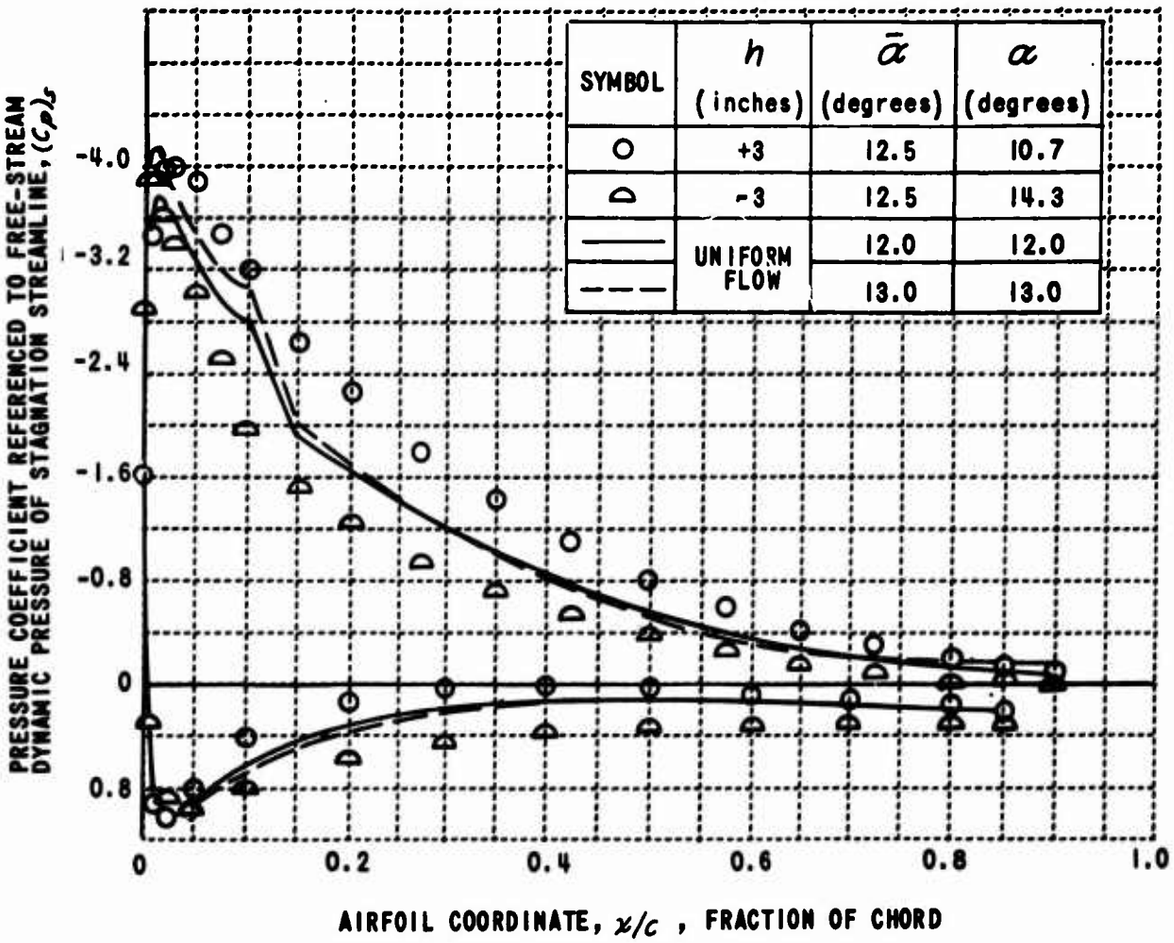

Figure 26. PRESSURE COEFFICIENT REFERENCED TO FREE-STREAM DYNAMIC PRESSURE OF STAGNATION STREAMLINE, $(C_p)_s$, VERSUS FRACTION OF CHORD, x/c , FOR $\bar{\alpha}$ = 12.5 DEGREES, UNIFORM FLOW AND NONUNIFORMLY SHEARED FLOW.

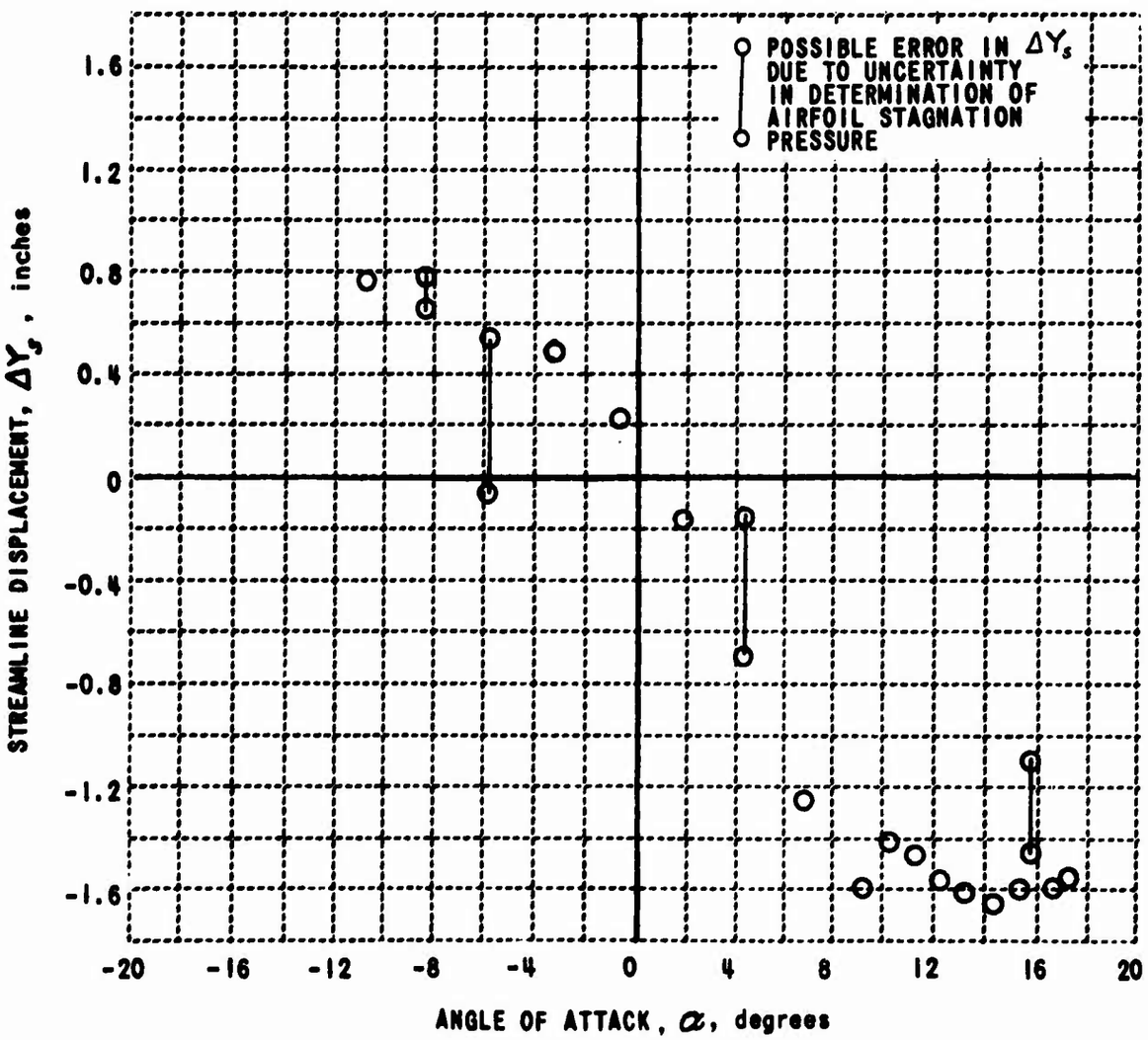

Figure 27. DISPLACEMENT OF NONUNIFORMLY SHEARED FLOW AIRFOIL STAGNATION STREAMLINE RELATIVE TO AIRFOIL MIDCHORD, h = -3 INCHES.

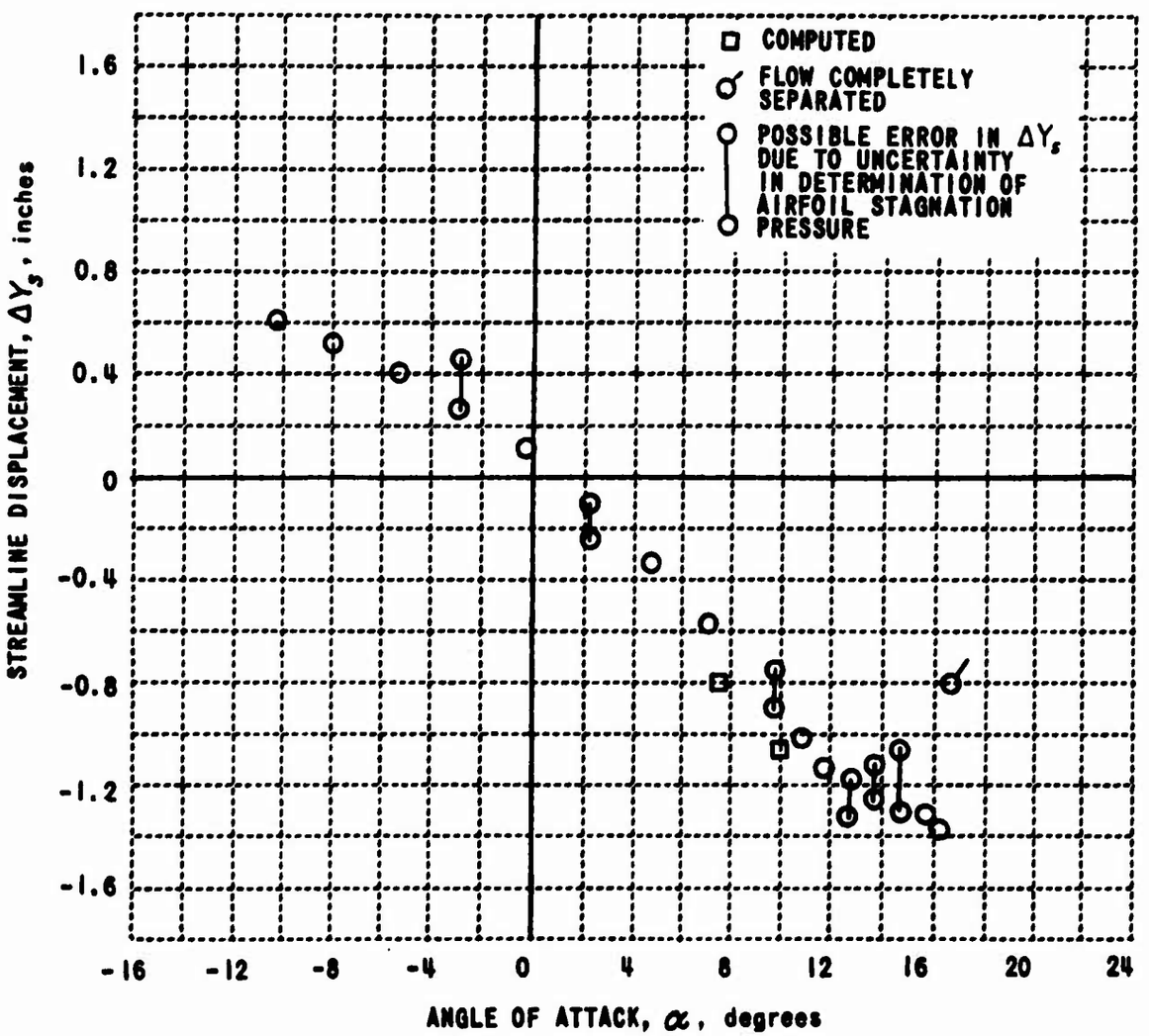

Figure 28. DISPLACEMENT OF NONUNIFORMLY SHEARED FLOW AIRFOIL STAGNATION STREAMLINE RELATIVE TO AIRFOIL MIDCHORD, h = -2 INCHES.

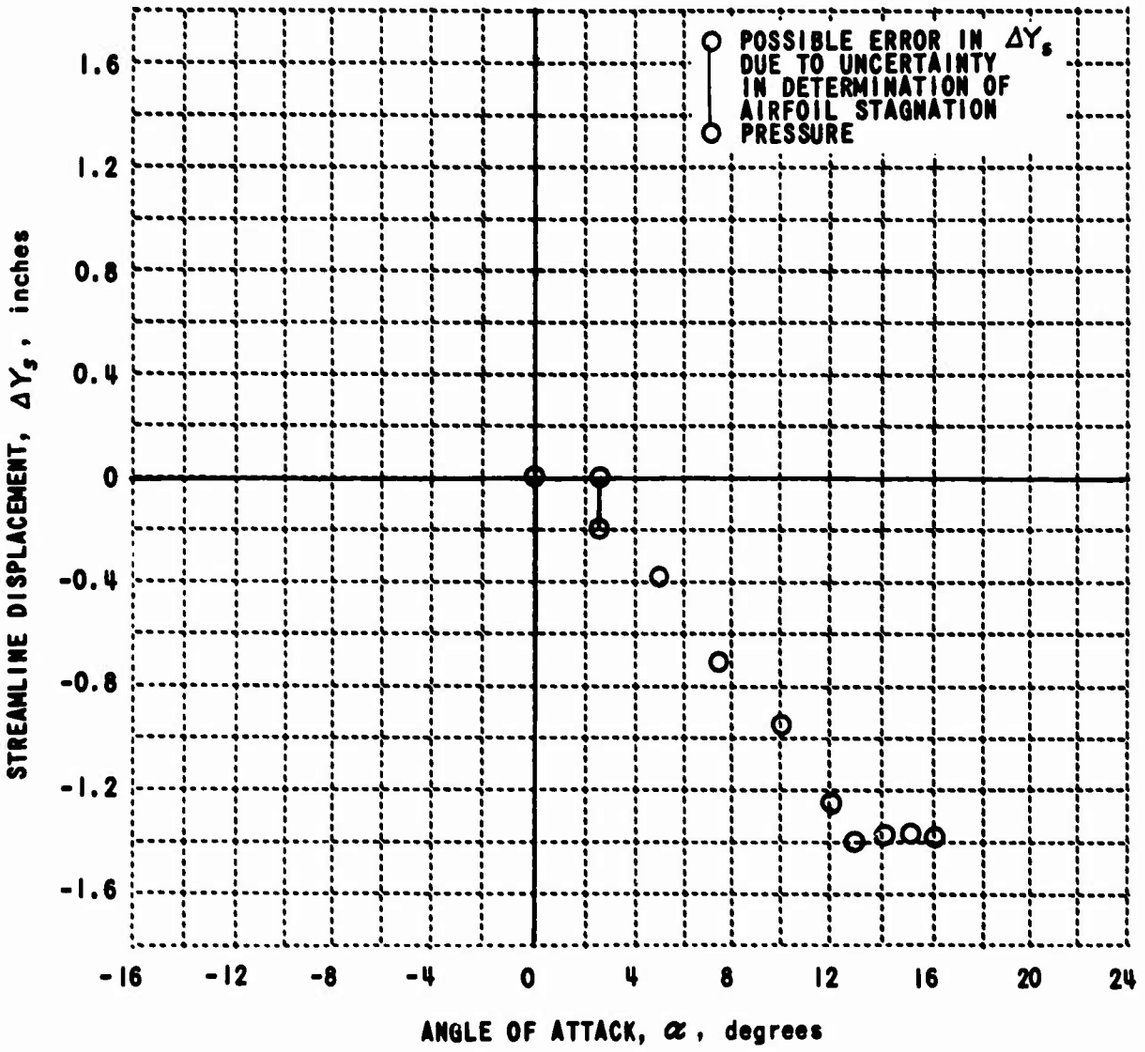

Figure 29. DISPLACEMENT OF NONUNIFORMLY SHEARED FLOW AIRFOIL STAGNATION STREAMLINE RELATIVE TO AIRFOIL MIDCHORD, h = -1 INCH.

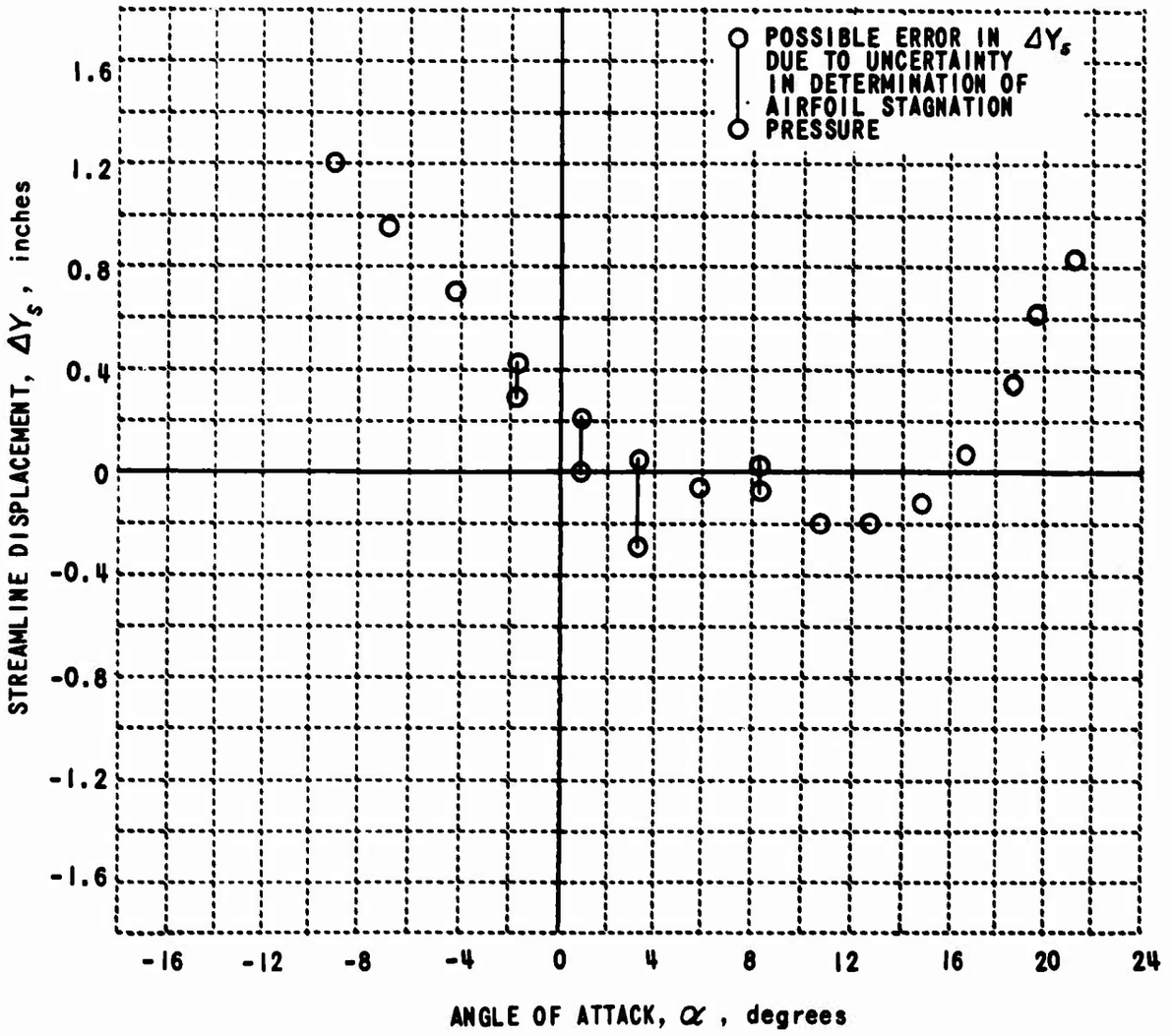

Figure 30. DISPLACEMENT OF NONUNIFORMLY SHEARED FLOW AIRFOIL STAGNATION STREAMLINE RELATIVE TO AIRFOIL MIDCHORD, h = +1 INCH.

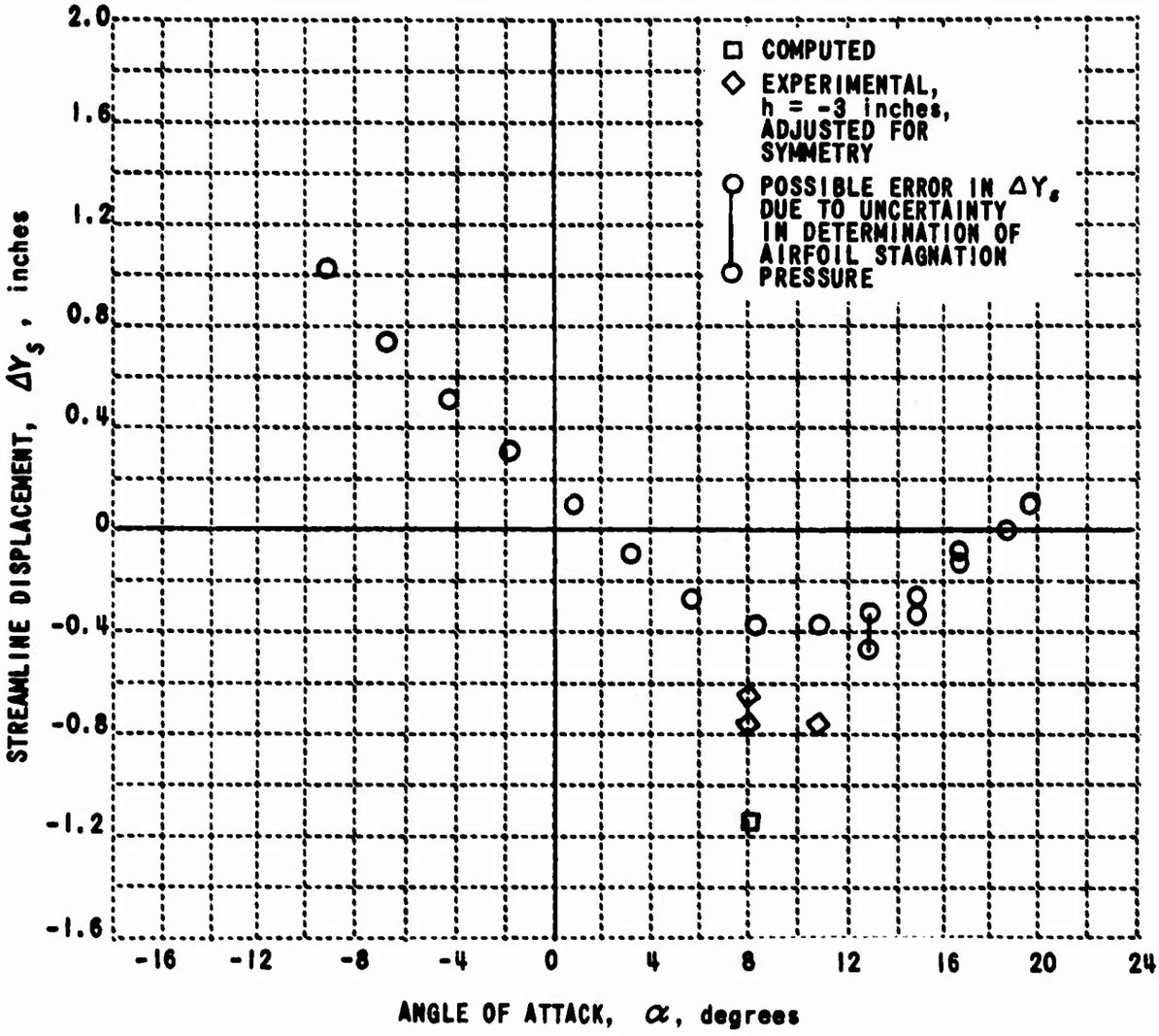

Figure 31. DISPLACEMENT OF NONUNIFORMLY SHEARED FLOW AIRFOIL STAGNATION STREAMLINE RELATIVE TO AIRFOIL MIDCHORD, h = +3 INCHES.

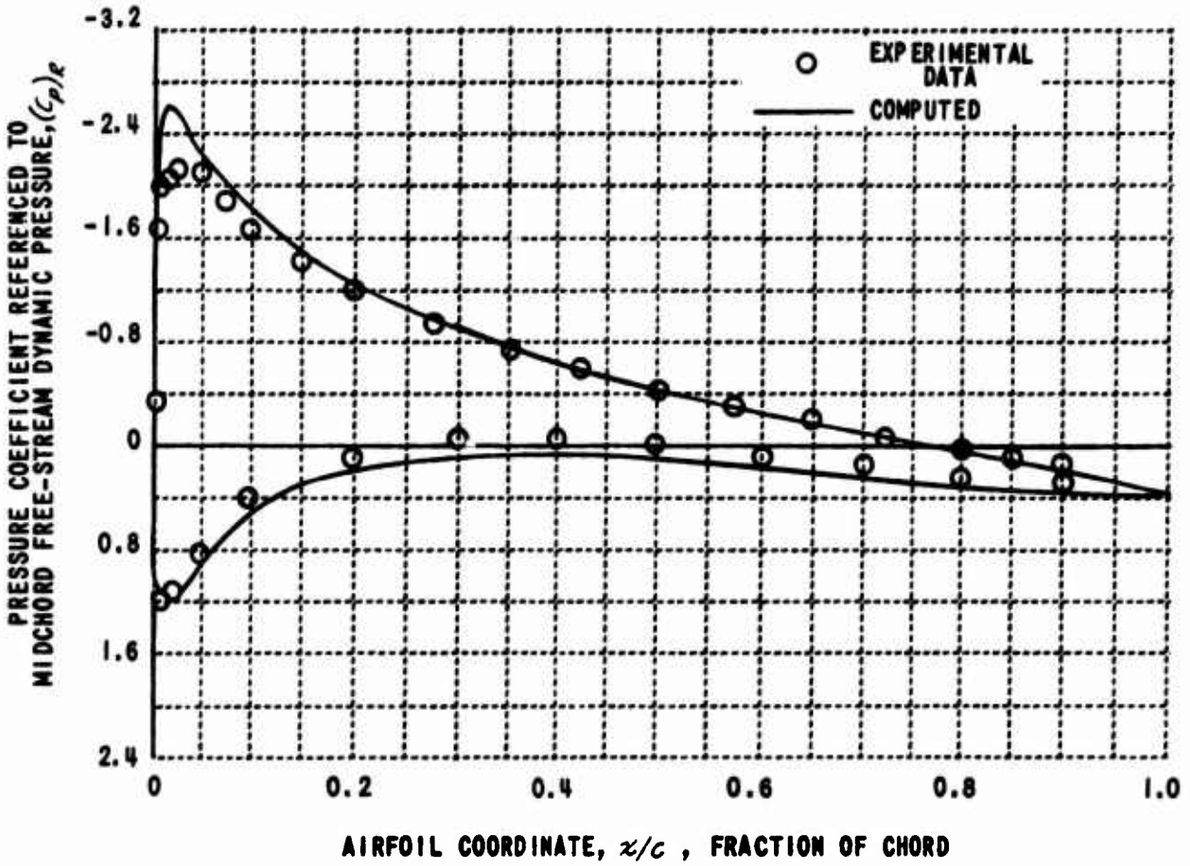

Figure 32. COMPARISON OF COMPUTED AND MEASURED PRESSURE COEFFICIENTS, $(C_p)_R$, VERSUS FRACTION OF CHORD, x/c , NONUNIFORMLY SHEARED FLOW, h = -2 INCHES, α = 7.1 DEGREES.

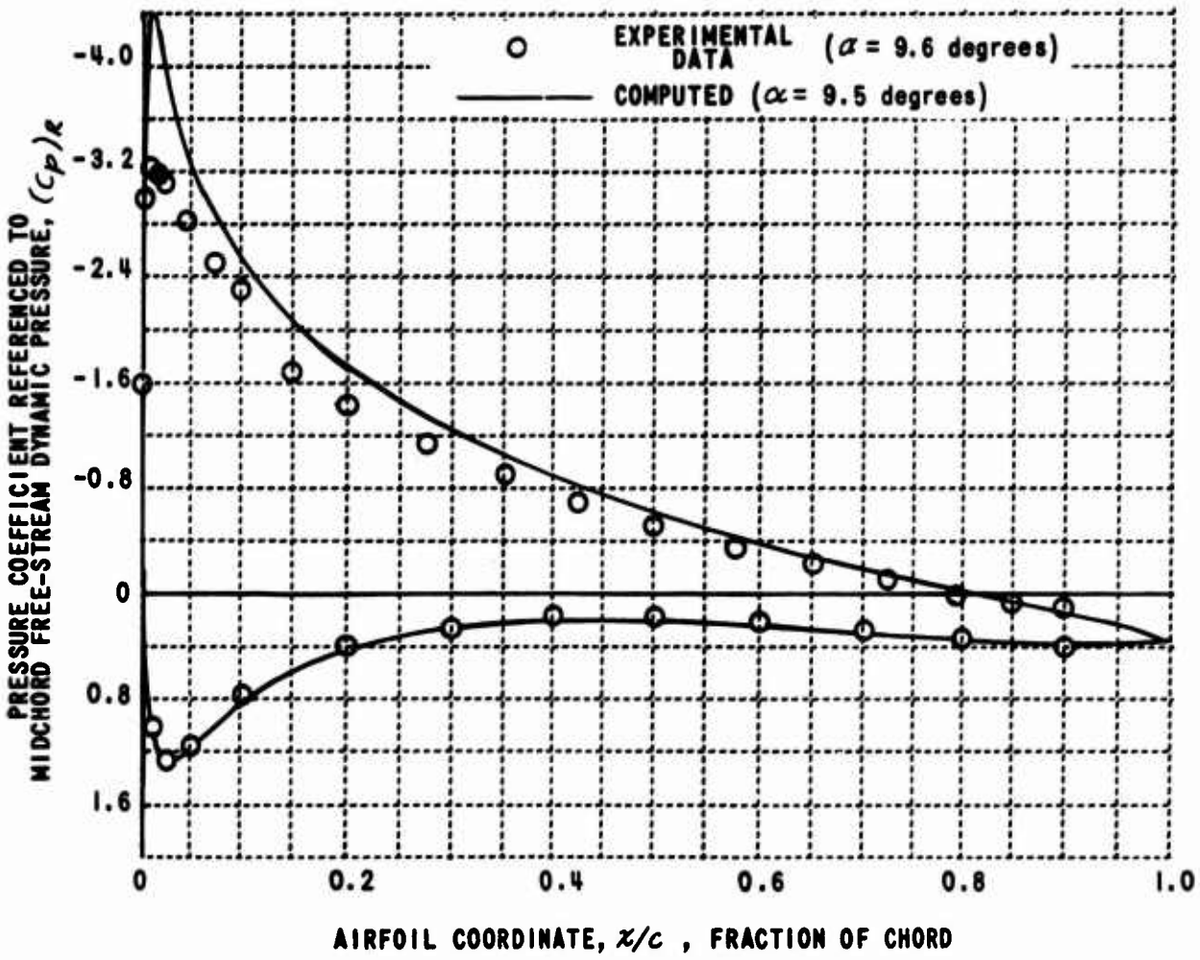

Figure 33. COMPARISON OF COMPUTED AND MEASURED PRESSURE COEFFICIENTS, $(C_p)_R$, VERSUS FRACTION OF CHORD, x/c , NONUNIFORMLY SHEARED FLOW, h = -2 INCHES, $\alpha \approx 9.5$ DEGREES.

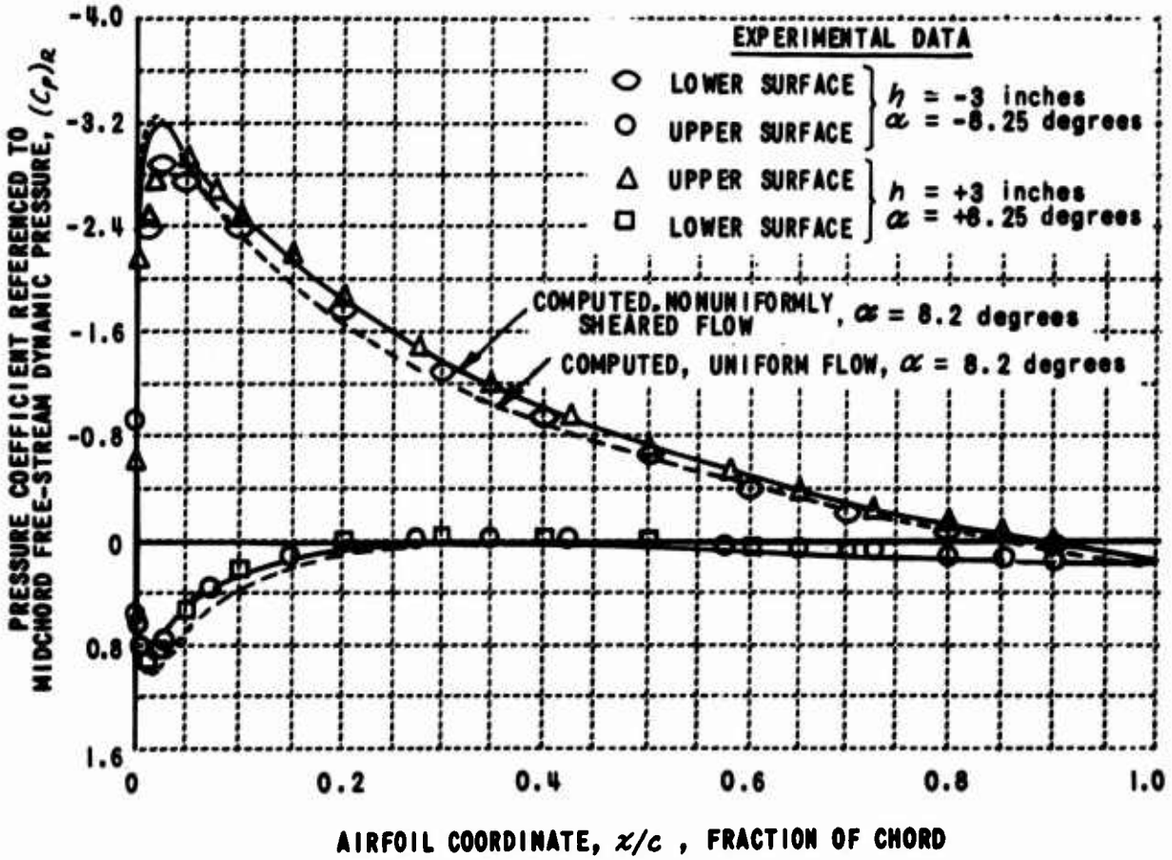

Figure 34. COMPARSION OF COMPUTED AND MEASURED PRESSURE COEFFICIENTS, $(C_p)_R$, VERSUS FRACTION OF CHORD, x/c , NONUNIFORMLY SHEARED FLOW, h = +3 INCHES, $\alpha \approx 8.2$ DEGREES.

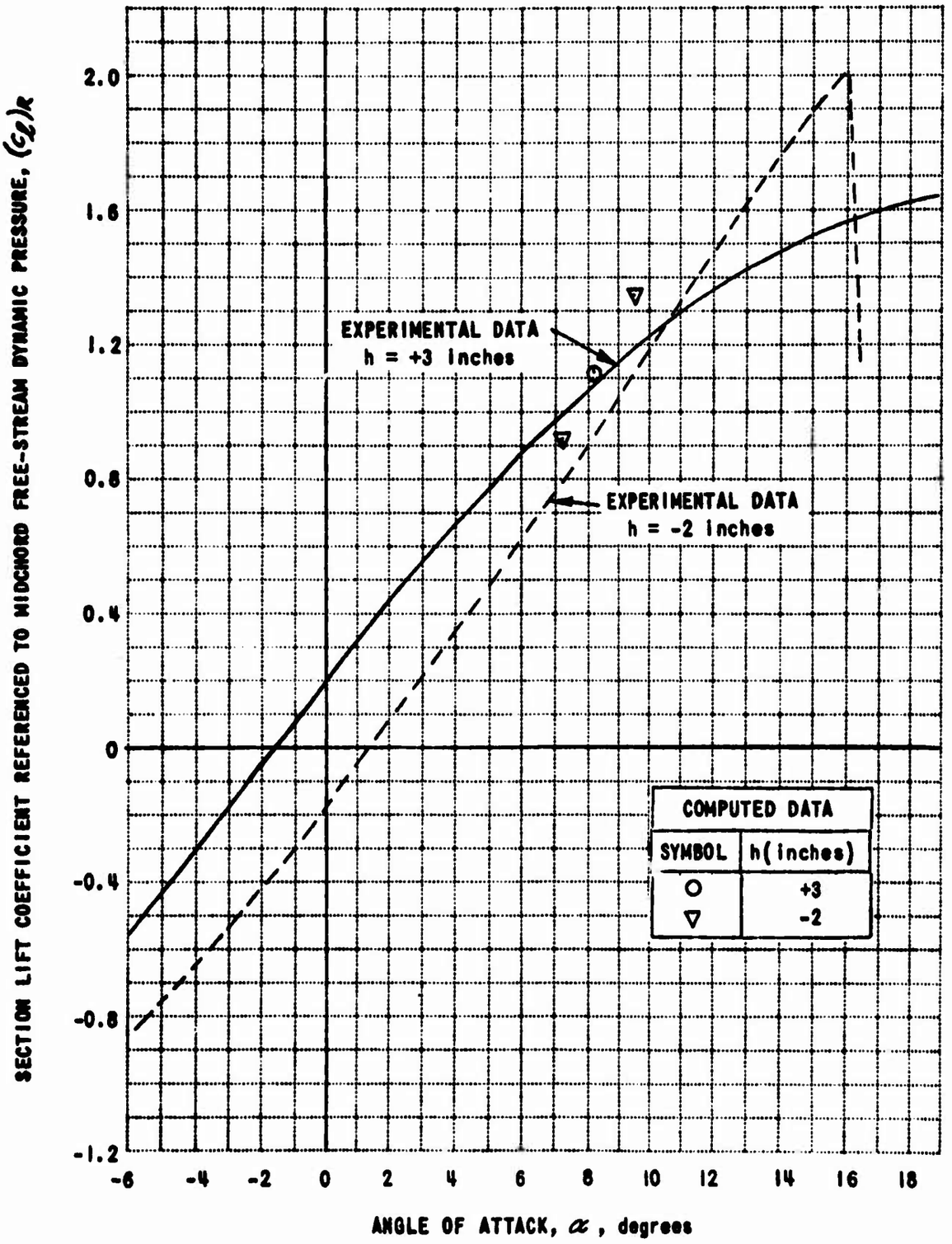

Figure 35. COMPARISON OF COMPUTED AND MEASURED SECTION LIFT COEFFICIENT REFERENCED TO MIDCHORD FREE-STREAM DYNAMIC PRESSURE, NONUNIFORMLY SHEARED FLOW.

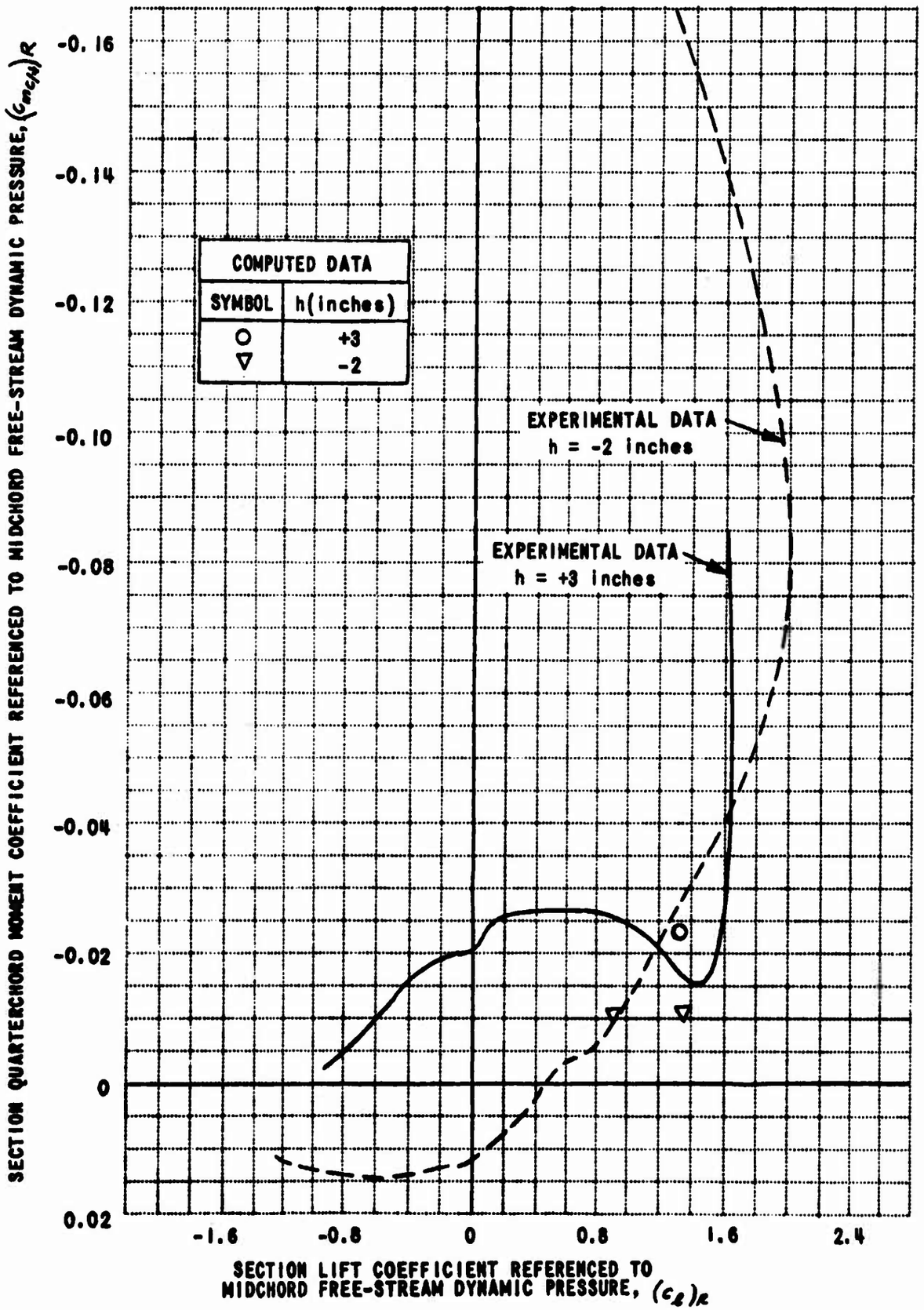

Figure 36. COMPARISON OF COMPUTED AND MEASURED SECTION QUARTERCHORD MOMENT COEFFICIENT, NONUNIFORMLY SHEARED FLOW.

REFERENCES

1. Tsien, H. S., "Symmetrical Joukowski Airfoils in Shear Flow", Quarterly of Applied Mathematics, Vol. I, No. 2, 1943, pp. 130 - 148.

2. Lighthill, M. J., "The Fundamental Solution for Small Steady Three-Dimensional Disturbances to a Two-Dimensional Parallel Shear Flow", Journal of Fluid Mechanics, Vol. 3, Vol. 3, 1957, pp. 113 - 144.

3. Jones, E. E., "The Forces on a Thin Airfoil in Slightly Parabolic Shear Flow", ZAMM, Vol. 37, 1957, pp. 362 - 370.

4. Sowyrda, A., Theory of Cambered Joukowski Airfoils in Shear Flow, CAL Report AI-1190-A-2, Cornell Aeronautical Laboratory, Inc., Buffalo, New York, September 1959.

5. Vidal, R.J., Hilton, J. H., and Curtis, J. T., The Two-Dimensional Effects of Slipstream Shear on Airfoil Characteristics, TREC TR 60-56, U. S. Army Transportation Research Command* Fort Eustis, Virginia, September 1959.

6. Vidal, R.J., Curtis, J.T., and Hilton, J.H., The Influence of Two-Dimensional Stream Shear on Airfoil Maximum Lift, TCREC TR 61-93, U. S. Army Transportation Research Command, Fort Eustis, Virginia, August 1961.

7. The Effects of Axisymmetric Slipstream Shear on Airfoil Characteristics, TCREC TR 61-138, U. S. Army Transportation Research Command* Fort Eustis, Virginia, December 1961.

8. Brady, W. G., Theoretical and Experimental Studies of Airfoil Characteristics in Nonuniform Sheared Flow, USAAML TR 65-17, AD 616617, U. S. Army Aviation Materiel Laboratories, Fort Eustis, Virginia, May 1965.

9. Brady, W. G., and Ludwig, G. R., Theoretical Studies of Impinging Uniform and Nonuniform Jets, TRECOM TR 64-42, U. S. Army Transportation Research Command* Fort Eustis, Virginia, August 1964.

* Now U. S. Army Aviation Materiel Laboratories

10. Phillips, B. L., "A Technique for the Numerical Solution of Certain Integral Equations of the First Kind", Journal of the Association for Computing Machinery, Vol. 9, 1962, pp. 84 - 97.

11. Twomey, S., "On the Numerical Solution of Fredholm Integral Equations of the First Kind by the Inversion of the Linear System Produced by Quadrature", Journal of the Association for Computing Machinery, Vol. 10, 1963, pp. 97 - 101.

12. Pope, A., and Goin, K. L., High-Speed Wind Tunnel Testing, First Edition, John Wiley and Sons, Inc., New York, New York, 1965, pp. 314-315.

13. von Kármán, Th., and Tsien, H. S., "Lifting-Line Theory for a Wing in Non-Uniform Flow", Quarterly of Applied Mathematics, Vol. 3, 1945, pp. 1 - 11.

DISTRIBUTION

US Army Materiel Command	5
US Army Mobility Command	3
US Army Aviation Materiel Command	5
US Army Aviation Materiel Laboratories	29
US Army R&D Group (Europe)	2
US Army Limited War Laboratory	1
US Army Research Office-Durham	1
US Army Test and Evaluation Command	1
US Army Medical R&D Command	1
US Army Engineer Waterways Experiment Station	1
US Army Combat Developments Command, Fort Belvoir	2
US Army Combat Developments Command Experimentation Command	3
US Army Command and General Staff College	1
US Army Aviation School	1
US Army Infantry Center	2
US Army Aviation Maintenance Center	2
US Army Electronics Command	2
US Army Aviation Test Activity, Edwards AFB	2
Air Force Flight Test Center, Edwards AFB	1
US Army Field Office, AFSC, Andrews AFB	1
Air Force Flight Dynamics Laboratory, Wright-Patterson AFB	1
Systems Engineering Group (RTD), Wright-Patterson AFB	3
Bureau of Ships, DN	1
Bureau of Naval Weapons, DN	5
Office of Naval Research	2
Chief of Naval Research	2
David Taylor Model Basin	1
Ames Research Center, NASA	1
Lewis Research Center, NASA	1
Manned Spacecraft Center, NASA	1
NASA Representative, Scientific and Technical Information Facility	2
NAFEC Library (FAA)	2
US Army Aviation Human Research Unit	2
US Army Board for Aviation Accident Research	1
Bureau of Safety, Civil Aeronautics Board	2
US Naval Aviation Safety Center, Norfolk	1
Federal Aviation Agency, Washington, D. C.	1
The Surgeon General	1
Defense Documentation Center	20

APPENDIX

MATHEMATICAL FORMULATION AND IMPLEMENTATION OF SHEARED FLOW AERODYNAMICS COMPUTER PROGRAM

FUNDAMENTAL EQUATIONS

The flow model on which the analysis is based is illustrated in Figure 2. The wind-tunnel walls are represented by vortex sheets of variable strengths $\gamma_i(x)$, where $i = 1$ refers to the lower wall and $i = 2$ refers to the upper wall. Likewise, the airfoil surfaces are represented by vortex sheets of variable strengths $\gamma_{A1}(x)$, $\gamma_{A2}(x)$, and $\gamma_{AL}(y)$.

Point (a), Figure 2, in the velocity profile marks the boundary, represented by the function $g(x)$, between different constant values of the vorticity. In Figure 2, the vorticity above this boundary is

$$\omega_+ = -\frac{U_2 - U_3}{L} = -\omega$$

and below this boundary is

$$\omega_- = \frac{U_1 - U_3}{L} = \omega.$$

The functions γ_1, γ_2, γ_{AL}, γ_{A1}, γ_{A2}, and g are the unknowns which are to be determined.

The velocity components u and v can be written*

$$\left.\begin{aligned} u(x,y) &= u_w + u_\omega + u_A \\ v(x,y) &= v_w + v_\omega + v_A \end{aligned}\right\} \qquad \text{(A-1)}$$

where (u_w, v_w) are contributed by the wind-tunnel wall singularity distribution, (u_ω, v_ω) arise from the vorticity ω in the shear flow, and (u_A, v_A) are the results of the airfoil singularity distribution. These follow directly from application of the Biot-Savart induction law, and are as follows:

$$u_w(x,y) = -\frac{1}{2\pi}\left\{(y-L)\int_{-\infty}^{\infty}\frac{\gamma_2(\xi)\,d\xi}{(x-\xi)^2+(y-L)^2} + (y+L)\int_{-\infty}^{\infty}\frac{\gamma_1(\xi)\,d\xi}{(x-\xi)^2+(y+L)^2}\right\} \qquad \text{(A-2)}$$

$$v_w(x,y) = \frac{1}{2\pi}\left\{\int_{-\infty}^{\infty}\frac{(x-\xi)\,\gamma_2(\xi)\,d\xi}{(x-\xi)^2+(y-L)^2} + \int_{-\infty}^{\infty}\frac{(x-\xi)\,\gamma_1(\xi)\,d\xi}{(x-\xi)^2+(y+L)^2}\right\} \qquad \text{(A-3)}$$

$$u_\omega(x,y) = \frac{\omega}{2\pi}\int_{-\infty}^{\infty}\left\{\int_{-L}^{g(\xi)}\frac{(y-\eta)\,d\eta}{(x-\xi)^2+(y-\eta)^2} - \int_{g(\xi)}^{L}\frac{(y-\eta)\,d\eta}{(x-\xi)^2+(y-\eta)^2}\right\}d\xi \qquad \text{(A-4)}$$

---

* Symbols used only in this appendix are defined as they are first introduced.

$$v_\omega(x,y) = -\frac{\omega}{2\pi}\int_{-\infty}^{\infty}\left\{\int_{-L}^{g(\xi)}\frac{(x-\xi)\,d\eta}{(x-\xi)^2+(y-\eta)^2} - \int_{g(\xi)}^{L}\frac{(x-\xi)\,d\eta}{(x-\xi)^2+(y-\eta)^2}\right\}d\xi \qquad \text{(A-5)}$$

$$u_A(x,y) = -\frac{1}{2\pi}\left\{\int_{y_{AL}}^{y_{AU}}\frac{\sqrt{1+[\ell'(\eta)]^2}\,(y-\eta)\,\gamma_{AL}\,d\eta}{[x-\ell(\eta)]^2+(y-\eta)^2} + \int_{x_L}^{x_T}\frac{\sqrt{1+[h'_{AU}(\xi)]^2}\,[y-h_{AU}(\xi)]\,\gamma_{A2}\,d\xi}{(x-\xi)^2+[y-h_{AU}(\xi)]^2} + \int_{x_L}^{x_T}\frac{\sqrt{1+[h'_{AL}(\xi)]^2}\,[y-h_{AL}(\xi)]\,\gamma_{A1}\,d\xi}{(x-\xi)^2+[y-h_{AL}(\xi)]^2}\right\} \qquad \text{(A-6)}$$

$$v_A(x,y) = \frac{1}{2\pi}\left\{\int_{y_{AL}}^{y_{AU}}\frac{\sqrt{1+[\ell'(\eta)]^2}\,[x-\ell(\eta)]\,\gamma_{AL}\,d\eta}{[x-\ell(\eta)]^2+(y-\eta)^2} + \int_{x_L}^{x_T}\frac{\sqrt{1+[h'_{AU}(\xi)]^2}\,(x-\xi)\,\gamma_{A2}\,d\xi}{(x-\xi)^2+[y-h_{AU}(\xi)]^2} + \int_{x_L}^{x_T}\frac{\sqrt{1+[h'_{AL}(\xi)]^2}\,(x-\xi)\,\gamma_{A1}\,d\xi}{(x-\xi)^2+[y-h_{AL}(\xi)]^2}\right\} \qquad \text{(A-7)}$$

where $h'(x) \equiv \frac{dh(x)}{dx}$, $h_{AU}(x)$ and $h_{AL}(x)$ are y - coordinates of the upper and lower aft surfaces, respectively, of the airfoil, $\ell'(y) \equiv \frac{d\ell(y)}{dy}$, $\ell(y)$ are x -coordinates of the leading edge of the airfoil, y_{AL}, y_{AU} are the y -coordinates of the lower surface and upper surface points, respectively, dividing the airfoil

leading-edge vortex sheet and airfoil upper and lower aft vortex sheets and (ξ,η) are dummy variables of integration corresponding to (x,y). The necessity for separate treatment of the airfoil leading edge is a result of the infinite slope there in terms of the y-coordinates of the airfoil surface.

BOUNDARY CONDITIONS

The boundary conditions which must be satisfied are

1. Velocity components normal to the wind-tunnel walls are zero, or

$$v(x,\pm L) = 0. \tag{A-8}$$

2. Velocity components normal to the airfoil surface are zero; i. e.,

$$\frac{dh_A}{dx} = \frac{v(x,h_A(x))}{u(x,h_A(x))}. \tag{A-9}$$

3. The boundary $g(x)$ is a streamline; i. e.,

$$\frac{dg}{dx} = \frac{v(x,g(x))}{u(x,g(x))},$$

where h_A represents either h_{AU} or h_{AL} as the case may be. This condition is satisfied if

$$\int_{-L}^{g(x)} u(x,y)\,dy = \frac{L}{2}(U_1 + U_3). \tag{A-10}$$

Also, the Kutta-Joukowski condition must be satisfied at the airfoil trailing edge; i. e., the velocity at the trailing edge is finite.

Equations (A-8), (A-9), and (A-10) with Equation (A-1) result in six nonlinear integral equations for the six unknown functions γ_1, γ_2, γ_{AL}, γ_{A1}, γ_{A2}, and g. It is possible to obtain a solution only by

recourse to a high-speed, high-storage-capacity digital computer. The nonlinearity in the problem arises through $g(x)$; if g were known, then solutions for the γ's could be obtained by a direct inversion procedure on the computer. The Kutta-Joukowski trailing-edge condition is applied by requiring that in the limit as the airfoil trailing edge is approached,the total circulation per unit chord approaches zero; i. e., (see Figure 2)

$$\lim_{x \to x_T} \left[\gamma_{A2}(x) - \gamma_{A1}(x) \right] = 0 \ . \qquad \text{(A-11)}$$

IMPLEMENTATION OF DIGITAL COMPUTER PROGRAM

Expressions for Velocity Components

It is assumed that the flow disturbance at the wind-tunnel walls is confined to $-D_W \leq 0 \leq D_W$ (see Figure 2), and that the flow disturbance near the flow centerline ($y = 0$) is confined to $-D_S \leq x \leq D_S$. In the far stream ($x < -D_W$, $x > D_W$) γ_1 and γ_2 are assumed constant; namely,

$$\left.\begin{aligned} \gamma_1(x) &= -U_1 \ , \\ \gamma_2(x) &= U_2 \ , \end{aligned}\right\} \quad \text{for} \quad x < -D_W \, , \; x > D_W \ .$$

For the purposes of numerical computation, the vortex sheets representing the wind-tunnel walls and the airfoil surfaces are divided into segments, Δx_i in length. The vortex-sheet strengths (γ_1 , γ_2 , γ_{AL} , γ_{A1} , and γ_{A2} in Figure 2) are assumed to be constant within increments Δx_i (but, of course, varying from segment to segment). Note that because of this assumed variation of vortex sheet strength, v is singular at the point where two vortex sheet segments of unequal strengths join.

The region between $x = -D_s$ and $x = +D_s$ is also divided into increments Δx_i. For the purpose of evaluating the integrals of Equations (A-2) and (A-3) numerically, the value of $g(x)$ is assumed to be constant in a given increment Δx_i, but varying from increment to increment.

Once the vortex sheets have been reduced to segments of constant singularity strength per unit length, the expressions for the velocity components u and v (Equation (A-1)) can be written

$$u(x,y) = \frac{1}{2\pi}\left[\frac{1}{2}\omega u_1 - (u_2 + u_3 + u_4 + u_5 + u_6)\right] \qquad \text{(A-12)}$$

and

$$v(x,y) = \frac{1}{2\pi}\left[-\omega v_1 + v_2 + v_3 + v_4 + v_5 + v_6\right]. \qquad \text{(A-13)}$$

Note that in Equations (A-2) through (A-7) and in Equations (A-12) and (A-13),

$$u_w = \frac{1}{2\pi}(u_2 + u_3) \quad , \quad v_w = \frac{1}{2\pi}(v_2 + v_3)$$

$$u_w = \frac{\omega}{4\pi} u_1 \quad , \quad v_w = \frac{\omega}{2\pi} v_1$$

$$u_A = \frac{1}{2\pi}(u_4 + u_5 + u_6) \quad , \quad v_A = \frac{1}{2\pi}(v_4 + v_5 + v_6) .$$

The terms u_i and v_i are associated with the various singularities as follows:

TERMS	ASSOCIATED WITH
u_1, v_1	Distributed vorticity
u_2, v_2	Lower wind-tunnel wall vortex sheet
u_3, v_3	Upper wind-tunnel wall vortex sheet
u_4, v_4	Airfoil leading-edge vortex sheet
u_5, v_5	Airfoil aft lower-surface vortex sheet
u_6, v_6	Airfoil aft upper-surface vortex sheet

These terms, expanded in terms of the contributions of the individual vortex sheet segments, become

$$u_1(x,y) = u_{1D} + \sum_{i=1}^{M_1} \Delta u_{1i} \tag{A-14}$$

$$u_2(x,y) = -U_1\, u_{2D} + \sum_{i=1}^{M_2} \gamma_{1i}\, \Delta u_{2i} \tag{A-15}$$

$$u_3(x,y) = U_2\, u_{3D} + \sum_{i=1}^{M_2} \gamma_{2i}\, \Delta u_{3i} \tag{A-16}$$

$$u_4(x,y) = \sum_{i=1}^{N_1} \gamma_{A1i}\, \Delta u_{4i} \tag{A-17}$$

$$u_5(x,y) = \sum_{i=1}^{N_2} \gamma_{A1i}\, \Delta u_{5i} \tag{A-18}$$

$$u_6(x,y) = \sum_{i=1}^{N_2} \gamma_{A2i}\, \Delta u_{6i} \tag{A-19}$$

$$v_1(x,y) = 2\left[v_{10} + \sum_{i=1}^{M_1} \Delta v_{1i}\right] \tag{A-20}$$

$$v_2(x,y) = -U_1\, v_{20} + \sum_{i=1}^{M_2} \gamma_{1i}\, \Delta v_{2i} \tag{A-21}$$

$$v_3(x,y) = U_2\, v_{30} + \sum_{i=1}^{M_2} \gamma_{2i}\, \Delta v_{3i} \tag{A-22}$$

$$v_4(x,y) = \sum_{i=1}^{N_1} \gamma_{AL_i}\, \Delta v_{4i} \tag{A-23}$$

$$v_5(x,y) = \sum_{i=1}^{N_2} \gamma_{A1_i}\, \Delta v_{5i} \tag{A-24}$$

$$v_6(x,y) = \sum_{i=1}^{N_2} \gamma_{A2_i}\, \Delta v_{6i} \tag{A-25}$$

where

$$\begin{aligned} u_{10} = {} & (x-D)\log\left\{\frac{[(x-D)^2+y^2]^2}{[(x-D)^2+(y+L)^2][(x-D)^2+(y-L)^2]}\right\} \\ & -(x+D)\log\left\{\frac{[(x+D)^2+y^2]^2}{[(x+D)^2+(y+L)^2][(x+D)^2+(y-L)^2]}\right\} \\ & +4\pi(|y|-L)+4y\left[\tan^{-1}\left(\frac{x-D}{y}\right)-\tan^{-1}\left(\frac{x+D}{y}\right)\right] \\ & +2(y+L)\left[\tan^{-1}\left(\frac{x+D}{y+L}\right)-\tan^{-1}\left(\frac{x-D}{y+L}\right)\right] \\ & +2(y-L)\left[\tan^{-1}\left(\frac{x+D}{y-L}\right)-\tan^{-1}\left(\frac{x-D}{y-L}\right)\right] \end{aligned} \tag{A-26}$$

$$u_{2D} = \pi + \tan^{-1}\left(\frac{x-D}{y+L}\right) - \tan^{-1}\left(\frac{x+D}{y+L}\right) \tag{A-27}$$

$$u_{3D} = -\pi + \tan^{-1}\left(\frac{x-D}{y+L}\right) - \tan^{-1}\left(\frac{x+D}{y-L}\right) \tag{A-28}$$

$$v_{1D} = (x-D)\tan^{-1}\left(\frac{y}{x-D}\right) - (x+D)\tan^{-1}\left(\frac{y}{x+D}\right) + \frac{1}{2}\, y \log \frac{(x-D)^2 + y^2}{(x+D)^2 + y^2} \tag{A-29}$$

$$v_{2D} = \frac{1}{2} \log \frac{(x-D)^2 + (y+L)^2}{(x+D)^2 + (y+L)^2} \tag{A-30}$$

$$v_{3D} = \frac{1}{2} \log \frac{(x-D)^2 + (y-L)^2}{(x+D)^2 + (y-L)^2} \tag{A-31}$$

$$\Delta u_{1i} = \left(x - x_i + \tfrac{1}{2}\Delta x_i\right) \log \frac{\left[\left(x - x_i + \frac{1}{2}\Delta x_i\right)^2 + \left(y - g_i\right)^2\right]^2}{\left[\left(x - x_i + \frac{1}{2}\Delta x_i\right)^2 + (y+L)^2\right]\left[\left(x - x_i + \frac{1}{2}\Delta x_i\right)^2 + (y-L)^2\right]}$$

$$- \left(x - x_i - \tfrac{1}{2}\Delta x_i\right) \log \frac{\left[\left(x - x_i - \frac{1}{2}\Delta x_i\right)^2 + \left(y - g_i\right)^2\right]^2}{\left[\left(x - x_i - \frac{1}{2}\Delta x_i\right)^2 + (y+L)^2\right]\left[\left(x - x_i - \frac{1}{2}\Delta x_i\right)^2 + (y-L)^2\right]}$$

$$+ 4(y - g_i)\left[\tan^{-1}\left(\frac{x - x_i + \frac{1}{2}\Delta x_i}{y - g_i}\right) - \tan^{-1}\left(\frac{x - x_i - \frac{1}{2}\Delta x_i}{y - g_i}\right)\right]$$

$$- 2(y+L)\left[\tan^{-1}\left(\frac{x - x_i + \frac{1}{2}\Delta x_i}{y+L}\right) - \tan^{-1}\left(\frac{x - x_i - \frac{1}{2}\Delta x_i}{y+L}\right)\right]$$

$$- 2(y-L)\left[\tan^{-1}\left(\frac{x - x_i + \frac{1}{2}\Delta x_i}{y-L}\right) - \tan^{-1}\left(\frac{x - x_i - \frac{1}{2}\Delta x_i}{y-L}\right)\right] \tag{A-32}$$

$$\Delta u_{2i} = \tan^{-1}\left(\frac{x - x_i + \frac{1}{2}\Delta x_i}{y+L}\right) - \tan^{-1}\left(\frac{x - x_i - \frac{1}{2}\Delta x_i}{y+L}\right) \tag{A-33}$$

$$\Delta u_{3i} = \tan^{-1}\left(\frac{x - x_i + \frac{1}{2}\Delta x_i}{y-L}\right) - \tan^{-1}\left(\frac{x - x_i - \frac{1}{2}\Delta x_i}{y-L}\right) \tag{A-34}$$

$$\Delta u_{4i} = \frac{1}{\sqrt{1+(l_i')^2}} \left[\frac{1}{2} \log \frac{\left[y - y_i + l_i'(x - l_i) + \frac{1+(l_i')^2}{2} \Delta y_i \right]^2 + \left[x - l_i - l_i'(y - y_i) \right]^2}{\left[y - y_i + l_i'(x - l_i) - \frac{1+(l_i')^2}{2} \Delta y_i \right]^2 + \left[x - l_i - l_i'(y - y_i) \right]^2} \right.$$

$$- l_i' \left\{ \tan^{-1} \left[\frac{y - y_i + l_i'(x - l_i) + \frac{1+(l_i')^2}{2} \Delta y_i}{x - l_i - l_i'(y - y_i)} \right] \right.$$

$$\left. \left. - \tan^{-1} \left[\frac{y - y_i + l_i'(x - l_i) - \frac{1+(l_i')^2}{2} \Delta y_i}{x - l_i - l_i'(y - y_i)} \right] \right\} \right] \qquad \text{(A-35)}$$

$$\Delta u_{5i} = \frac{1}{\sqrt{1+(h_{ALi}')^2}} \left[\tan^{-1} \left[\frac{x - x_i + h_{ALi}'(y - h_{ALi}) + \frac{1+(h_{ALi}')^2}{2} \Delta x_i}{y - h_{ALi} - h_{ALi}'(x - x_i)} \right] \right.$$

$$- \tan^{-1} \left[\frac{x - x_i + h_{ALi}'(y - h_{ALi}) - \frac{1+(h_{ALi}')^2}{2} \Delta x_i}{y - h_{ALi} - h_{ALi}'(x - x_i)} \right]$$

$$\left. + \frac{1}{2} h_{ALi}' \log \frac{\left[x - x_i + h_{ALi}'(y - h_{ALi}) + \frac{1+(h_{ALi}')^2}{2} \Delta x_i \right]^2 + \left[y - h_{ALi} - h_{ALi}'(x - x_i) \right]^2}{\left[x - x_i + h_{ALi}'(y - h_{ALi}) - \frac{1+(h_{ALi}')^2}{2} \Delta x_i \right]^2 + \left[y - h_{ALi} - h_{ALi}'(x - x_i) \right]^2} \right] \qquad \text{(A-36)}$$

Δu_{6i} is the same expression as Δu_{5i} with h_{ALi}, h_{ALi}' replaced by h_{AUi}, h_{AUi}'.

$$\Delta v_{1i} = \left(x - x_i + \frac{1}{2} \Delta x_i \right) \tan^{-1} \left(\frac{y - g_i}{x - x_i + \frac{1}{2} \Delta x_i} \right)$$

$$- \left(x - x_i - \frac{1}{2} \Delta x_i \right) \tan^{-1} \left(\frac{y - g_i}{x - x_i - \frac{1}{2} \Delta x_i} \right)$$

$$+ \frac{1}{2} (y - g_i) \log \frac{(y - g_i)^2 + \left(x - x_i + \frac{1}{2} \Delta x_i \right)^2}{(y - g_i)^2 + \left(x - x_i - \frac{1}{2} \Delta x_i \right)^2} \qquad \text{(A-37)}$$

$$\Delta v_{2i} = \frac{1}{2} \log \frac{\left(x - x_i + \frac{1}{2}\Delta x_i\right)^2 + (y+L)^2}{\left(x - x_i - \frac{1}{2}\Delta x_i\right)^2 + (y+L)^2} \tag{A-38}$$

$$\Delta v_{3i} = \frac{1}{2} \log \frac{\left(x - x_i + \frac{1}{2}\Delta x_i\right)^2 + (y-L)^2}{\left(x - x_i - \frac{1}{2}\Delta x_i\right)^2 + (y-L)^2} \tag{A-39}$$

$$\Delta v_{4i} = \frac{1}{\sqrt{1+(\ell_i')^2}} \left\{ \tan^{-1} \left[\frac{y - y_i + \ell_i'(x - \ell_i) + \frac{1+(\ell_i')^2}{2}\Delta y_i}{x - \ell_i - \ell_i'(y - y_i)} \right] \right.$$

$$- \tan^{-1} \left[\frac{y - y_i + \ell_i'(x - \ell_i) - \frac{1+(\ell_i')^2}{2}\Delta y_i}{x - \ell_i - \ell_i'(y - y_i)} \right]$$

$$\left. + \frac{1}{2}\ell_i' \log \frac{\left[y - y_i + \ell_i'(x - \ell_i) + \frac{1+(\ell_i')^2}{2}\Delta y_i\right]^2 + \left[x - \ell_i - \ell_i'(y - y_i)\right]^2}{\left[y - y_i + \ell_i'(x - \ell_i) - \frac{1+(\ell_i')^2}{2}\Delta y_i\right]^2 + \left[x - \ell_i - \ell_i'(y - y_i)\right]^2} \right\} \tag{A-40}$$

$$\Delta v_{5i} = \frac{1}{\sqrt{1+(h_{ALi})^2}} \left\{ \frac{1}{2} \log \frac{\left[x - x_i + h_{ALi}'(y - h_{ALi}) + \frac{1+(h_{ALi}')^2}{2}\Delta x_i\right]^2 + \left[y - h_{ALi} - h_{ALi}'(x - x_i)\right]^2}{\left[x - x_i + h_{ALi}'(y - h_{ALi}) - \frac{1+(h_{ALi}')^2}{2}\Delta x_i\right]^2 + \left[y - h_{ALi} - h_{ALi}'(x - x_i)\right]^2} \right.$$

$$- h_{ALi}' \left\{ \tan^{-1} \left[\frac{x - x_i + h_{ALi}'(y - h_{ALi}) + \frac{1+(h_{ALi}')^2}{2}\Delta x_i}{y - h_{ALi} - h_{ALi}'(x - x_i)} \right] \right.$$

$$\left. \left. - \tan^{-1} \left[\frac{x - x' + h_{ALi}'(y - h_{ALi}) - \frac{1+(h_{ALi}')^2}{2}\Delta x_i}{y - h_{ALi} - h_{ALi}'(x - x_i)} \right] \right\} \right\} \tag{A-41}$$

Δv_{6i} is the same expression as Δv_{5i} with h_{ALi} , h_{ALi}' replaced by h_{AUi} , h_{AUi}' .

In these expressions (Equations (A-14) through (A-41)), M_1 is the number of increments into which the region $-D_S \leq x \leq D_S$ is subdivided, M_2 is the number of segments into which each of the wind-tunnel wall vortex sheets between $-D_W \leq x \leq D_W$ is subdivided, γ_i is the singularity strength of the i^{th} vortex sheet segment, N_1 is the number of segments into which the airfoil leading-edge vortex sheet is subdivided, N_2 is the number of segments into which the vortex sheets representing the aft upper and lower surfaces of the airfoil are each subdivided, (x_i, g_i) are the coordinates of the midpoint of the i^{th} segment of $g(x)$ between $-D_S \leq x \leq D_S$, $(x_i, \pm L)$ are coordinates of the midpoint of the i^{th} segment of wind-tunnel wall vortex sheet, (x_i, h_{AU_i}) and (x_i, h_{AL_i}) are the coordinates of the midpoint of the i^{th} segments of airfoil upper and lower vortex sheets, respectively, (ℓ_i, y_i) are the coordinates of the midpoint of the i^{th} segment of airfoil leading-edge vortex sheet, and $(\Delta x_i, \Delta y_i)$ are the projections on the x and y axes of the segment length. The prime denotes differentiation; e. g.,

$$\ell' \equiv \frac{d\ell}{dy} \quad , \quad h' \equiv \frac{dh}{dx} .$$

The principal values of the inverse tangents is to be understood, and logarithms are natural logarithms. The general computational procedure adopted is as follows:

1. An initial shape of the dividing streamline, $g^{(0)}(x)$, is assumed.

2. The boundary conditions that the flow is tangential at the wind-tunnel walls and the airfoil surface, together with the approximation to $g(x)$, are used to determine the singularity strength distribution of the vortex sheets representing the walls and airfoil surfaces. The boundary conditions at the wind-tunnel walls and at the airfoil surface are satisfied at discrete points, x_i, corresponding to the segments Δx_i of vortex sheets along these surfaces.

3. The second approximation, $g^{(1)}(x)$, is determined on the basis of the mass flow continuity requirement based on Equation (A-10).

4. The iteration proceeds for the adjusted boundary by going back to Step 2 with the new approximation to $g(x)$.

Boundary Conditions - "Smoothing" Technique

When the velocity components u and v, Equations (A-12) through (A-41), are substituted into the equations for the boundary conditions, Equations (A-8) and (A-9), and including Equation (A-11), there results $2M_2 + N_1 + 2N_2 + 1$ linear equations in terms of $2M_2 + N_1 + 2N_2$ unknown γ_i's. This, of course, is an overdetermined set of equations. (As noted in the body of this report, this overdeterminacy is very likely a result of the particular assumptions inherent in the method of numerical analysis adopted; in particular, constant singularity strength along small segments of the vortex sheets.) The "solution" of this set of equations is effected by means of a smoothing process, based on the results presented in References 10 and 11. This approach was resorted to because of the unsatisfactory behavior of solutions obtained by direct inversion of the system of equations (see Figures 3 and 4). The set of equations can be written

$$\sum_{i=1}^{M_2} A_{ij}\,\gamma_{1i} + \sum_{i=1}^{M_2} B_{ij}\,\gamma_{2i} + \sum_{i=1}^{n} C_{ij}\,\gamma_{3i} = D_j \,. \qquad \text{(A-42)}$$

(The γ_{3i} are the values of γ on the airfoil, and $n = N_1 + 2N_2$.) It is assumed that the D_j are in error by some small amount, ϵ_j. At the same time, it is known from experiment that the γ_{1i}, γ_{2i}, and γ_{3i} are smoothly varying quantities. To achieve this in the mathematical solution, it is proposed to minimize second differences of the γ_i. Thus it is desired that

$$\sum_{i=2}^{M_2-1} (\gamma_{1(i-1)} - 2\gamma_{1i} + \gamma_{1(i+1)})^2 + \sum_{i=2}^{M_2-1} (\gamma_{2(i-1)} - 2\gamma_{2i} + \gamma_{2(i+1)})^2$$

$$+ \sum_{i=1}^{n} (\gamma_{3(i+1)} - 2\gamma_{3i} + \gamma_{3(i+1)})^2$$

be a minimum, subject to

$$\sum_{j=1}^{(2M_2+n+1)} \epsilon_j^2 \quad = \text{constant.}$$

The γ_{3i} are continuous around the airfoil surface; hence, the convention is adopted that $\gamma_{30} \equiv \gamma_{3n}$, $\gamma_{31} \equiv \gamma_{3(n+1)}$ to insure this.

The development follows closely that outlined in Reference 11, and details are omitted here. The results can be stated simply in matrix form. If Equation (A-42) is written in matrix form

$$[A][\gamma] = [D], \tag{A-43}$$

then the desired solution is obtained from

$$[A^*A + \bar{K}H][\gamma] = [A^*][D] \tag{A-44}$$

where the matrix $[A^*]$ is the transpose of the matrix $[A]$, $\bar{K}$ is an arbitrary constant, and the matrix $[H]$ is

$$[H] = \left[\begin{array}{c|c|c} H_1 & 0 & 0 \\ \hline 0 & H_1 & 0 \\ \hline 0 & 0 & H_2 \end{array}\right], \tag{A-45}$$

a $(2M_2+n)$ by $(2M_2+n)$ matrix, where

$$\left[H_1\right] = \begin{bmatrix} 1 & -2 & 1 & 0 & 0 & 0 & . & . & . & 0 \\ -2 & 5 & -4 & 1 & 0 & 0 & . & . & . & 0 \\ 1 & -4 & 6 & -4 & 1 & 0 & . & . & . & 0 \\ 0 & 1 & -4 & 6 & -4 & 1 & . & . & . & 0 \\ 0 & 0 & 1 & -4 & 6 & -4 & . & . & . & . \\ . & . & . & . & . & . & . & . & . & . \\ 0 & . & . & . & 1 & -4 & 6 & -4 & 1 & 0 \\ 0 & . & . & . & 0 & 1 & -4 & 6 & -4 & 1 \\ 0 & . & . & . & 0 & 0 & 1 & -4 & 5 & -2 \\ 0 & . & . & . & 0 & 0 & 0 & 1 & -2 & 1 \end{bmatrix} \qquad \text{(A-46)}$$

an M_2 by M_2 matrix, and

$$\left[H_2\right] = \begin{bmatrix} 6 & -4 & 1 & 0 & 0 & 0 & . & 0 & 1 & -4 \\ -4 & 6 & -4 & 1 & 0 & 0 & . & 0 & 0 & 1 \\ 1 & -4 & 6 & -4 & 1 & 0 & . & 0 & 0 & 0 \\ 0 & 1 & -4 & 6 & -4 & 1 & . & . & . & . \\ . & . & . & . & . & . & . & . & . & . \\ . & . & . & . & . & . & . & . & . & . \\ 0 & 0 & 0 & . & . & 1 & -4 & 6 & -4 & 1 \\ 1 & 0 & 0 & . & . & 0 & 1 & -4 & 6 & -4 \\ -4 & 1 & 0 & . & . & 0 & 0 & 1 & -4 & 6 \end{bmatrix} \qquad \text{(A-47)}$$

an n by n matrix.

If $\bar{K} = 0$, the solution obtained represents a "least squares" optimum solution with no smoothing. As $\bar{K}$ is increased from a zero value, more and more smoothing is evident in the solutions obtained, but in general the sum $\sum \epsilon_j^2$ becomes larger also. The uniform flow solution shown in Figure 4 was obtained with $\bar{K} = 0.1$; the sheared flow solutions (Figures 32 through 34) were computed with $\bar{K} = 0.3$. An indication of the order of magnitude of the ϵ_i is afforded for any particular solution by noting the airfoil trailing edge values of γ_{A2} and γ_{A1} (Equation (A-11)); in a typical calculation, they differed in magnitude by approximately 2 percent and $\epsilon \sim 0.003$.

Iterative Technique

Given the input values of $q_i^{(j-1)}$ for the j^{th} iteration and once the system of equations for the γ_i has been solved based on $q_i^{(j-1)}$, the velocity components u and v can be computed from Equations (A-32) through (A-41) for any value of x and y in the flow. The technique used in the computer program to obtain input values $q_i^{(j)}$ for the $(j+1)^{th}$ iteration was as follows. At the x_i centered on segments corresponding to the constant q_i, the integral equation (mass flow continuity)

$$\int_{-L}^{q_i^{*(j-1)}} u\,dy + (v - u q_i')\Big|_{(x_i,\, q_i^{(j-1)})} = \frac{1}{2}(U_1 + U_3) \qquad \text{(A-48)}$$

is solved numerically for $q_i^{*(j-1)}$. The term $(v - u q_i') = 0$ if the flow normal to the curve $q^{(j-1)}(x)$ is zero. The input $q_i^{(j)}$ for the $(j+1)$ iteration is then

$$q_i^{(j)} = \frac{1}{2}\left[q_i^{(j-1)} + q_i^{*(j-1)}\right]. \qquad \text{(A-49)}$$

Initially, calculations were made using

$$g_i^{(j)} = g_i^{*(j-1)} ,$$

but these calculations failed to converge.

Once the calculation has resulted in a converged solution, the stagnation streamline dynamic pressure is determined by computing the mass flow between the airfoil surface and the wind-tunnel wall; i. e. ,

$$\int_{-L}^{h_L(x)} u(x, y)\, dy .$$

Finally, the airfoil stagnation streamline dynamic pressure is $\frac{1}{2}\rho\left[U(y_*)\right]^2$ where

$$\int_{-L}^{y_*} U(y)\, dy = \int_{-L}^{h_{AL}(x)} u(x, y)\, dy .$$

BLANK PAGE

Unclassified

Security Classification

DOCUMENT CONTROL DATA - R&D

(Security classification of title, body of abstract and indexing annotation must be entered when the overall report is classified)

1. ORIGINATING ACTIVITY (Corporate author)	2a. REPORT SECURITY CLASSIFICATION
Cornell Aeronautical Laboratory, Inc. Buffalo, New York 14221	Unclassified
	2b. GROUP

3. REPORT TITLE

Theoretical and Experimental Investigation of the Aerodynamic Properties of Airfoils Near Stall in a Two-Dimensional Nonuniformly Sheared Flow

4. DESCRIPTIVE NOTES (Type of report and inclusive dates)

5. AUTHOR(S) (Last name, first name, initial)

Brady, W. G.
Ludwig, G. R.

6. REPORT DATE	7a. TOTAL NO. OF PAGES	7b. NO. OF REFS
June 1966	120	13

8a. CONTRACT OR GRANT NO.	9a. ORIGINATOR'S REPORT NUMBER(S)
DA 44-177-AMC-268(T)	
b. PROJECT NO.	USAAVLABS Technical Report 66-35
Task 1P125901A14203	
c.	9b. OTHER REPORT NO(S) (Any other numbers that may be assigned this report)
d.	AF-2035-S-1

10. AVAILABILITY/LIMITATION NOTICES

Distribution of this document is unlimited.

11. SUPPLEMENTARY NOTES	12. SPONSORING MILITARY ACTIVITY
	US Army Aviation Materiel Laboratories Fort Eustis, Virginia

13. ABSTRACT

A theoretical method, which requires the use of a digital computer, was developed to predict pressure distributions on an airfoil in an inviscid two-dimensional nonuniformly sheared flow. The theory is applicable to airfoils of arbitrary profile and to nonuniformly sheared flows which can be represented by segments with linear velocity profiles. To test the developed theory, aerodynamic characteristics of an airfoil were investigated both theoretically and experimentally in a relatively simple two-dimensional nonuniformly sheared flow consisting of two segments with shears of equal magnitude but of opposite sign. Agreement between computed and experimental pressure distributions was good and on the basis of these results, a mechanism is postulated by which the large variations in lift previously observed in a two-dimensional nonuniformly sheared flow can occur.

DD FORM 1 JAN 64 1473

Unclassified

Security Classification

14. KEY WORDS	LINK A		LINK B		LINK C	
	ROLE	WT	ROLE	WT	ROLE	WT
Aerodynamics Airfoil Shear Flow Fluid Dynamics Wind Tunnel						

INSTRUCTIONS

1. ORIGINATING ACTIVITY: Enter the name and address of the contractor, subcontractor, grantee, Department of Defense activity or other organization *(corporate author)* issuing the report.

2*a*. REPORT SECURITY CLASSIFICATION: Enter the overall security classification of the report. Indicate whether "Restricted Data" is included. Marking is to be in accordance with appropriate security regulations.

2*b*. GROUP: Automatic downgrading is specified in DoD Directive 5200.10 and Armed Forces Industrial Manual. Enter the group number. Also, when applicable, show that optional markings have been used for Group 3 and Group 4 as authorized.

3. REPORT TITLE: Enter the complete report title in all capital letters. Titles in all cases should be unclassified. If a meaningful title cannot be selected without classification, show title classification in all capitals in parenthesis immediately following the title.

4. DESCRIPTIVE NOTES: If appropriate, enter the type of report, e.g., interim, progress, summary, annual, or final. Give the inclusive dates when a specific reporting period is covered.

5. AUTHOR(S): Enter the name(s) of author(s) as shown on or in the report. Enter last name, first name, middle initial. If military, show rank and branch of service. The name of the principal author is an absolute minimum requirement.

6. REPORT DATE: Enter the date of the report as day, month, year; or month, year. If more than one date appears on the report, use date of publication.

7*a*. TOTAL NUMBER OF PAGES: The total page count should follow normal pagination procedures, i.e., enter the number of pages containing information.

7*b*. NUMBER OF REFERENCES: Enter the total number of references cited in the report.

8*a*. CONTRACT OR GRANT NUMBER: If appropriate, enter the applicable number of the contract or grant under which the report was written.

8*b*, 8*c*, & 8*d*. PROJECT NUMBER: Enter the appropriate military department identification, such as project number, subproject number, system numbers, task number, etc.

9*a*. ORIGINATOR'S REPORT NUMBER(S): Enter the official report number by which the document will be identified and controlled by the originating activity. This number must be unique to this report.

9*b*. OTHER REPORT NUMBER(S): If the report has been assigned any other report numbers *(either by the originator or by the sponsor)*, also enter this number(s).

10. AVAILABILITY/LIMITATION NOTICES: Enter any limitations on further dissemination of the report, other than those imposed by security classification, using standard statements such as:

(1) "Qualified requesters may obtain copies of this report from DDC."

(2) "Foreign announcement and dissemination of this report by DDC is not authorized."

(3) "U. S. Government agencies may obtain copies of this report directly from DDC. Other qualified DDC users shall request through _____."

(4) "U. S. military agencies may obtain copies of this report directly from DDC. Other qualified users shall request through _____."

(5) "All distribution of this report is controlled. Qualified DDC users shall request through _____."

If the report has been furnished to the Office of Technical Services, Department of Commerce, for sale to the public, indicate this fact and enter the price, if known.

11. SUPPLEMENTARY NOTES: Use for additional explanatory notes.

12. SPONSORING MILITARY ACTIVITY: Enter the name of the departmental project office or laboratory sponsoring *(paying for)* the research and development. Include address.

13. ABSTRACT: Enter an abstract giving a brief and factual summary of the document indicative of the report, even though it may also appear elsewhere in the body of the technical report. If additional space is required, a continuation sheet shall be attached.

It is highly desirable that the abstract of classified reports be unclassified. Each paragraph of the abstract shall end with an indication of the military security classification of the information in the paragraph, represented as *(TS)*, *(S)*, *(C)*, or *(U)*.

There is no limitation on the length of the abstract. However, the suggested length is from 150 to 225 words.

14. KEY WORDS: Key words are technically meaningful terms or short phrases that characterize a report and may be used as index entries for cataloging the report. Key words must be selected so that no security classification is required. Identifiers, such as equipment model designation, trade name, military project code name, geographic location, may be used as key words but will be followed by an indication of technical context. The assignment of links, rules, and weights is optional.

3682-66